Gradient Grain Growth

A thesis submitted in partial fulfilment

of the requirements for the degree of

MASTERS OF ENGINEERING

IN MECHANICAL ENGINEERING

by

NICHOLAS JAMES BREEUWER

University of Canterbury

2020

PREFACE

This thesis is in partial fulfilment of a Masters of Engineering in Mechanical Engineering.

This research was conducted under the supervision of senior supervisor Associate Professor Dr Catherine Bishop and co-supervised by Professor Dr Milo Kral and Associate Professor Dr Daniel Lewis.

Dr Bishop and Dr Kral are in the Department of Mechanical Engineering, University of Canterbury, New Zealand.

Dr Lewis is in the Department of Materials Science and Engineering, Rensselaer Polytechnic Institute, NY, USA.

Masters start date	01/03/2019
Masters finish date	01/05/2020

ACKNOWLEDGEMENTS

I would like to acknowledge the following people and organisations that have made this research possible:

Firstly I would like to thank my supervisor Dr Catherine Bishop for her unwavering support and guidance throughout my masters. Her understanding and board knowledge of all things materials is impressive. She has inspired many deep conversations during my undergraduate degree and this work. Her passion, mentorship and attention to detail have made this work so enjoyable.

I would like to thank Dr Milo Karl for his support and guidance on all things practical during this work and the opportunity to broaden my knowledge of materials and failure analysis during the many consulting jobs.

I would also like to thank Dr Daniel Lewis for inspiring the idea of gradient grain growth.

I would like to thank Shaun Mucalo for helping with the design of the gradient samples and teaching me to use the equipment and for fixing anything that broke along the way. I would like to thank Shaun for all the stimulating off topic conversations.

I would like to thank soon-to-be Dr Oscar Torres-Matheus for the many hours of mentorship and teaching as a lab demonstrator during my undergraduate degree, and for educating me about Venezuela and all of the political banter and theoretical conversations during lunchtimes in the office.

I would like to thank Alice Young for her mentorship during my undergraduate degree and helping so much with the experiments and for doing the EBSD work.

I would also like to thank my family and friends for all the support and encouragement.

Lastly, I want to thank my loving wife Katie for her encouragement, understanding and constant support during this work.

ABSTRACT

Inhomogeneous material properties such as corrosion resistance, strength and creep can be found in cast or formed metals which are heat treated. The spatial variation comes from the gradient in grain sizes, which is a problem for any industry which forms/bends high strength metals such as in petrochemical refinery.

The aim of this masters project was to investigate the rate of grain growth in brass which has a gradient in grain sizes. This was following on from prior work by Dr Dan Lewis (assistant supervisor) who found not-normal grain growth in simulated gradient grain growth calculations.

Grain size engineering is one of a few methods engineers use to strengthen metals. One way to control grain size is through controlled solidification. The higher the undercooling (temperature difference between the liquid metal and the temperature at which solidifications begins) the higher the nucleation rate of new grains and thus the smaller the solidified grain size. Another method is through cold work followed by a heat treatment. Cold work is when a metal is deformed below a material-specific temperature called the recrystallisation temperature. Cold work causes the generation and motion of defects called dislocations. A dislocation is a line defect in the lattice. These harden the metal by generating internal strain in the metal. This is known as strain hardening. Strain hardening makes the metal harder but less ductile. When given enough thermal energy, atoms are able to move around which allows point and line defects to combine and eliminate each other. This is recovery and recrystallisation. These processes restore the original material properties; however, the size of the grains in the material will be reduced. A smaller grain size strengthens the material and is known as the Hall-Petch relationship. If the metal is left in this elevated thermal state, then atoms are able to migrate from one grain to the next. This results in a kinetic process where large grains increase in size and small grains shrink and disappear. Overall, the mean grain size increases, and this is the process known as grain growth.

Simulations of grain growth in 2D were performed by Dr Lewis. A higher rate of grain growth occurred in samples which had a higher spatial gradient in grain size. The present work set out to test if the same phenomenon occurred experimentally.

The metal in this work was 70/30 brass, an alloy with 70 wt.% Cu and 30 wt.% Zn. It has high ductility, and is a classical metal for grain growth studies.

The gradient in grain sizes was created in this project using tensile cold work. A sample with constantly changing cross section was deformed to a known total gage deformation. This was followed by a series of interrupted heat treatments to recrystallise then grow grains. The grain size was measured after each heat treatment using large-scale optical images, and image analysis software ImagePro 10 was used to identify the grain boundaries. Because the stored cold work was dependant on the location, recrystallisation was able to be tracked as it progressed down the sample. Then the grain growth was also measured in the same sample which had a gradient in grain sizes. The rates of both recrystallisation and grain growth agreed with literature values in each analysis area. However due to using interrupted heat treatments there was significant thermal lag which may have altered the detailed results.

This work focuses on tracking recrystallisation and measuring the grain growth in a series of gradient samples at five different temperatures. It includes developing a new method for material testing which would suit high-throughput material design for industries such as the petrochemical and nuclear sector which require high levels of testing before a new alloy can be put into service.

CONTENTS

LIST OF FIGURES

LIST OF TABLES

1 INTRODUCTION

1.1 MOTIVATION

This research was driven by an industrial problem of anisotropic material properties in high temperature steels that have been formed then heat treated. The anisotropic properties are caused by a gradient in grain sizes. A metals grain size has an effect on corrosion resistance and more importantly the strength and creep resistance.

Recrystallisation and grain growth are well understood in materials with homogeneous grain sizes, but little research has been done in materials with a gradient in grain size. Dr Lewis's (assistant supervisor) modelling of grain growth detected an anomalous increase in the rate constant for grain growth in samples with a larger gradients in grain sizes. No previous experimental study had investigated that prediction.

1.2 RESEARCH OBJECTIVES

This work set out to develop a method to create a gradient in grain sizes in one sample using tensile cold work in 70/30 brass and then to track the grain size using optical methods to measure the recrystallisation and grain growth rates.

1.3 RESEARCH ACHIEVEMENTS

This work showed that isotropic FEA was able to accurately predict the mean strain in a sample by comparison to DIC, even well past the elastic limit.

The use of DIC for measuring strain and deformation was validated by direct comparison to strain gauges and linear extensometers.

A method to electropolish large brass samples using simple equipment to a quality suitable for EBSD was developed.

The equivalence of tensile and rolled cold work to achieve the same reduction in original grain size was validated.

Digital grain boundary detection using large scale optical images was shown to be more effective and efficient than EBSD in this study.

Recrystallisation and grain growth behaviour determined here for each analysed subdomain on the gradient sample were broadly consistent with literature studies.

There was a detectable increase in the growth rate with the larger starting grain sizes. This was most prominent in the 700 °C sample. This increase in growth rate was not expected and was hypothesised to relate to the larger grains being excluded from analysis due to touching the edge of the micrographs.

A new method to determine the critical strain anneal conditions using a single sample was developed. This will enable high-throughput materials engineering when developing new engineering metals.

A poster of preliminary work was presented by my supervisor at Material Science and Technology (MS&T19) in Portland, OR.

1.4 THESIS CHAPTER ORGANISATION

Chapter 1: Introduction

This chapter introduces the research with a brief motivation for the research. It also has a summary of the research achievements and layout of this thesis.

Chapter 2: Literature Review and Background

This chapter details all the underlaying concepts of this research. This section is broken into four major subsections: *Thermomechanical processing, Properties, Gradient grain sizes and Methods*

Chapter 3: Method.

This chapter provides a comprehensive description on the processes and techniques used to complete this work.

Chapter 4: Results

All the raw results for grain size and hardness are shown here.

Chapter 5: Recrystallisation

The analysis of recrystallisation based on results from Chapter 4 is presented. This chapter describes the reason that measuring recrystallisation in one sample is important. It also shows how the recrystallisation varies with both temperature and time.

Chapter 6:Grain Growth

The analysis of grain growth based on results from Chapter 4 is presented. This chapter centres around how the rate of grain growth varies with both temperature and time. It also shows that the composition of the samples did not vary from the as received brass.

Chapter 7: Cold Work Grain size and Hardness

This chapter compares cold work from rolling to tensile cold work on the reduction in area and to the recrystallised grain size. It also shows the measured strain from DIC and associated errors and the relationship between the grain size and the position along the samples. The relationship between hardness and both grain size and recrystallisation is discussed.

Chapter 8: Conclusions and Future work

This chapter is broken into two main sections, a summary and conclusions section and future work section. The future work section is broken into three sections, further experiments to conduct on both grain growth and recrystallisation, and a method improvements section for both DIC and the electro polishing, and a section on a new process to speed up the testing of new materials.

Chapter 9: References

This chapter has all the references and resources used in this work.

Chapter 10: Appendix

The rough calculations to determine the rate of heat transfer and temperature rise in a sample during heat treatment are included here.

2 LITERATURE REVIEW AND BACKGROUND

OVERVIEW

Materials engineering is used by industry to strengthen materials [1]–[3]. Grain size engineering is one of these techniques, normally done commercially through cold work followed by a heat treatment. During heat treatment the material will go through recovery, recrystallisation, and then, if kept at an elevated temperature, will enter the grain growth phase [3]. When a material's grain size is reduced, mechanical properties will change, e.g. yield strength is increased [3]. Conversely, when the grain size is increased, the creep resistance is increased [4].

This chapter has been broken into four sections: thermomechanical processing, properties, gradient grain sizes, and methods.

2.1 THERMOMECHANICAL PROCESSING

This section describes what happens to a polycrystalline material during cold work, recovery, recrystallisation and grain growth. It also describes the recrystallisation and grain growth kinetics, critical strain and the governing equations.

2.1.1 COLD WORK

When a metal is cold worked most of the energy put into the material is released as heat caused by friction, but there is energy stored in the lattice, most of which is dislocation or strain energy [5]. The dislocations disrupt the regular arrangement of the atoms in the lattice, altering the bond lengths between the atoms. These bonds act like small springs, storing energy.

The increase in the dislocation density causes the material to simultaneously increase in hardness while decreasing in ductility. This phenomenon is known as strain hardening. Strain hardening is caused by dislocations restricting the formation and motion of other dislocations [3]. The internally stored energy in the dislocations is released during heat treatment, which lowers the temperature required to begin the recovery and recrystallisation process. Therefore, a sample that is heavily cold worked will recover and recrystallise at a lower temperature and will therefore enter the grain growth phase much sooner than a sample which has not been cold worked [3]. The formation of dislocation bands or slip lines is not a random event, but instead occurs in preferred planes that are related to the crystallographic orientation of the lattice [3]. These slip bands appear as parallel lines in the microstructure as shown in Figure 2-1.

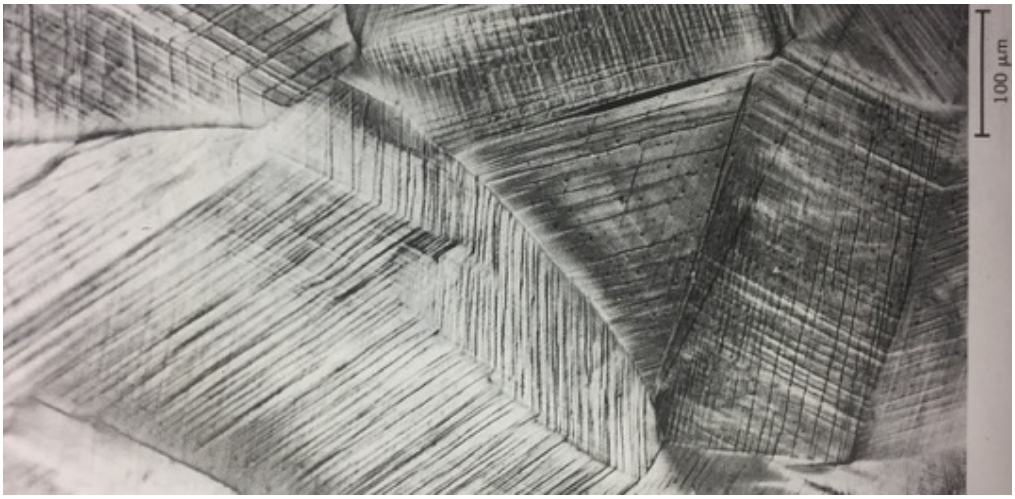

Figure 2-1 Slip lines after 33% cold work in brass, shown as long thin parallel lines within the grain structure [3].

2.1.1.1 FORMATION OF TWINS

A twin is a special grain boundary where the orientation of the two grains is related by symmetry as shown in Figure 2-2. There are two types of twins: deformation twins and annealing twins. Deformation twins are formed when a stress is applied to the lattice at temperatures below that which individual atoms are mobile. Annealing twins are formed at elevated temperatures following cold work.

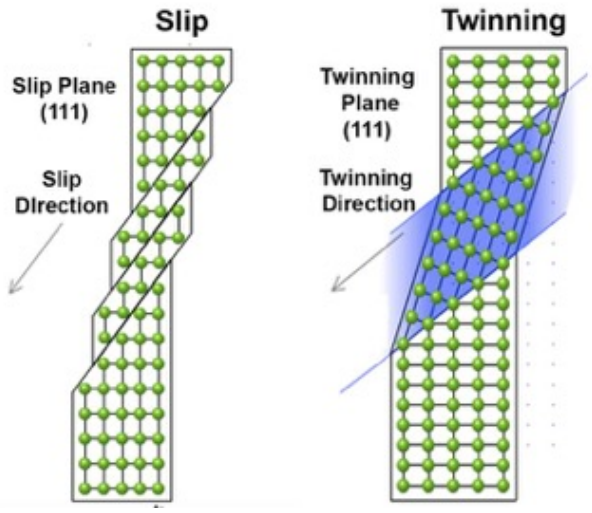

Figure 2-2 Two methods of displacing atoms in fcc metals. Slip shown on the left which occurs during cold work and annealing twins shown on the right that form at elevated temperatures after cold work. [6]

A deformation twin volume is often lens shaped and small (less than 100 μm); whereas, an annealing twin volume is much larger, and often appears to have parallel sides and to span the full parent grain.

Not all materials form deformation twins at the same rate. Face centred cubic (FCC) metals do not mechanically twin easily and normally require large amounts of deformation when compared to body centred cubic (BCC) or hexagonal close packed (HCP) metals which twin during yielding and often well before macroscopic deformation [7]. However, FCC metals with low stacking fault energies (such as Cu, Mg and Ni) have a tendency to form deformation twins when deformed at high strain rates or low temperatures [8]. This is because the deformation mode is via twinning over dislocation slip. Xiao et al. found that a high strain rate or low temperature, increased the formation of twins. The distance between the twins was also decreased independently with either higher strain rates or lower temperatures [9].

2.1.2 Heat Treatment

During heat treatment following cold work the dislocation density of the material will be reduced. This is described as recovery. During recovery, atoms are able to move more freely within the lattice due to the increased thermal energy. This enables opposite dislocations and opposite point defects to combine, which eliminates some defects in the lattice.

Following recovery, recrystallisation will take place with the nucleation of new strain free grains. The nucleation rate is related to the amount of cold work stored in the material. The higher the percentage of cold work, the higher the nucleation rate and finer the recrystallised microstructure. The growth of the strain free grains is driven by the change in internal energy from the recovered grains (which are still in a strained, higher energy state) and the strain free recrystallised grains. The new grains will grow, consuming all the original material until the grains meet at the newly formed grain boundaries.

If left at high temperature, recrystallisation will be followed by grain growth. Grain growth is where the larger grains increase in size consuming smaller grains, thus increasing the mean grain size.

This process of recrystallisation and grain growth is shown in Figure 2-3 of a brass sample. During recrystallisation, the original material properties will be restored to the original unstrained state but

with an increase in the yield strength according to Hall-Petch effect described later. The formation of annealing twins is also during the recrystallisation process. [2], [3].

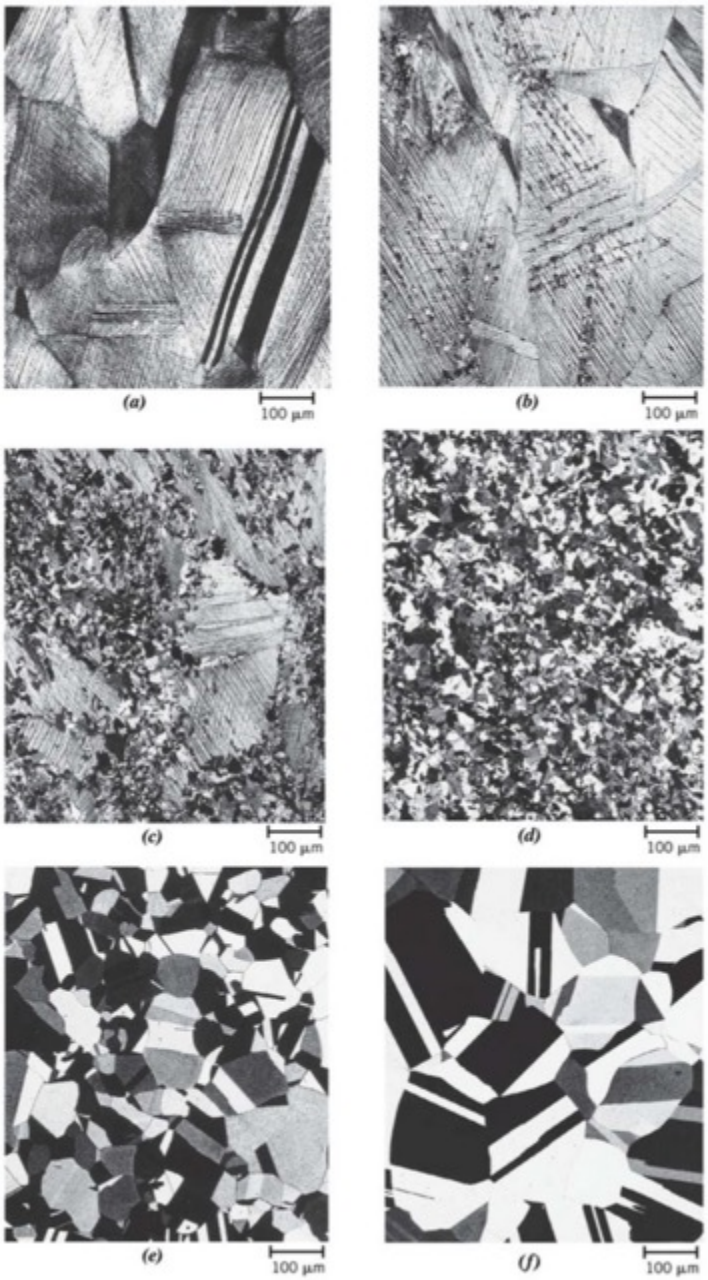

Figure 2-3 Micrographs of brass showing the stages of nucleation, recrystallisation then grain growth during heat treatment following 33 % cold work. (a) After 33 % cold worked. (b) Nucleation of new grains after 3 seconds at 580 °C. (c) Continued nucleation after 4 seconds at 580 °C showing the growth of the new strain free grains. (d) Complete recrystallisation after 8 seconds at 580 °C. (e) Grain growth after 15 minutes at 580 °C. (f) Further grain growth after 10 minutes at 700 °C [3] The rectangular regions are annealing twin volumes inside parent grains.

2.1.3 DEZINCIFICATION

Brass is made of copper and zinc, but can contain small portions of other alloying elements such as lead [10]. During recovery, recrystallisation or grain growth experiments, the temperature of the heat treatment is often in the vicinity of 400 – 900 °C. This is sufficiently hot to melt pure alloying elements such as zinc or lead, which have melting temperatures of 419.5 °C and 327.4 °C,

respectively [11]. The vapour pressures of these alloying elements are over the vapour pressure of copper at heat treatment conditions. There have been recorded cases of weight loss in samples during heat treatment [11], [12]. This weight loss is due to dezincification, where sublimation of zinc takes place from the surface. The vapour pressure of lead is much lower than that of zinc and lead has not been found to sublime. When zinc sublimes from the surface it creates a copper rich region as shown in Figure 2-4 [11], [13].

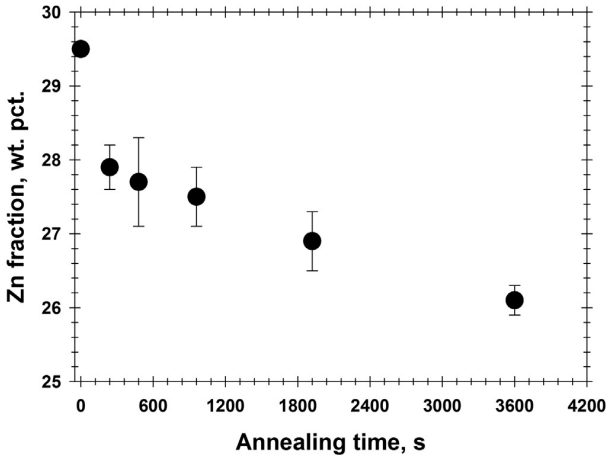

Figure 2-4 Zinc fraction in the mid plane of a 1 mm thick sample annealed at 900 °C [13]

2.1.4 Critical Strain for Recrystallisation

There is a minimum amount of cold work that a material must have to initiate recrystallisation, known as the critical strain [14]. Below the critical strain limit the nucleation rate for new grains is low while the growth rate of the already large grains is significant to outweigh any newly formed grains [15].

Chotinuchit showed that the critical strain was a function of concentration of zinc in a copper zinc alloy as well as the annealing temperature Figure 2-5A. Figure 2-5B shows that the recrystallised grain size decreases with critical strain for four annealing temperatures in 70/30 brass.

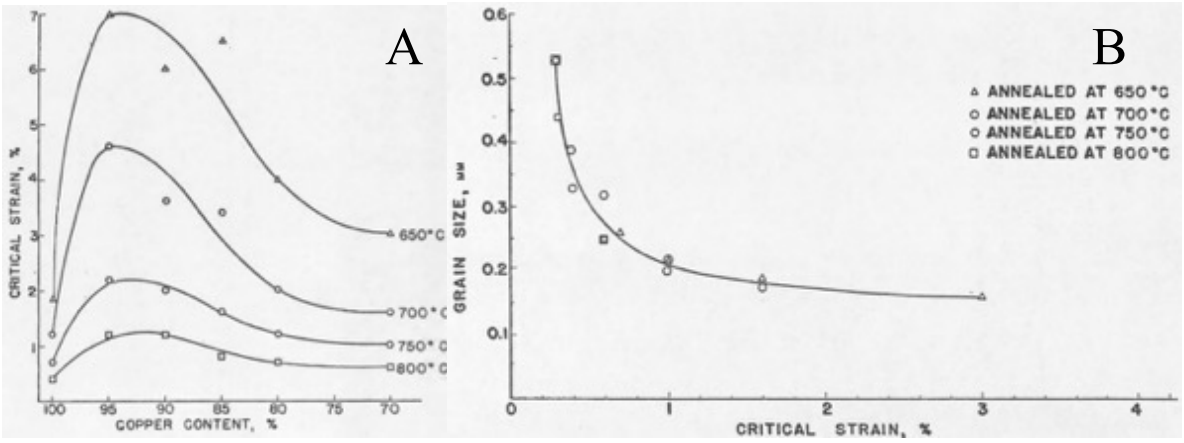

Figure 2-5 A) Critical strain vs copper content in Cu-Zn alloys various set annealing temperatures. Figure 2-5B) Recrystallised grain size vs critical strain for 70/30 brass [15].

2.1.5 Recrystallisation Kinetics

The amount of material that has recrystallised can be modelled by the Avrami equation [16], [17].

$$y = 1 - \exp(-kt^n)$$

Equation 1 Fraction transformed [18]

Where y is the fraction transformed, t is the time, while k and n are time independent constants for that material and process. The temperature of the heat treatment plays an important role in the transformation time required. This is shown for pure copper in Figure 2-6 for six different temperatures.

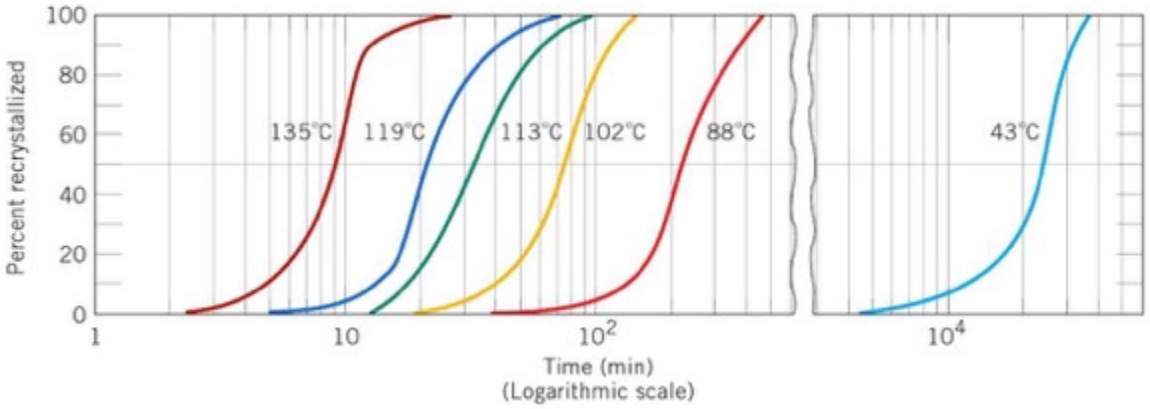

Figure 2-6 Fraction recrystallised as a function of time for pure Cu annealed at several temperatures [3].

2.1.6 Grain Growth

Grain growth happens through the movement of grain boundaries. A grain boundary is an interface between two grains. Grain boundaries can be divided into two groups: low angle grain boundaries and high angle grain boundaries. Low angle grain boundaries generally have an ordered or discrete dislocation structure; whereas, high angle grain boundaries have a disordered structure [19]. Grain boundaries have an energy associated with them. As grains grow there is a reduction in the total grain boundary area and thus a reduction in the total grain boundary energy [5]. This is the driving force for grain growth to occur. The physical way a grain boundary moves is through atoms detaching from the lattice of one grain and reattaching at the adjacent grain's lattice. This can be though as short-range motion and is why the rate of grain growth increases with increased thermal activity [20].

2.1.6.1 Rate of Growth

The speed that the grain boundaries move is proportional to the radius of curvature of the boundary. As a grain grows the rate usually slows. The growth of the grains in isotropic systems can be modelled by the grain growth equation [2], [3], [21].

$$d^n - d_0^n = k_0 \, e^{\left(\frac{-Q}{RT}\right)}$$

Equation 2 Isotropic grain growth [3].

Where d is the mean grain size at time t, a_0 is the initial mean grain size, R is the universal gas constant, Q is the activation energy for grain growth for that material, T is the temperature in Kelvin, n is the kinetic growth exponent and k_0 is a material constant [28].

2.1.6.2 Growth Laws

There are specific relationships that govern which grains grow and which are consumed [2], [23]. These relationships are related to the size of the grains relative to the neighbouring grains, the number of neighbouring grains, and the angle of the grain boundary and the crystallographic misorientation to the neighbouring grains [5]. Figure 2-7 shows the relationship between which grain will grow and which will be reduced in 2D. In Figure 2-7A there are six complete grains, one of which has five sides and one has seven. According to the relationships described above, the central grain, which has five neighbours, will be consumed (shown with a minus sign) by the grain on the left (shown with a plus) which has seven neighbouring grains. This will continue until the central grain is isolated from the growing grain as shown in Figure 2-7B. This process will continue in a cascading effect until the grains all have the same number of sides and the same number of neighbouring grains. This process was first described by von Neumann in 1952 as the N – 6 rule, where if a grain has less than six neighbours then it will be consumed and if it has more than six it will grow.

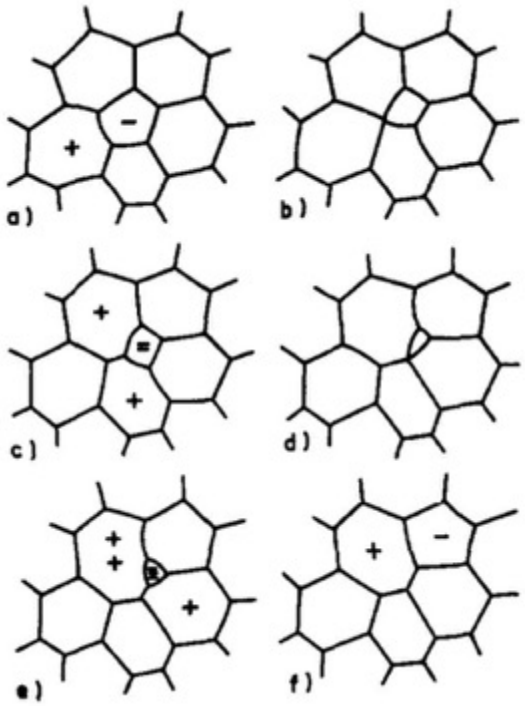

Figure 2-7 Illustration of the N – 6 relationships of isotropic grain growth in 2D. Growing grains are shown with a plus (+) and grains being consumed are shown with a minus (-) [23].

2.1.6.3 Maximum Grain Size

The predicted maximum size of any grain in a homogenous material, is twice the average grain size, provided there is not abnormal grain growth [5]. Normal grain growth is when individual grains stay very close to the average grain size. Abnormal grain growth is when select grains grow much faster than the surrounding fine-grained matrix creating a skewed or bimodal grain size distribution.

Abnormal grain growth is predicted to occur when all three of the following conditions are met: there is a presence of a second phase particle, when the average grain size is below an upper limit for that material and there is at least one grain which is much larger than the average grain size [5].

2.1.6.4 Grain Boundary Drag

The diffusion rate of solute atoms is generally slower than that of the bulk material and therefore will reduce the mobility of a grain boundary. Rollett et al explained the decreased mobility as being a result of the change in chemical gradient, which was due to the absorption of the solute either into, or away from the grain boundary. Where any change, either into or away from the grain boundary, increases the chemical gradient away from the lowest energy state. The chemical gradient then acts as a drag force for grain boundary mobility [19].

The presence of a particle or second phase solute can alter the mobility of the grain boundary depending if the material is attracted to or repelled by the grain boundary [13], [24]. Konkova et al. identified grain boundary pinning in brass due to precipitates rich in lead and tin forming on the grain boundary during an isothermal anneal. These precipitates were found on high angle grain boundaries. This resulted in the grain growth exponent n ~ 4, which is much lower than others found [25]–[27]

2.1.7 Materials for Grain Growth

Numerous metal alloys were investigated for grain growth experiments including aluminium alloys, iron alloys, zirconium alloys, titanium alloys, and lastly copper alloys.

2.1.7.1 Aluminium Alloys

Commercial aluminium alloys can form precipitates during heat treatment. Aluminium is somewhat challenging alloy to polish as it quickly forms oxides on the surface, and oxidises heavily during heat treatments in atmospheric furnaces [28]. There is literature on the grain growth of some series of aluminium [29], [30].

2.1.7.2 Iron alloys

Both ferric and austenitic iron alloys form deformation and annealing twins making optical grain growth studies hard. Polishing is easy, including electropolishing. They require high temperatures for grain growth and therefore long periods while the samples heat up. This would make interrupted heat treatments difficult [31].

2.1.7.3 Zirconium Alloys

Zirconium alloys are soft and can develop deformation twins during the polishing process which makes them a difficult alloy to polish [32].

2.1.7.4 Titanium Alloys

Titanium alloys are challenging to polish as they are very hard therefore requiring long preparation times [33]. Titanium alloys can have small grain sizes making optical methods of grain boundary identification hard. Titanium alloys also require a significantly high temperature for grain growth to occur, and like the iron alloys, this will create timing issues while the samples heat to the furnace temperature when using interrupted heat treatments [33].

2.1.7.5 Copper Alloys

Alpha brass, which is a binary alloy with under ~ 35 wt. % zinc, does not form precipitates as shown by the Cu – Zn binary phase diagram in Figure 2-8. All the copper alloys are easy to mechanically

polish using electro polishing and electro etching, making grain identification easy [28]. There is significant grain growth data available for copper alloys: 70/30 brass is a classical alloy for grain growth experiments and data for the critical strain anneal, grain size reduction with cold work etc. is available or comparison [34].

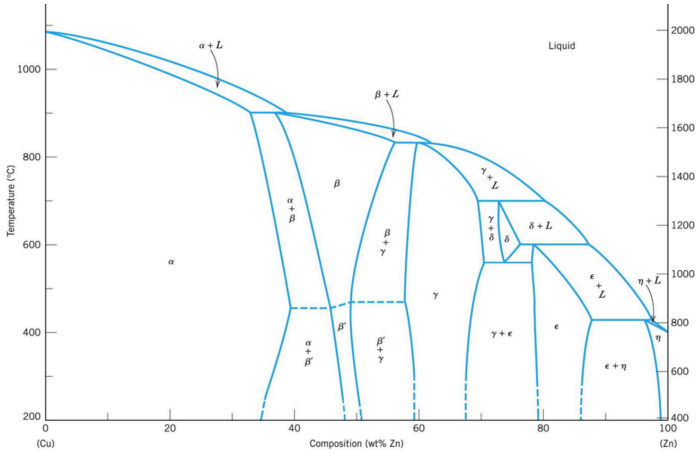

Figure 2-8 Binary phase diagram of copper and zinc [35]. Alpha brass is denoted with an α and is roughly under ~ 35 wt. % zinc.

2.1.7.6 Grain Growth Data for Brass

70/30 brass is a classical material for grain growth studies, there are many data sets to compare to, such as those from Ghauri et.al. [36] Rhee et.al. [37] Kirby and Walker [34] as shown here in Figure 2-9 through to Figure 2-12. The data from these figures is used in the grain growth chapter to compare the results of this study.

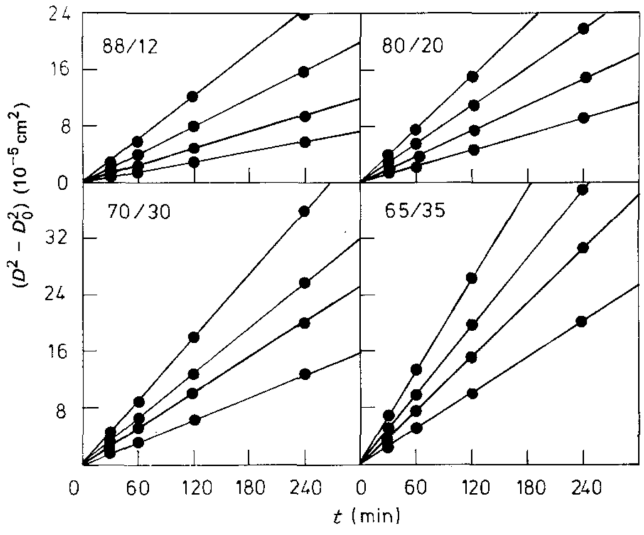

Figure 2-9 Grain growth isotherms of brass wires with differing compositions as indicated, the annealing temperatures are 600 °C ,650 °C, 700 °C, and 750 °C [36].

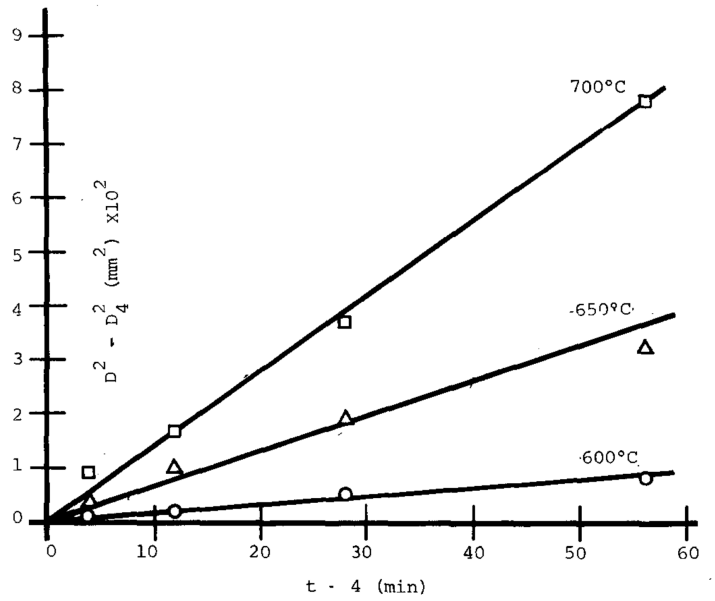

Figure 2-10 Grain growth data for 70/30 brass analysed by S. K. Rhee [37], with original data from Walker [34]

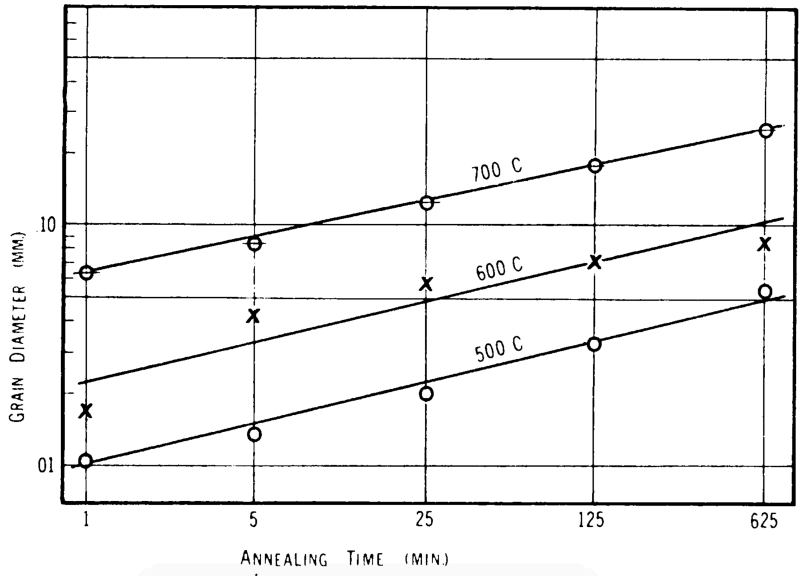

Figure 2-11 Grain growth data for cold rolled 0.044-inch-thick 70/30 brass isothermally heat treated in a molten salt bath [26]

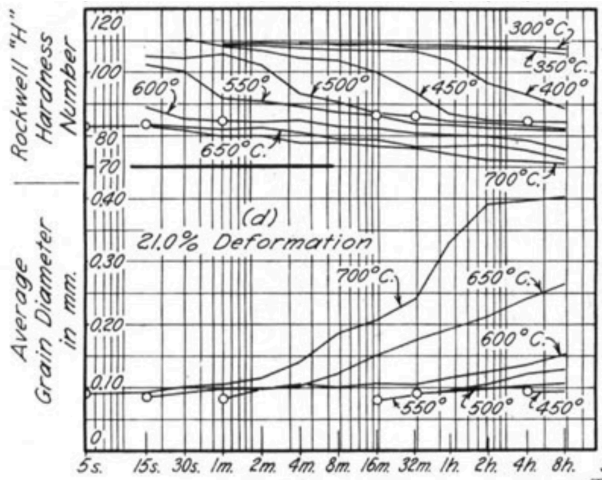

Figure 2-12 Grain growth and hardness data for cold rolled 70/30 brass heat treated in a molten lead bath [34]

2.2 PROPERTIES

The strength and ductility of a material is dependent on the grain size, as is the corrosion resistance.

2.2.1 HALL-PETCH

A reduction in the grain size of a single crystal is predicted to increase the yield stress from an initial yield stress σ_0 according to the empirical Hall-Petch equation [18].

$$\boldsymbol{\sigma = \sigma_0 + k\, d^{-1/2}}$$

Equation 3 Hall-Petch [18].

Where d is a linear measure of grain size, and k is a material constant. The relationship is believed to be caused by the grain boundaries blocking the movements of dislocations. A plot of the Hall-Petch effect is shown in Figure 2-13 for 70/30 brass.

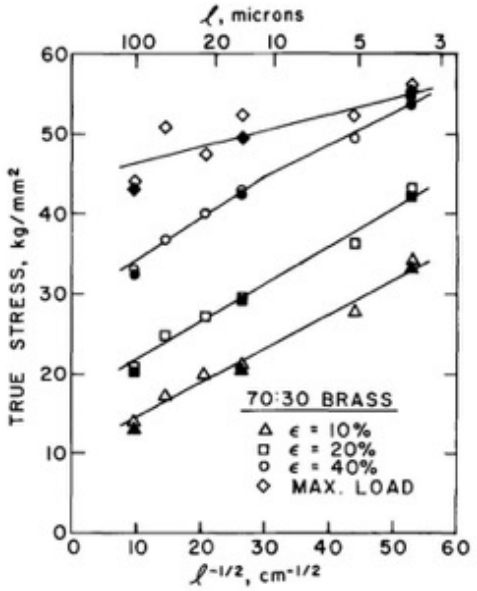

Figure 2-13 Shows the Hall-Petch relationship. As grain size decreases in 70/30 brass the stress increases. This is indicated by the iso-strain lines increasing with decreasing grain size. [38].

2.2.1.1 Inverse Hall-Petch

Meyers et al. identified that the Hall-Petch equation was only an approximation, and that the use of another material property exponent n which would lie between - 0.3 and - 0.7 would be more accurate. The Hall–Petch equation predicts an ever-increasing yield strength up to the amorphous limit. However, there is still an unexplained deviation in the trend once the grain size is reduced below roughly 25 - 50 nm [39]–[41]. Figure 2-14 shows the break down in the Hall-Petch equation in copper, lead and nickel. There is a decrease in yield strength and hardness below a critical grain size [42], [43]. Others have found a plateau in the yield strength and hardness [39], [44].

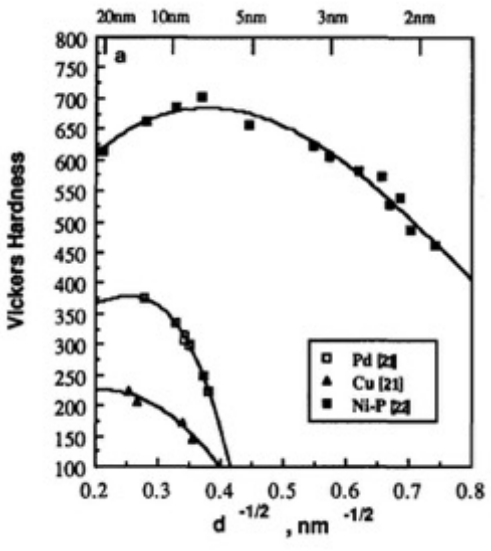

Figure 2-14 Inverse Hall-Petch effect in lead copper and a nickel alloy [41].

Further studies have shown that there is a change in the deformation mechanism from dislocation motion in large grains to grain boundary sliding [40], [45], [46], triple junction diffusional creep [41] and Coble creep [47] in the nanoscale grain sizes. Schuh et al. have suggested that select alloying elements may be able to suppress the breakdown in the Hall-Petch effect down to the amorphous limit [44].

2.3 Gradient Grain Sizes

Having a gradient in grain sizes is not a new problem. The fabrication industry has been producing gradients in grain sizes every time a cross section of metal is bent and heat treated or cast. Recently gradients in grain sizes have been created in additive manufactured metals. Research of gradient grain sizes is also not new as the properties of materials are altered by the grain size. The strength of gradient nanosized grain microstructures is higher than uniform grain size materials. Grain growth simulations in 2D have shown larger growth rates with higher spatial gradients in grain sizes.

2.3.1 Fabrication Industry

When a piece of thick metal is bent, there are varying amounts of cold work stored in the material. One side is in compression, and the opposite side is in tension. To regain some of the previous material properties and to relieve the internal stress of cold work, a heat treatment is often used. Upon heat treatment, through recovery and recrystallisation there will be a gradient microstructure in the material. This microstructure varies with the amount of cold work as shown in Figure 2-15. The material properties will vary through the cross section, which could be problematic if the variation is large and is used in a high strength application such as aircraft or large buildings.

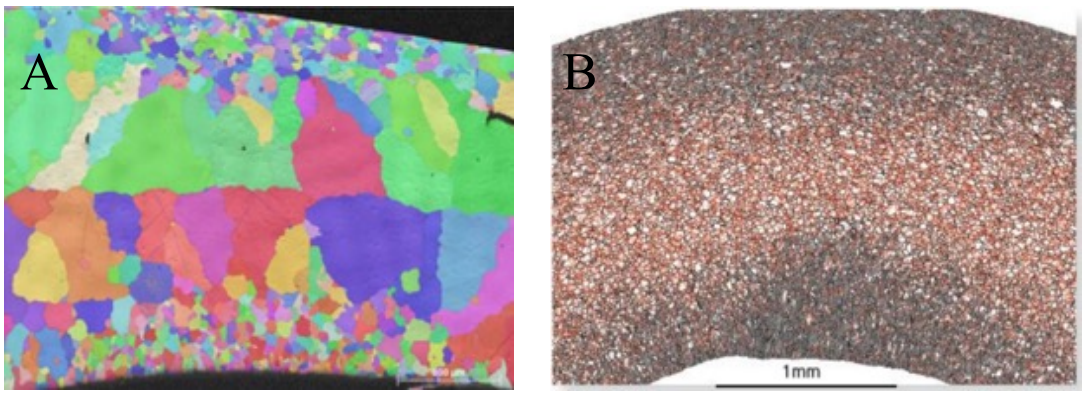

Figure 2-15 EBSD images of gradient grain sizes a) Grain map taken from zircaloy-4 after 3-point bending. Note the coarse internal grains and fine external grains [48]. B) Mosaic grain boundary map from a bent nickel tube made up of 90 image tiles, the black areas indicate grain boundaries that are > 10 °, red are twin boundaries, and grey are > 2 °. Again note the coarse grains along the central axis and fine grains at the top and bottom [49].

2.3.2 Additive Manufactured Microstructures

Three Dimensional (3D) printed microstructures are formed in numerous ways. One process is selectively laser melting a very fine powder of metal in an inert atmosphere. This builds up a structure in thin layers. This process requires complex post manufacture heat treatments which result in very anisotropic and heterogeneous properties of the final printed part [50]. These anisotropic properties can be from processing defects between the layers, which causes de-bonding and stress concentrations, through to changes in the grain structure from equiaxed to columnar grains caused by the rapid heating and cooling of the metal as shown in Figure 2-16.

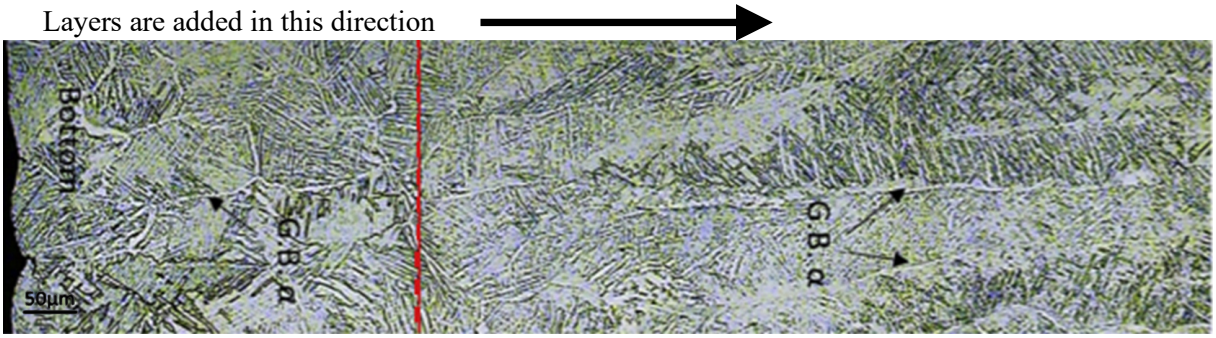

Figure 2-16 3D printed microstructure of Ti-6Al-4V by selective laser melting. Note the change in grain morphology from the left where the grains are equiaxed and to the right where they are columnar [51].

The grain shape alters the properties of the material and is dependent on the build direction of the 3D part [51]. The grain morphology in 3D printed metals is similar to metals which have been bent then recrystallised as shown in Figure 2-15.

2.3.3 Nanograined Alloys

There have been numerous studies in nanograined metals as shown in Figure 2-17 which have been shown to have increased mechanical properties such as strength and hardness over the same material with an homogeneous microstructure [39], [41], [43], [44], [46], [52].

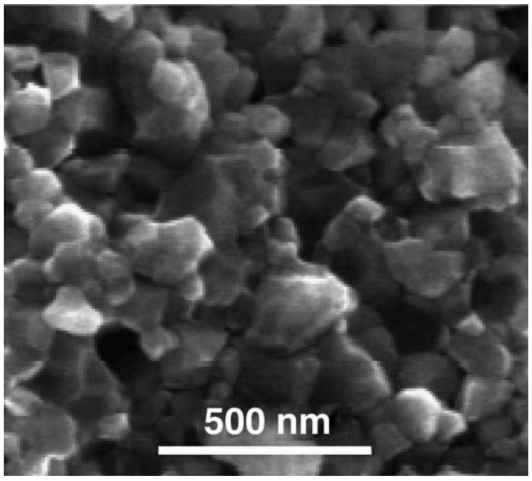

Figure 2-17 Micrograph of a fracture surface taken with a SEM of a nanocomposite of Al_2O_3 – TiO_2 – MgO, where the grains are in the order of 100 nm. It was formed by high pressure sintering (P ~ 1 GPa) at 850 °C for 30 min [39]

However, the increase in strength and hardness comes with the detriment to ductility, with as little as three percent elongation before brittle like failure [53]. As the size of a grain is reduced the volume fraction of atoms involved in the grain boundaries is increased. Meyers et al. showed that if a grain was assumed to have a cubic shape, then the volume fraction of interfaces grew from 3 % with a 100 nm grain size to 30 % with a grain size of 10 nm and to 50 % with a 5 nm grain. Most mechanical testing involving nanograined material is performed on micro or nanoscale test pieces [39], [52]. This is to reduce the chance of the sample containing a defect[39]. It is widely accepted that the chance of encountering a low reading test increases with the size of the test piece [3].

2.3.4 Nanotwinned Mechanical Properties

There has more recently been work by Cheng et al in creating a gradient of grain sizes in nanotwinned samples to further enhance the mechanical properties, specifically to increase the ductility. A sample of a gradient microstructure is shown in Figure 2-18.

Figure 2-18 SEM image of the microstructure of a gradient nanotwinned copper sample [52]

Changes in microstructures can be seen in nature from the hierarchical structure of bone and muscle to the changes in dentine and enamel to orientate the structures with favourable loading conditions in order to prevent breakage and excessive wear [54]. Cheng et al. were able to increase the yield and ultimate tensile strength and ductility of the gradient nanotwinned copper samples over the non-gradient nanotwinned samples as shown in Figure 2-19 [52].

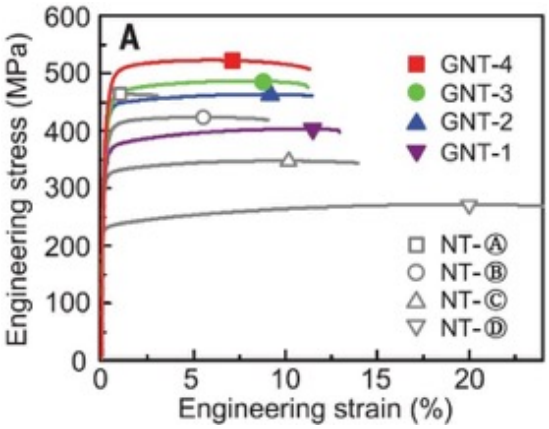

Figure 2-19 Stress strain curves of Gradient Nano Twinned (GNT) copper and Nano Twinned (NT) showing the increased strength and ductility for the GNT samples 1 – 4 (colour) over NT samples a – d (grey) [52].

The process that was used to create the gradient in grain sizes was electro-deposition. This process of manufacturing is slow and costly whereas cold work followed by a heat treatment is fast and requires low technology. If similar benefits can be obtained in gradient grain sizes developed with cold work then this would be of great interest to industry.

2.3.5 SIMULATION

Dr Lewis, from the Rensselaer Polytechnic Institute, USA (assistant supervisor) has a group modelling grain growth using Surface Evolver [55]. The samples that they have studied had non-uniform microstructures. The samples all had an identical mean grain area but with different gradients in the grain size. They have detected an increase in the rate of grain growth in the samples which have

a higher gradient of grains sizes as shown in Figure 2-20 [56]. Existing empirical models do not explain why this is. Indeed, while the rate of grain growth with samples with non-gradient grain sizes is well established, these models do not hold true when there is a gradient of grain sizes [57].

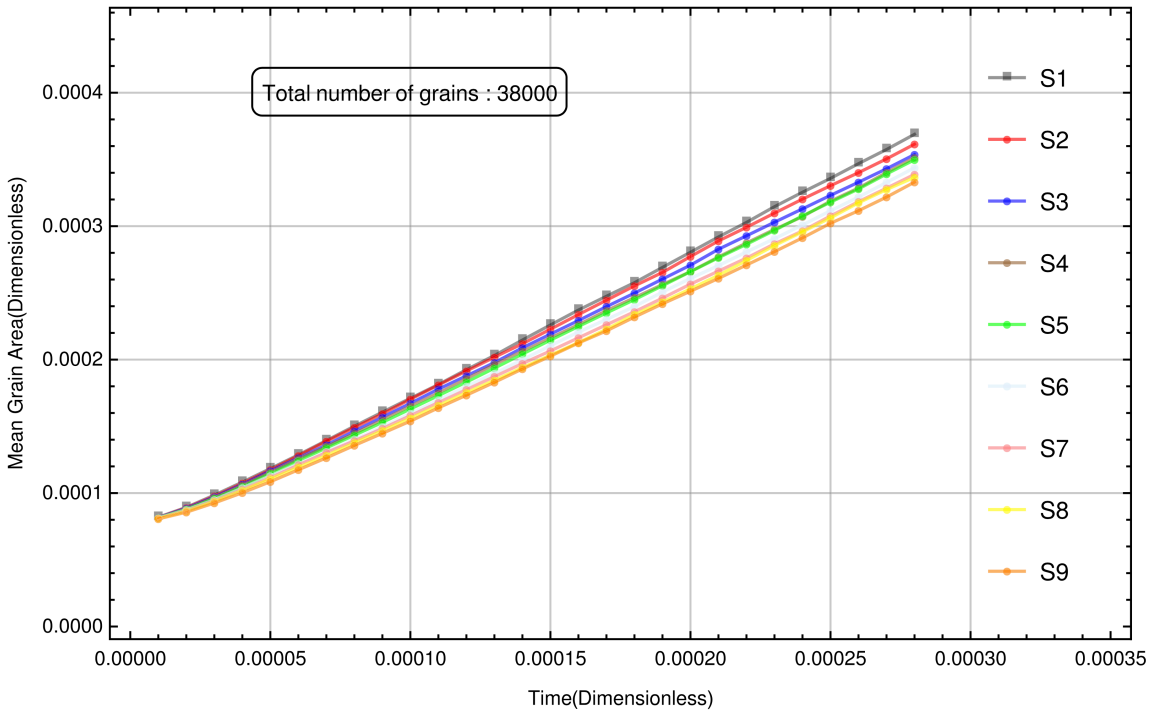

Figure 2-20 Simulated grain growth in samples with a gradient in grain sizes. Note S1 has the highest gradient in grain size and S9 has the most uniform grain size [56]

2.4 METHODS

2.4.1 CREATING GRADIENT GRAIN STRUCTURES.

As shown in section 2.3, there are many ways to create a gradient grain structure. In research grain size manipulation is traditionally done by reducing the cross-sectional area of metals by rolling followed by a recrystallisation heat treatment. But recently Bishop et al. has used cold work created using tension to create a gradient in grain sizes in Incoloy 800H [58]. The sample was non-uniform and after recrystallisation had a constantly changing grain size.

Chotinuchit used an asymmetric tapered tensile sample with linearly changing cross sectional area that was deformed using tensile cold work to measure the critical strain in alpha brass. Microstructural analysis was optical with grain size determined by the Heyn line intercept method that is now included in ASTM Standard E112 [59]. The method of strain determination is not given in the thesis, but hardness indents were used as fiducial markers evenly spaced along the gage. The maximum deformation reported was 10 % strain. No error bars or indication of grain size distributions or sampling method were presented.

2.4.2 Recording Macro and Microstructure

Revealing the macro and microstructure of a material is important in determining things such as what phases/structures are present, the grain size and grain shape. The methods used to observe these range from simple optical microscopes through to using electron microscopes. An optical microscope uses visible light reflected off the surface of the sample that is magnified through lenses. The magnification is limited by the resolution of the light waves to around 1000X [60]. An electron microscope uses a beam of focused electrons that interacts with the sample. The resolution of electron microscopes is far greater than that of light microscopes because the wavelength of an electron is up to 100,000 shorter than that of visible light [61]. There are two main types of electron microscope, Transmission Electron Microscopes (TEM) and Scanning Electron Microscopes (SEM).

2.4.2.1 TEM

A TEM uses a beam of focused high energy electrons and very thin samples around 100 nm thick that some of the electrons are able to pass through. The detector is directly under the sample and records the information from the few electrons that were able to pass through the material and were not deflected or scattered. The resolution in TEM is limited to above 50 million magnification, but images have been taken that are sub 50 pm [62].

2.4.2.2 SEM

An SEM uses a similar beam of highly focused electrons that quickly raster's (moves) across the surface. The amount of information that can be gathered depends on the detectors that are installed, such as the topography and the composition of the sample. One of these techniques is called Electron Back Scatter Diffraction (EBSD). The back scattered electrons are diffracted by a volume of atoms close to the surface of a crystalline sample as shown in Figure 2-21 [62].

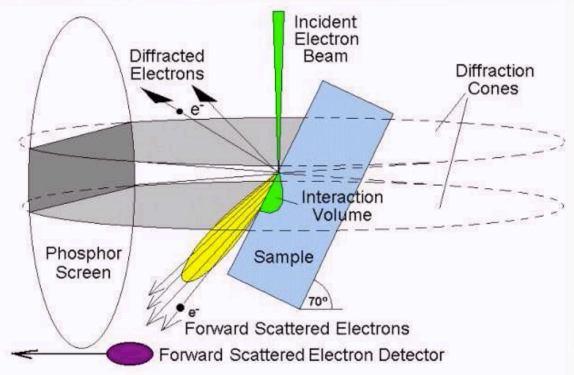

Figure 2-21 Interaction of the sample with the beam of electrons used in SEM to construct Kikuchi maps [49]

Consider the volume of atoms from a crystal lattice with planes separated by a distance d, as shown in Figure 2-22. If the incident waves are at the correct angle θ then the diffracted electrons will constructively interfere according to Bragg's law [18].

$$\mathbf{n\lambda = 2d \sin \theta}$$

Equation 4 Braggs law [18].

Where n is a positive integer, λ is the wavelength of the electrons, d is the interplanar spacing, and θ is the diffraction angle.

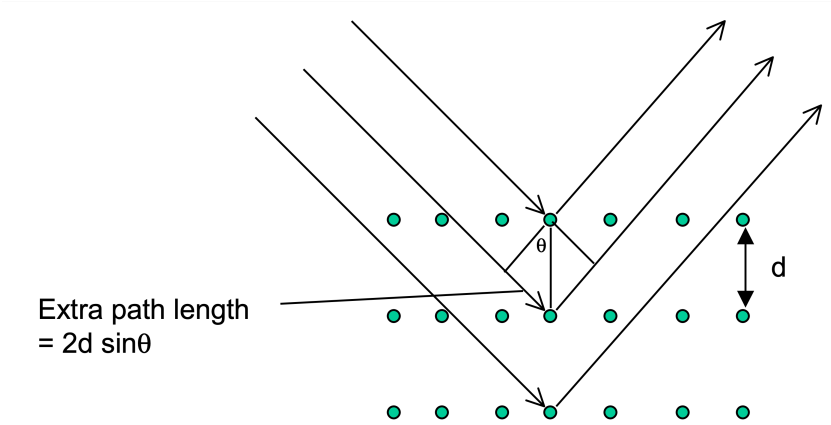

Figure 2-22 Illustration of Bragg's law, showing the extra distance travelled by the electrons that penetrate further into the sample before being deflected by an atom marked by a green circle [61]

The electrons that are constructively diffracted from the surface form bands or rings that originate from the sample. These bands can be used to construct Kikuchi maps when they impact a phosphorus screen as shown in Figure 2-23.

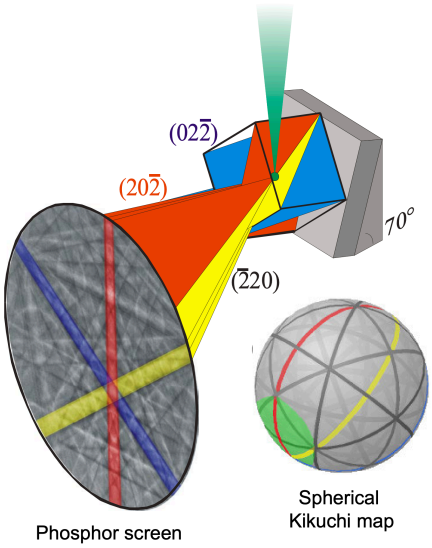

Figure 2-23 Schematic of how the diffracted electron bands shown in yellow blue and red are used to construct Kikuchi maps [61]

The spherical Kikuchi maps are an identifier to a particular phase and orientation of material. The identification is by the orientation and interaction of these bands. As the electron beam raster's over the sample it is possible to detect a change in the lattice orientation down to ~ 0.5° by a shift in the Kikuchi maps position [63]. When there is a shift in the Kikuchi map over a threshold value, it signifies a change in crystal orientation from one grain to the next. When a completely new map is present it signifies a different phase is present. The lattice orientation is a way of determining how each voxel is orientated in the bulk of the sample.

Texture can be random through to almost single crystal where each grain only has a slight variation to the neighbouring grains. Texture can be portrayed though a colour map such as displayed in Figure

2-24, where each grain's Miller indices are represented as a colour from the orientation triangle[61], [63]–[65].

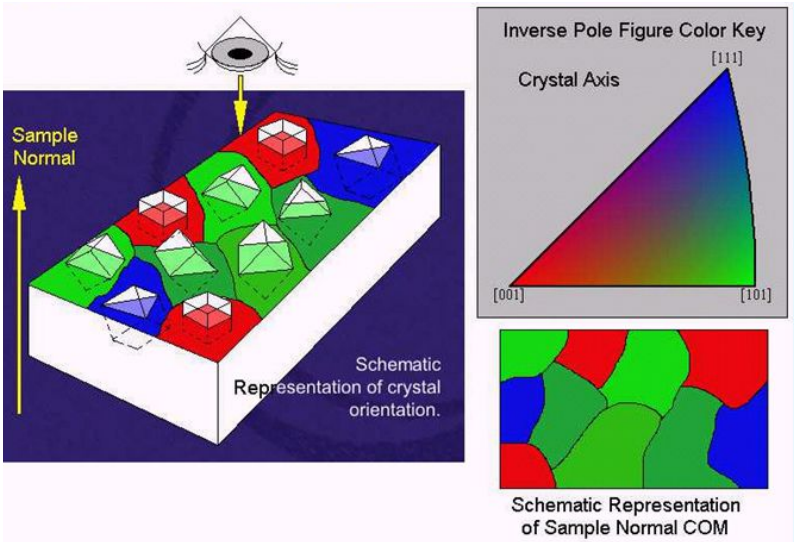

Figure 2-24 Crystal orientation maps [66]

Grain boundary maps can easily be created from EBSD maps through digital post processing. Then statistical data can be gathered such as grain size distribution and grain boundary character distribution.

2.4.2.3 Optical Emission Spectroscopy

Optical Emission Spectroscopy (OES) is a method of accurately measuring the atomic composition of a metal. OES works by removing some of the surface atoms with a high temperature spark discharge. The atoms are then sucked into a chamber for analysis. The high temperature spark used to erode the surface excites the atoms and ions that are removed which causes the electrons to jump valance bands. The excited atoms then emit a photon with a spectrum which is unique to that element, the spectrum is caused by the individual electrons dropping back to the original location as shown in Figure 2-25 [67].

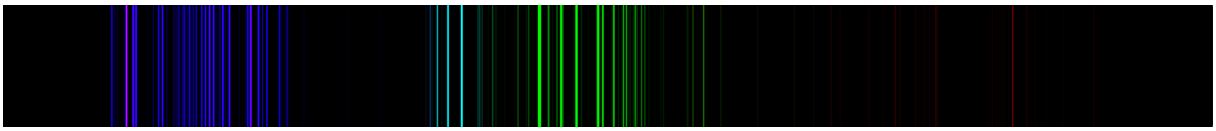

Figure 2-25 Optical Emission Spectrum of Iron with 26 electrons [68]

The spectrum of light from the sample is analysed against known reference spectra to determine the elements present. The intensity of each spectrum determines the quantity of that particular atom in the sample [67].

2.4.3 Sample Preparation

The method used to record the microstructure dictates the sample preparation technique. For optical measurements the sample is polished flat to remove any surface defects, then an etchant is used to expose the grain boundaries. The etchant can be either chemical or electrical. An acid will preferentially attack the grain boundaries as will an electrical current passed through a sample when

the sample is in an electrolyte. This will show grain boundaries as darker areas under the microscope like those from Figure 2-3.

EBSD maps require much higher levels of polish to produce maps which are of usable quality. Firstly, hard cloths are used (silicon carbides papers) to flatten the surface, similar to those used for optical. This is followed by soft cloths which have a suspension of very fine grinding paste. This is to remove any surface damage created by the hard cloths. Following mechanical polishing, a sample may require further processing by electropolishing or ion milling [69].

2.4.4 Digital Image Analyses of Grain Boundaries

With computers becoming faster with more memory and software algorithms getting better, computer assisted image processing is now more reliable and faster than by hand [70]. What would have involved counting grain boundaries by hand that intercepted a series of lines as is described in the standard ASTM E112-13 can now be done more accurately by analysing the whole micrograph, using an image processing software such as ImageJ or ImagePro by Cybernetics [59], [70], [71]. Measuring area and grain size using digital methods is more repeatable than by hand as it requires a skilled and trained operator to be able to identify the correct features. Also, human eyes can easily be tricked or generate bias in the results [72]. The American Society for Testing and Materials (ASTM-E562) estimates about 15 minutes per image to measure the volume fraction of an identifiable constituent or phase with an experienced user [73].

Campell et al. used both optical and digital methods to measure the grain area, the digital methods were within 10% of the manual measurements and were all within the operator variation [72].

2.4.5 Strain Measurements

Strain measurements can be taken in a few ways, either directly by using a sensor mounted to the surface of the sample, or a more recent method is using a non-contact process which involves tracking a point or points with a camera and digitally measuring the displacement [74] [75].

2.4.5.1 Physical Strain Gauges

Physical strain gauges come in many forms. There are strain gauges which work by measuring a change in resistance of an extremely fine wire which is glued directly to the surface in a rosette. The wire is stretched with the sample which it is glued too. The reduction in cross section of the wire increases in resistance. These gauges have a few limiting features, they can only deform to around 25 % strain because above that the glue which holds the gauge to the surface may start de-bonding and the gauge will not deform with the sample. They can only be used up to the linear elastic limit of the wire which they are made from making them unsuitable for very ductile materials e.g. rubber. They are sensitive to temperature variations [74].

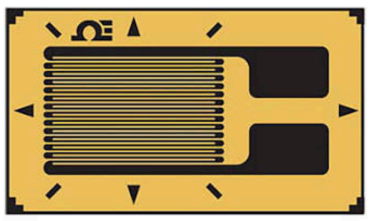

Figure 2-26 Single foil type resistive strain gauge. The black is the metallic foil which will thin out when deformed which will increase the resistance [76].

The most common reusable strain gauge is an extensometer. This measures a deflection over a known distance which can be converted to strain. Most of these devices are a resistive style strain gauge, but the strain gauge is mounted onto an arm. These sensors are much larger than a wire-based strain gauge, but they can be taken to very high levels of deformation because the strain gauge is working on a lever and not directly on the sample as shown in Figure 2-27.

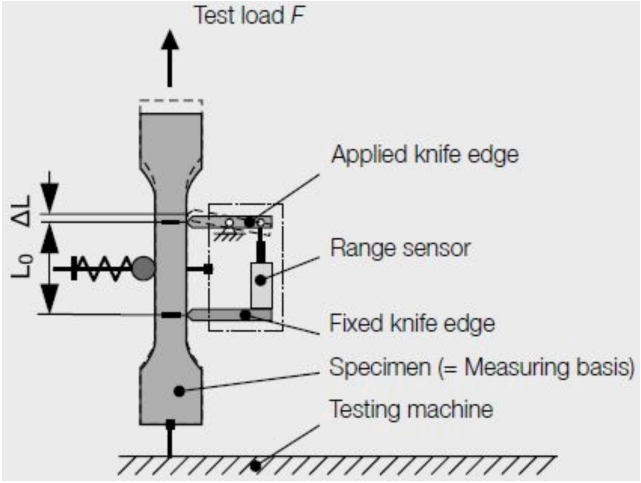

Figure 2-27 Schematic of extensometer for strain measurement. The knife edge arms can either be connected to a Linear Variable Dependant Transformer (LVDT) as shown, or the arm may be solidly mounted and have a set of foil type strain gauges which will measure the strain and thus deflection in the arm [77].

2.4.5.2 Optical Strain Measurement

A video extensometer works by tracking two features on the surface of a sample with a camera or laser. The software is able to measure the change in distance between these two points during deformation which is converted to strain similar to an extensometer [75]. There are more sophisticated optical techniques which track more points and are able to measure strain in three dimensions if two cameras are used, such as Digital Image Correlation (DIC). DIC uses a very large number of speckle (in the 10,000s) on the surface and is able to measure the change in position of each dot relative to the neighbouring dots [78]. The displacement map is converted to strain and can be output as an overlay map, see Figure 2-28.

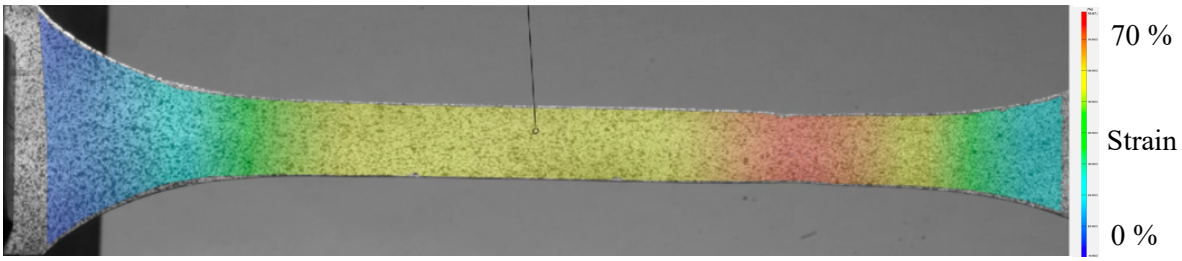

Figure 2-28 Screen shot from GOM correlate showing Von Mises equivalent strain just before failure of an annealed 70/30 brass dog bone sample which is showing approximately 70 % strain in the necked region just before failure.

The speckle quality is very important and will greatly affect the resolution of the information that is able to be gathered. There are key factors that determine a good speckle: Contrast, Randomness, Anisotropy and Adhesion. The higher the contrast the speckle has with the background the better the computer can track individual dots. If the speckle has a pattern or is periodic nature, then the full field displacement may be compromised. The speckle should take up roughly half the surface of the sample. The speckle should not have any directionality, the distance between the pattern should be

equal in all directions. And finally, the speckle must adhere to the sample surface without flaking while also deforming with the surface [78], [75], [79], [80].

3 METHODS

OVERVIEW

This chapter describes the techniques and processes that were used to design and create the samples used in this research project.

It describes the modelling method used to design the gradient samples, the process of machining the samples, the techniques used to prepare the samples for DIC, the mechanical deformation and set up along with the image recording during deformation. The heat treatment process is described along with the temperature and times. The mechanical polishing process and electro-polishing to reveal the grain boundaries is described, along with the process of identifying grain boundaries using Image Pro 10.

The end of this chapter is dedicated to validating the process and methods used, where DIC is validated against strain gauges and linear extensometers. Then DIC is compared to FEA and finally optical methods of detecting grains are compared to EBSD.

3.1 70/30 Brass

The material chosen for this study was a low alloy brass, namely 70/30 brass which is ~ 70 wt.% copper and 30 wt.% zinc. The reason that this composition was chosen was all the classical grain growth data available used this composition. It is easy to mechanically grind and electro polish to reveal the grain boundaries. It is easy to heat treat at low temperatures and does not react with the atmosphere. The downside is that it forms annealing twins during heat treatment.

A low alloy brass sheet 3 mm thick was purchased from The Little Metal Company in Sockburn, Christchurch, and conformed to C26000 which has the composition shown in Table 3-1.

Table 3-1 Composition of C26000 in weight percent. [81]

Element	Weight percent (%)
Cu	68.5-71.5
Zn	Remainder
Fe	0.05
Pb	0.07
Other	0.15

All the brass used in this research came from the same sheet which had the composition measured prior and post heat treatment using an Oxford Foundry Master Xpert, OES. This was to check for loss of zinc due to dezincification during heat treatments, and to check for high concentrations of elements that may prevent normal grain growth by pinning the grain boundaries, namely lead.

Two as-received samples (~ 30 mm x 30 mm) taken from opposite ends of the sheet were prepared by grinding down one face by 0.1 - 0.3 mm with 180 and through to 400 grit SiC paper to remove any surface contamination. The two heat treated gradient samples 5B and 9B, were ground down until the samples measured ½ the original thickness. These four samples were measured by OES.

3.2 Gradient Sample Design using Finite Element Analysis

The method of designing the gradient sample using computer aided design is described as well as the methods of refining the model. The goal is to use a non-uniform von Mises plastic strain to obtain a gradient in recrystallised grain size.

3.2.1 Ansys Modelling

The purpose of the tensile sample was to minimise the strain variation in the Y direction and to achieve a peak strain in the X direction around 40 % von Mises. Here X is the coordinate along the gauge and Y is the transverse coordinate.

The Computer Aided Design (CAD) package Solidworks was used to draw the samples initially in 2 D. Only one quarter of the sample was needed. This was done because the samples have two-fold symmetry which reduced the computational time used to solve the stress fields.

The samples were analysed in the Finite Element Analysis (FEA) package ANSYS. Only the strain and deflection required to produce a set strain were measured. The model was increased to full shape and 3D once the strain profile was improved sufficiently, which was theoretically redundant but was done for completeness.

The modelling method used in ANSYS was Structural Mechanical deformation at 25 °C. The mesh was adaptive using a program-controlled size. With the adaptive control still on the mesh size was forced down from 0.5 mm to 0.3 mm then to 0.1 mm to increase the accuracy and to check for convergence of the model.

The left side of the sample was fixed in all directions at 20 mm from the end of the sample. This was to simulate the jaws of the electromechanical tester gripping the sample. Likewise, the right side was deformed 20 mm from the end of the sample. The model with boundary conditions is shown in Figure 3-1. All the samples were deformed to a set displacement.

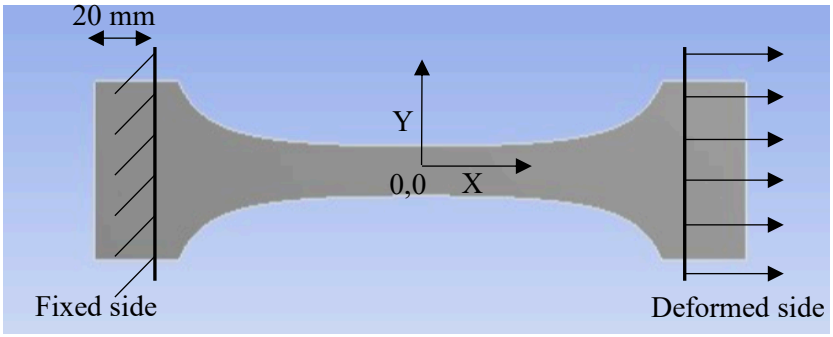

Figure 3-1 A gradient sample with the boundary conditions used in FEA. The left side of the sample was fixed in all dimensions at a distance of 20 mm from the end of the sample to simulate the jaws of the electro mechanical tester, and likewise on the right the sample was deformed at a distance of 20 mm from the end of the sample.

The mechanical properties of the brass were manually entered as the default data for brass was only up to the isotropic elastic limit, and this calculation went well into the plastic regime. Therefore, a custom strain profile was loaded which went up to 50 % strain as shown in Figure 3-2.

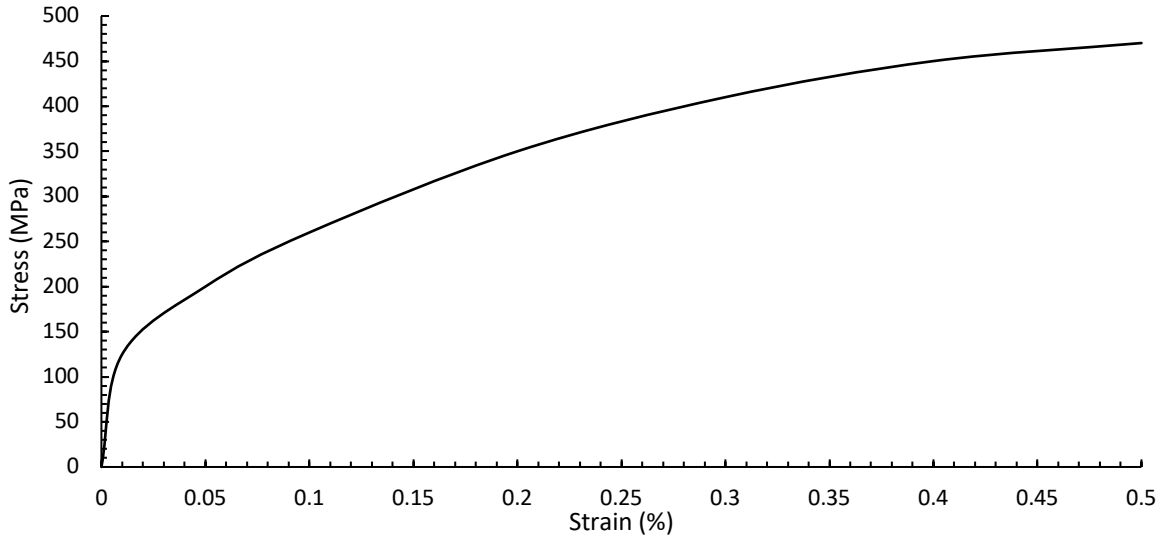

Figure 3-2 Engineering Stress-Strain plot used in ANYSIS. This data was obtained from a dog bone sample stamped from a unrelated sheet of 70/30 brass during preliminary work on DIC speckle optimisation.

The custom profile stopped at 50 % as this was getting close to when the sample would begin necking and it was past the intended strain limit in the design.

Four tensile sample designs were looked into: one which had straight sections, another with large radius curves, the third had a parabolic arc, and finally sine driven curves.

3.2.2 Straight Sections

A sample with straight sections joined with large radii to reduce stress concentrations was the first sample design as it had a relatively linearly changing cross section. Figure 3-3 shows the large distribution of equivalent plastic strain in both the X and Y directions. This model was not refined further.

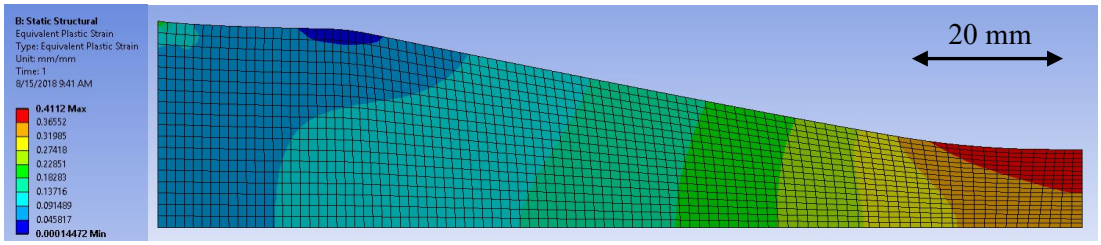

Figure 3-3 Equivalent plastic strain of the straight sample

3.2.3 Large Radius curve

The second design was a large single radius. This sample also had a constantly changing cross section however as shown in Figure 3-4 the strain profiles were still largely changing in the both the X and Y directions. This model was also not refined further.

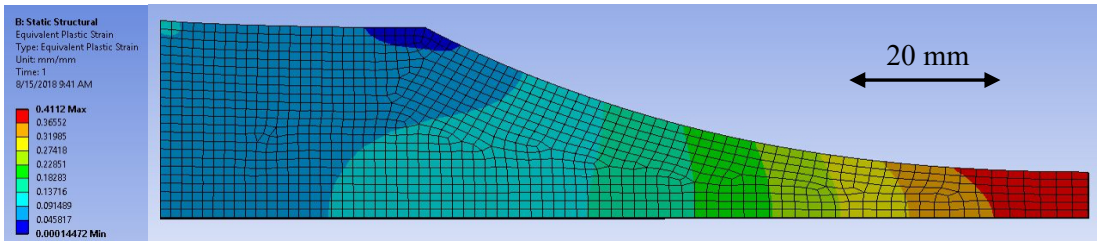

Figure 3-4 Equivalent plastic strain of the large radius sample

3.2.4 Parabolic Arc curves

The third sample design was a single large parabolic arc. This design had a better stress profile than the two previous models but still had significant changes in the strain profile in the Y direction as shown in Figure 3-5. This model was also not refined further.

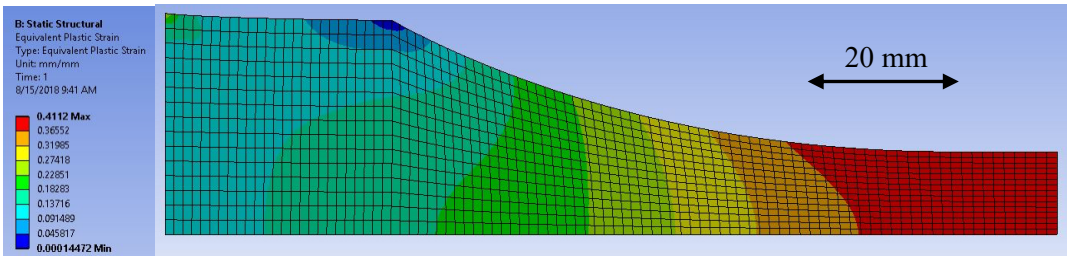

Figure 3-5 Equivalent plastic strain of the parabolic arc sample

3.2.5 SINE CURVE

The last design was using a sine driven curve. This produced the least distribution of strain in the Y-direction as shown in the full sample in Figure 3-6. This model was further refined to produce even less variation in the Y-direction strain profile.

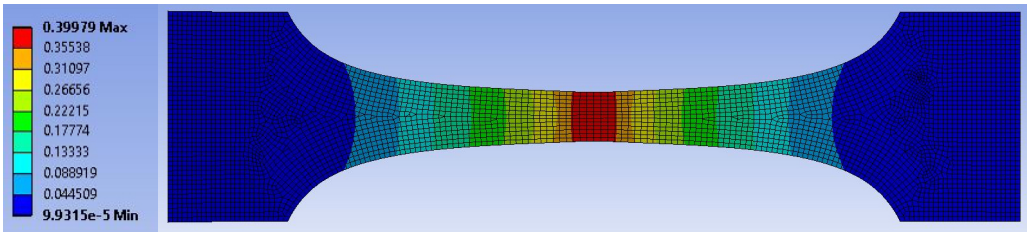

Figure 3-6 Equivalent plastic strain of the sine driven curve sample

The sample in Figure 3-6 has a profile of $Y_{max}(X) = \frac{5}{\sin(\frac{\pi X}{130})}$ with a minimum gauge width of 12.5 mm and length of 130 mm before deformation. The amount of deflection was varied to understand the change in peak strain. A deflection of 25 mm resulted in a peak equivalent plastic strain of ~ 40 %. The mesh was refined to check for convergence of the models, as shown in Figure 3-7.

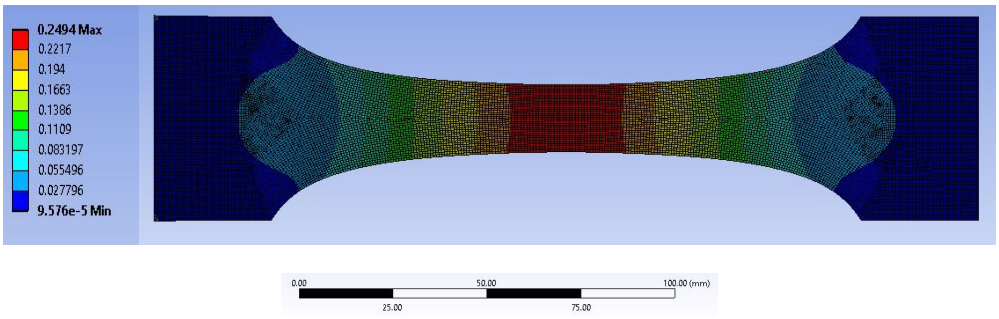

Figure 3-7 Equivalent plastic strain with a very fine mesh and a deflection of 15 mm lowered the peak strain to ~ 25 %.

3.3 SAMPLE MANUFACTURE

3.3.1 MACHINING

The gradient sample shape was converted to a DXF file format then G-Code was generated using a G-Code generator. Twenty samples were milled using a 16 mm carbide end mill from blanks of brass that had been roughed out on a band saw. The CNC milling machine used two roughing passes and two finishing passes. The sides of the samples were then hand sanded with 600 grit SiC paper to remove any tooling marks and sharp edges. The front face of the sample then had masking tape applied to protect the surface and prevent any scratches.

Three homogeneous grain growth samples were also cut from the plate at the same time but had a standard dog bone shape with a straight 12.5 mm gauge. These were the same overall length as the gradient samples. After deformation the homogenous samples were cut into two pieces.

3.3.2 INITIAL HEAT TREATMENT

The samples all required a recrystallisation heat treatment prior to deformation. This was because the brass sheet was in the ¼ hard condition, which means that after the final rolling steps during

manufacture there was no final heat treatment. This leaves the brass with a large amount of stored cold work. It also served to increase the starting grain size a small amount.

All of the samples were suspended between two metal rods with a gap of 5 mm. This was to increase the air circulation in the furnace and to provide a more consistent heat treatment. The initial heat treatment was at 600 °C for one hour, then the samples were left to cool down with the furnace turned off and the door propped open.

3.4 Digital Image Correlation

The samples were recorded during deformation to compare the ANSYS model to the actual strain results. DIC is a post deformation measurement technique used to optically measure strain. DIC works by tracking points on a samples surface. During deformation the change of one particle's position relative to the surrounding particles is used to calculate strain. DIC requires special sample preparation and consistent images during deformation to work effectively [75].

3.4.1 Sand Blasting and Paint Application

The front faces of the samples were re-polished with 1200 grit SiC paper to remove the oxide layer formed during the initial heat treatment, then masking tape was re-applied to protect the surface and prevent any scratches. The back sides of all the samples were dry sandblasted with fine quartz granite. The samples were held about 300 mm from the nozzle so that the granite would only matt the surface and not remove too much material, as recommended by Correlated Solutions [79]. Then the speckles of matt black paint were applied using a can of modified acrylic flat black from Rust-Oleum by Painter's Touch. The paint was applied in full sun at 90 ° to the sample, a slight wind drifted a light coating of "overspray" onto the sample, shown in Figure 3-8.

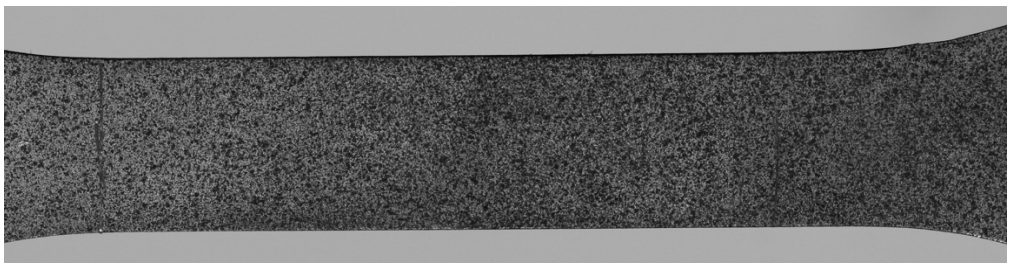

Figure 3-8 Ideal speckle pattern with good contrast, good speckle size variation and without any repetitive pattern

The idea was to drift small particles of paint onto the sample. Any large droplets of paint would not be carried by the wind and therefore would miss the sample. Another reason for letting the wind carry the droplets was to allow the paint to form a skin (where the paint droplets form a dryer surface) mid-air. This reduced the wet out or spreading of the liquid once the paint was on the sample. The samples were then left to dry for 24 hours.

The process of paint application is very sensitive to variation in speckle size and quantity. Figure 3-9 shows different sized hand drawn speckle and a gradient of spray-painted samples. Sample 6 represents the best preforming method.

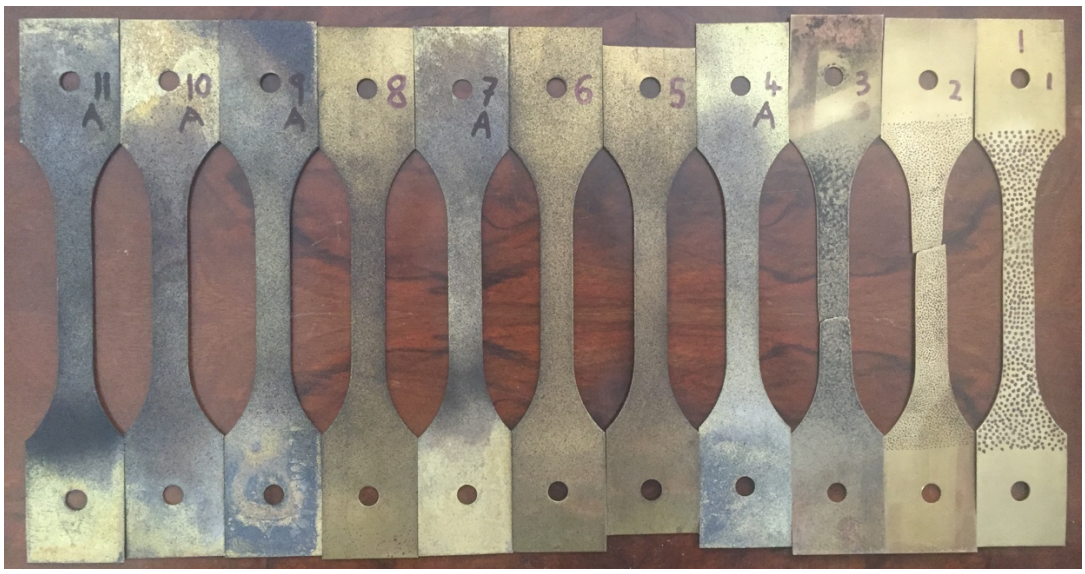

Figure 3-9 Differences in speckle patterns between hand-drawn dots samples 1, 2 and sprayed 3 through to 11. Sample 3 was sand blasted after painting. The sprayed samples have a gradient of speckle from light, sample 4, through to dark, sample 11. The A stands for annealed after sandblasting. The ideal amount of speckle is around sample 6.

3.4.2 Image Quality, Number and Setup

A custom built 100 W LED flood light was used for illuminating the samples so that a faster shutter speed could be used which reduced blurring of the image. A flat white backing was placed behind the samples in the tensiometer to reduce background light noise. During the deformation process roughly 400 images per sample were taken using a Canon EOS 30D Digital Single Lens Reflex (DSLR) with a fixed 100 mm lens. The focus was set at 2.2 m, aperture was 9, and shutter speed was 1/500 s. The settings were left in manual mode to prevent them automatically changing during the recording. The image resolution was 2336 pixels × 3504 pixels and was taken in RGB.

3.4.3 GOM Correlate

A free 2D version of GOM correlate (v2.01) was used to analyse the images [82]. However, some processing was done using the Professional 3D version. The images were imported, and GOM converts the image sequence into black and white. A region of interest was placed around the sample (done purely to reduce computational time). There are only two variables that can be adjusted, the "Speckle Size" and "Separation Distance". GOM has a speckle quality function that checked how well the image sequence is able to be correlated. Therefore, the two variables could be adjusted and optimised for each sample. Once the calculations were complete the deformation was converted into von Mises equivalent plastic strain. Then line profiles could be used to extract strain from different locations on the sample.

3.5 Deformation

An MTS 810 electromechanical tester was used to deform all the samples at 5 mm/minute.

The samples were held with knurled jaws with pressure set at 3000 psi, the bottom jaw was closed first, then the tester was set to zero force before the top jaw was closed. This prevents the jaws from applying any deformation to the samples during closure. The jaws were axially aligned to prevent twisting and distortion of the sample. The gradient samples were deformed to 25 mm, then the cross

head was allowed to return to a zero-force condition over a period of 10 seconds. This was so that the elastic strain portion of the deformation could be optically recorded.

At this stage the gradient samples were identified with numbers from 1-20, this was engraved on the sand blasted backside.

The homogeneous grain growth samples were deformed using the same set up as for the gradient samples. However, the samples were deformed to 40 % strain. This was done using a strain gauge mounted on the back side of the gauge section. The strain gauge stopped the crosshead once 40 % engineering strain was recorded. Again, the sample was allowed to come back to a zero-force position to allow the elastic strain to be recorded. After deformation the homogenous samples were cut in half and the grip section was removed. They were then engraved on the back face with letters from A-F.

3.6 Heat Treatments

Heat treatments were performed in a Nabertherm N20/HR box furnace with a PID C-16 controller.

The furnace temperature was stabilised for at least 30 minutes prior to any heat treatments.

The heat treatment samples were laid flat on a piece of open mesh stainless steel that was suspended in the centre of the furnace. This was to prevent any differential heating effects of laying the brass directly on the furnace floor or anything that had a high thermal mass.

The order which the samples were placed into the furnace was always the same (sample 1a first, then 1b etc) and was the same order when the samples were removed. This was to ensure that all the samples had an equal amount of time in the furnace.

Once the samples had spent the desired amount of time in the furnace they were quickly removed by grabbing the grip section of the sample (where the electro mechanical tester gripped) with tongs, and plunged into a 10 L bucket of fresh water at room temperature and left to cool.

The average time to place four samples into the furnace was around 8 s. The time to remove the same four samples and plunge them into water was around 10 s.

3.6.1 Grain Growth Heat Treatments

The heat treatments for the first grain growth samples started with an initial heat treatment of 500 °C for 12 min. This was based on preliminary work. The times for each heat treatment are recorded in Table 3-2.

Table 3-2 Heat treatment times at 500°C for samples 1a-2b.

	Time (minutes)	
Heat treatment number	*1a and 1b*	*2a and 2b*
0	*12*	*12*
1	*17*	*22*
2	*22*	*32*
3	*27*	*42*
4	*32*	*52*
5	*37*	*62*
6	*47*	*82*
7	*57*	*102*
8	*67*	*122*
9	*77*	*162*
10	*87*	*182*
11	*97*	*222*
12	*107*	*282*
13	*127*	
14	*147*	
15	*167*	
16	*207*	
17	*247*	
18	*287*	
19	*347*	

3.6.2 Recrystallisation Heat Treatments

The recrystallisation samples did not have an initial 12-minute heat treatment, and the first heat treatments were at very short times so that recrystallisation could be measured in the high strain portions of the sample. The heat treatment times are shown in Table 3-3.

Table 3-3 Heat treatment times and temperatures for the recrystallisation samples

	Sample Designation and Temperature				
	5a-b 500°C	*6a-b 550 °C*	*7a-b 600 °C*	*8a-b 650°C*	*9a-b 700 °C*
Time (Minutes)	*2*	*2*	*2*	*2*	*2*
	6	*6*	*6*	*4*	*3*
	10	*10*	*10*	*6*	*5*
	14	*14*	*14*	*8*	*7*
	22	*22*	*22*	*12*	*11*
	30	*30*	*30*	*16*	*15*
	40	*40*	*40*	*21*	*20*
	50	*50*	*50*	*26*	*25*
	60	*60*	*60*	*31*	*30*
	80	*80*	*80*	*40*	*35*
	100	*100*	*100*	*50*	*45*

3.6.3 Homogenous (control sample) Heat Treatments

The homogenous samples were heat treated at the same time as the recrystalising samples but for varying times as shown in Table 3-4.

Table 3-4 Heat treatment times and temperatures for the homogenous control samples

	Sample Designation and Temperature				
	A *500 °C*	*B* *550 °C*	*C* *600 °C*	*D* *650 °C*	*E* *700 °C*
Time (Minutes)	*1*	*1*	*1*	*1*	*0.5*
	3	*2.5*	*2.5*	*2.5*	*1.5*
	5	*5*	*5.5*	*5*	*2.5*
	8	*8*	*8*	*8*	*5*
	15	*15*	*15*	*15*	*10*

3.6.4 Temperature Measurements

The temperature of a gradient sample was recorded to measure the time taken to heat up to the furnace temperature. This was repeated for every temperature used in this research. The equipment used to log the temperature was a digital National Instruments data recorder and a 2.5 mm probe K-type thermocouple. The thermocouple was imbedded in the centre of the sample, which was at the 60 mm bin location, which is where the sample had the largest thermal mass. This was done by drilling a 2.5 mm hole and peening the brass to get the best thermal contact between the brass and the probe. The sample was quickly placed in the furnace in the same way as the rest of the heat treatment samples and left until the temperature of the sample had stabilised. For the 500 °C, 600 °C, and 700 °C temperatures the sample was pulled out of the furnace and plunged into water while the temperature was still being recorded to measure the cooling rate.

3.7 Sample Preparation for Microscopy

The process of grinding and polishing the samples for microscopy is explained so that the grain size could be measured. This involved mechanically grinding and polishing the samples before an electro polish was used. Two independent methods were used to reveal the grain boundaries, initially electro etching and then an acid etch.

3.7.1 Mechanical Polishing

All the grinding and polishing was done using a 8 inch Buehler Vector semi-automatic grinder-polisher with an LC 250 power head.

The first grinding stage was to flatten the samples, as during deformation the samples had become much thinner in the gauge/narrow section. A purpose-built jig was used to attach the samples to the polisher with double sided tape. This decreased the time required to grind the samples as it allowed three whole samples to be flattened at once. The first stage of flattening was done using Buehler CarbiMet 180 grit SiC paper that was liberally cooled/lubricated with running water to prevent the samples heating up. The first grinding stage required many pad changes as there was a substantial amount of material to be remove. Once the samples were flat the SiC paper was changed out for 240 then 320, 400, 600, 1200, and finally 2500 grit SiC paper. After each grinding step change in paper the samples were thoroughly washed to remove all contamination/loose material and then inspected to make sure that the grinding marks from the previous step were completely removed. The speeds were decreased at each step change from around 350 rpm with the course papers down to 120 rpm with the

finer papers. The force was also decreased from 100 N down to 50 N. The samples were not put back onto the power head once removed; therefore, the powerhead was only used for the first polish and was not used again.

Before all polishing steps the samples were washed in the ultrasonic cleaner with dish washing detergent and thoroughly rinsed in fresh water then ethanol, then dried using forced hot air from a hairdryer. Washing the samples between each step prevented contamination of the polishing cloths and increased the quality of the final polish.

The first three steps in polishing were using Buehler TexMet pads that was initially charged with Hyprez Five Star abrasive paste; however, the polishing compound was changed to Buehler MetaDi Supreme diamond suspension once the pad was worn in significantly and had a build-up of compound. The size of the polishing compound was decreased from 9 μm, down to 3 μm, and finally 1 μm. Each grade polishing compound had a different TexMet pad.

The final polishing step was using a long nape Buehler MicroCloth pad and 1 μm Buehler MetaDi Supreme diamond suspension. Care was taken with this step to polish for the shortest amount of time to avoid the long nape pad rounding the edges of the sample and causing topological effects due to differential hardness in the sample.

After the initial grinding and polishing, the samples were generally only re-polished with the 3 μm, and 1 μm steps, depending on how much oxidation had formed on the sample surface, after heat treatments.

3.7.2 Electro Polishing

After the mechanical polishing steps the samples were electropolished in a purpose built electro polishing bath using a Power Tech MP3090 40 A power supply, a deep sided 5 L plastic container, a 316 stainless plate anode the same size as the bath, and stainless forceps to hold the samples. The electrolyte solution was based on published recommendations by George F. Vander Voort [60] and the ratios are

- 1 part ethanol 99.9 %
- 1 part 85 % phosphoric acid
- 2 parts deionised water

The batch volume mixed was 4 L, as that was enough to have a 70 mm gap between the bottom of the sample and the base anode.

The current was closely controlled as to avoid electro pitting the samples. Generally the current was between ~ 8 – 9 A which equated to ~ 10 V with new electrolyte, but was slightly decreased as the electrolyte was consumed down to around 7 A and 7 V before replacing the solution. The samples were placed with the narrow section of the sample just under the surface of the electrolyte while the wide part (the grip end) of the sample was only10 - 15 mm from the anode. This placed the sample at about a 30 - 40 ° angle. This was done to even out the current density down the length of the sample, preventing the narrow section of the sample from entering the pitting regime.

The current and voltage was recorded for a new solution of electrolyte with the above technique in an attempt to determine the correct current to use for polishing and etching these samples, shown in Figure 3-10. However, this was unsuccessful because the plot has a linear relationship and did not

display the typical nonlinear trend. There is a slight deviation at 4.5 - 5 A which was much lower than current used to polish. The difficulty was suspected to have been because the surface area of the sample was nonuniform and thus the current density down the sample was also constantly changing.

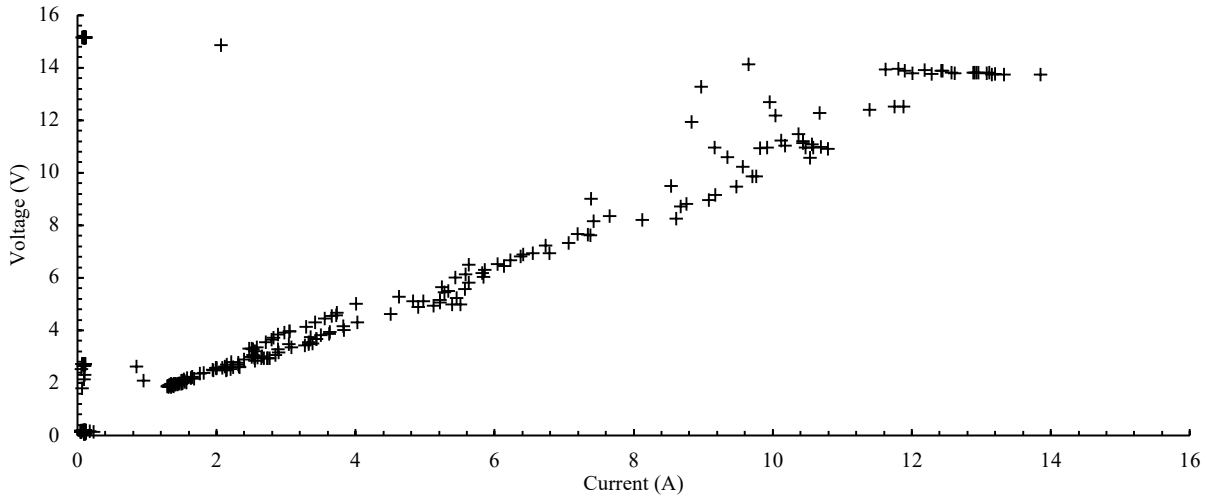

Figure 3-10 Current voltage plot during electro polishing and electro etching.

Once the sample was in the electrolyte the sample was aggressively agitated in a large circular pattern before the power supply was turned on. This was to reduce the hydrogen bubbles collecting on the samples.

The sample was constantly agitated while polishing and was polished for between 20-45 seconds or until a satisfactory polish was obtained.

Many problems were encountered during electropolishing.

- The strength of the acid was increased from 65 % up to 85 % to increase the acid concentration and reduce the electro affects which decreased pitting as shown in Figure 3-11D.
- Constantly having to adjust the current as the solution wore out.
- Altering the agitation speed of the sample to avoid the hydrogen bubbles affecting the quality and to keep the electrolyte on the surface of the sample from becoming stale as shown in Figure 3-11C.
- Tilting the sample in an attempt to keep the current density down the length of the sample consistent, and to reduce the fringing affects due to the high rates of curvature on the edges. If the sample came close to the anode, then the risk of electro affects increased as shown in Figure 3-11B.
- If the sample was agitated too slowly, then pits would form around the edge of the hydrogen bubbles that sat on the surface of the brass as shown in Figure 3-11C.

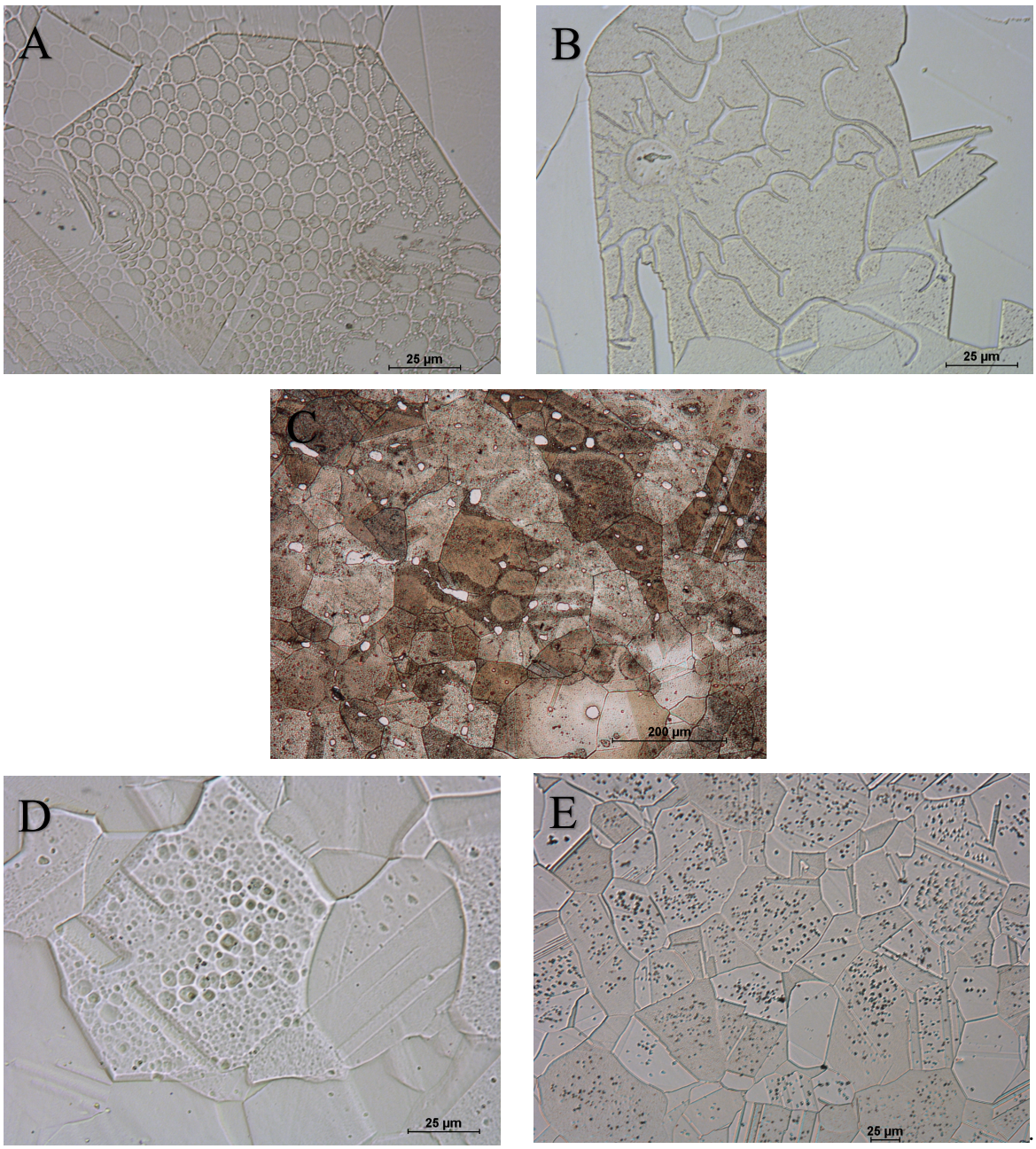

Figure 3-11 Failed electro etched samples. A) spiders web caused by electrolyte contamination. B) Electro tracks inside grains, caused by the sample becoming close to the anode and electricity tracking on the surface of the sample. C) Hydrogen bubbles formed on the surface causing differential polishing, this section was also over electropolished. D) Micro electro pitting caused by a high current density, note that one grain is heavily pitted while the neighbouring grains are unaffected. E) Electro pitting also caused by a high current density.

3.7.3 Etching

The samples were then etched to reveal the grain boundaries. Two methods were used, originally electro etching, which was replaced by an acid etch due to the inconsistent and difficulty of using electro etching.

3.7.3.1 Electro Etching.

Etching was done using the same equipment and electrolyte but by reducing the current and reducing the agitation speed. This caused the sample to enter the electro etching regime by reducing the current density on the sample surface.

The samples were again placed in the electrolyte at an angle and agitated at a much slower speed which just fast enough to prevent bubbles sticking on the surface of the sample. Then the power supply was connected. The time to etch would vary from 20 to 40 seconds depending on the electrolyte concentration. The final etch is shown in Figure 3-12B). The current to etch would also vary between ~ 1.8-3.5 A which was around ~ 3.5-5 V. The time to etch the samples increased as the electrolyte was consumed.

However, this method was fraught with issues. The main issue again was getting the whole sample into the correct regime. The edges and the thinner portions of the gauge section would stay in the polishing regime due to the higher rates of curvature or the reduced area and would fail to etch or would be pitted from the previous electro polishing step. This would require the sample to be mechanically re-polished starting again at the 3 μm polish, if the pitting was severe then the sample may require grinding starting at the 600 grit SiC paper.

There were many issues with the electro etching similar to those of the electro polishing steps.

- It was very hard to keep the whole sample in the etching regime and avoid the polishing regime around the edges and in the narrow section of the sample. Often the sample would be over etched in one section and under etched in another.
- Determining the correct amount of time to etch was difficult.
- If the sample was agitated to slow the small hydrogen bubbles would cause a small circular shape. If agitated too fast, then the bubbles would cause streaks across the surface.

3.7.3.2 Acid Etch

After an intensive amount of trial and error testing of recommended acid etches [28][60][83][84], a solution of acid was made up according to George F. Vander Voort [60]. Most of the etches tested produced colour changes depending on grain orientation shown in Figure 3-12C. The colour changes made the automated process of detecting grain boundaries much more difficult. The final etching solution was made up of

- 10 grams $Fe(NO_3)_3$
- 50 ml of HCl (32%)
- 50 ml Ethanol and
- 100 ml Deionised Water

The cleaned and dried sample was immersed completely and quickly into the solution and agitated very slightly to prevent bubbles forming on the etched surface. The sample was only immersed for around 7-10 seconds. The results are shown in Figure 3-12A. If the sample was left in the solution for too long, the grain boundaries would become wide and resolution was poor, the sample then required a re-polish, most often starting at 3 μm. If the sample was not etched long enough, the grain boundaries were too faint, and detection was a problem. The sample was then re-immersed in the etch for a longer period to deepen and darken the grain boundaries.

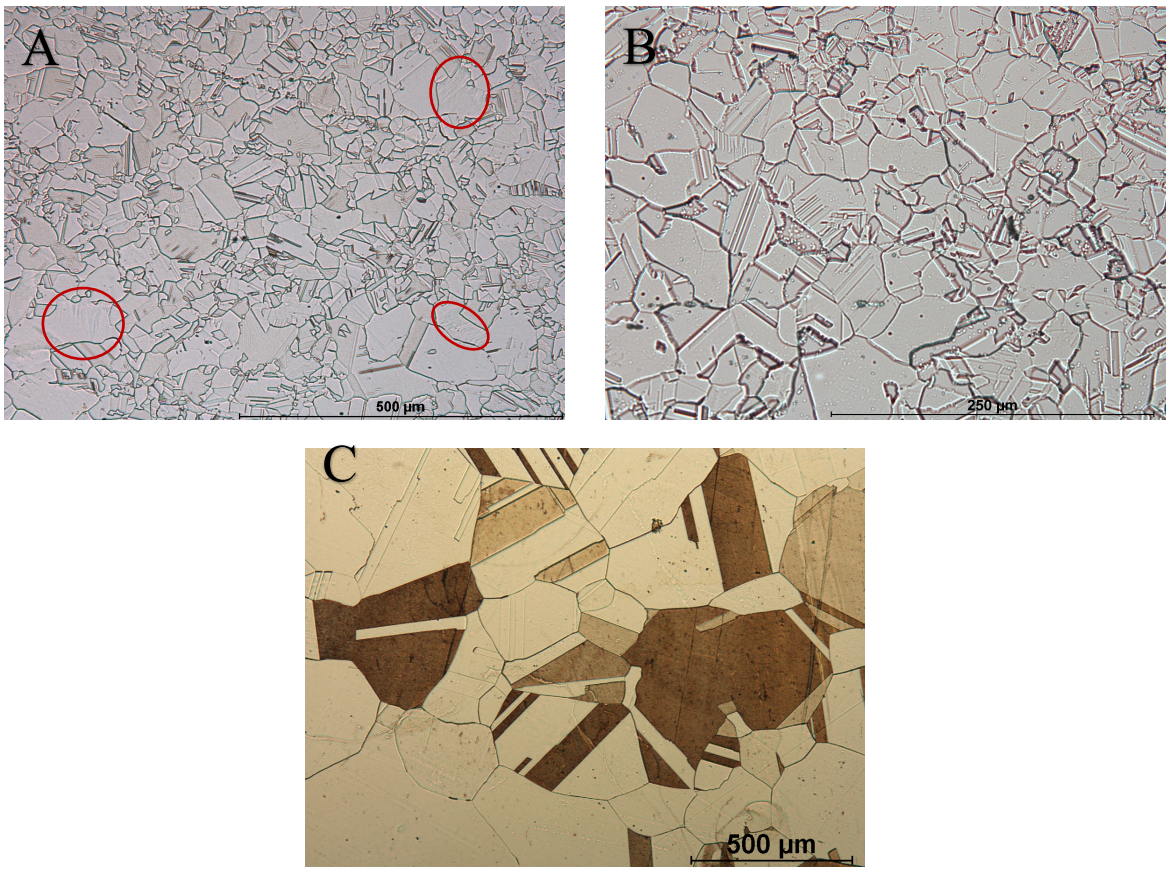

Figure 3-12 Different etches A) Iron nitrate acid etch, there are still un-recrystallised grains in this micrograph identified with red circles, the grains have slip lines on the surface. B) Electro etch, note the much wider grain boundaries than the iron nitrate acid etch, taken at 200x. C) Acid ferric chloride etch. Note the large colour contrast between the grains which is dependent on the grain orientation.

3.8 IMAGING

After the samples were ground, but before being polished, the samples were cut in half with a slow speed 0.5 mm diamond saw made by Buehler IsoMet rotating at 200 rpm.

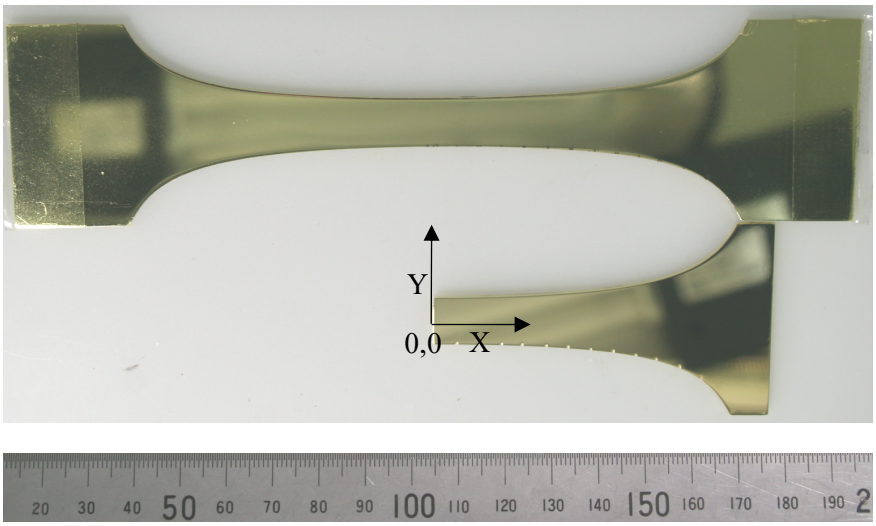

Figure 3-13 Gradient sample after polishing showing one replicate which was cut from the gradient sample after polishing.

Each half of the sample was a replicate as they should have identical properties. The replicates were then engraved with the original sample number plus either an A or B on the back side where the electromechanical tester griped the sample. Both replicates were then marked along one edge using the same 0.5 mm diamond saw and the micrometre slide adjuster to precisely move the sample. The first mark was at 2.5 mm from the centre, then 5 mm, and every 5 mm after that up to 60 mm. These fiducial marks were used to locate analysis regions shown in Figure 3-14. The reason for the first bin being at 2.5 mm was due to the initial difficulty in electro-etching the small end of the samples.

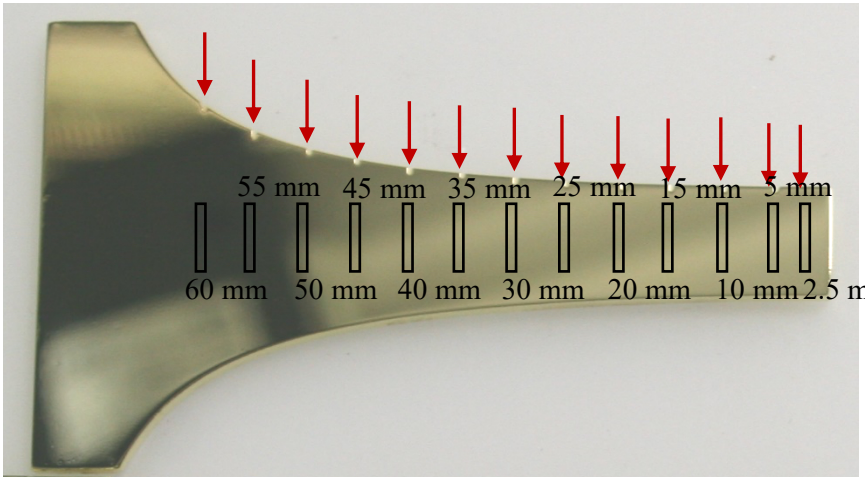

Figure 3-14 A replicate sample showing the markings on the top edge indicated with red arrows and the associated analysis bin locations.

A minimum of ten overlapping images were captured in a vertical line at each bin location using a Leica DMIRM inverted microscope fitted with a Nikon camera. The images were 1280 x 960 pixels and were saved as JPEG image files. No optical filters were used. Magnifications of 100x and 200x were used depending on the size of the grains at the bin location. The images were captured using Nikon software with an auto whiting feature that emphasise the grain boundaries and flattened the image colour.

A total of over 25,000 images were taken in this work. Not all of these images were analysed at the time of thesis submission.

The homogeneous samples also had a minimum of 10 images taken. A rectangular region was imaged which was 5 images tall by 2 images wide. The purpose of this was to reduce the chances that a single large grain would be on the edge of the micrograph and be removed from the statistics.

3.9 Optical Methods of Measuring Grain Boundaries.

The grain boundary images captured were analysed using Media Cybernetics ImagePro 10 which had an add on called the Grain app [85]. The individual images from the bins were manually stitched back together into a single long image as shown in Figure 3-15.

Figure 3-15 Ten images stitched together using ImagePro. This is the 20 mm bin on sample 5a after 60 minutes at 500 °C

The Grain app was used to automatically detect the grain boundaries. The ROI (region of interest) was set to NONE as the whole image was analysed. The edge type was set to STEP. The CLEAN ALL BORDERS was checked so that any grain that touched the edge of the image were excluded. The only settings changed was the calibration, which depended on the magnification of the images. The EDGE WIDTH and SENSITIVITY were adjusted, which was to correctly threshold the image without under detecting or over detecting the grain boundaries. These two settings were recorded along with the ASTM grain size and the average grain area. ImagePro shows grain boundaries as a blue line as shown in Figure 3-16.

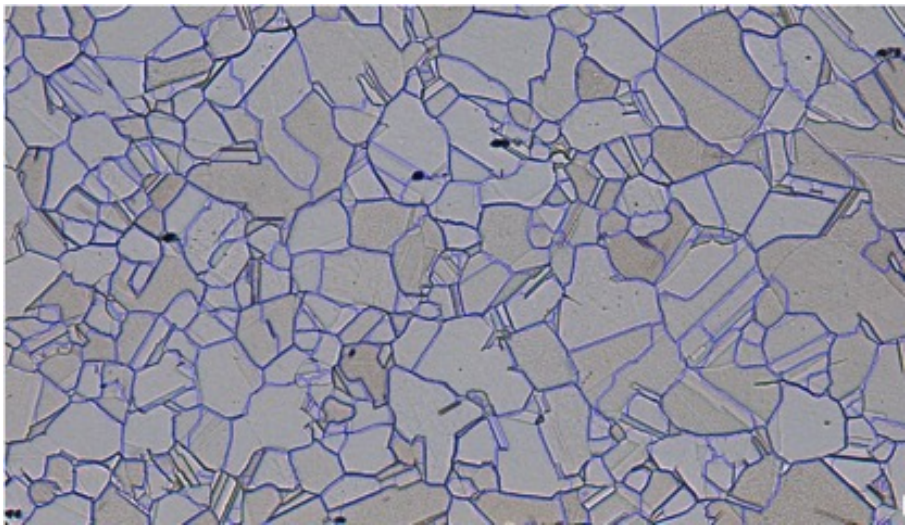

Figure 3-16 Optical image of a gradient sample showing the grain boundaries after being detected using ImagePro 10

Originally ImageJ with the MorphoLibJ add on was used to identify grain boundaries; however, the processing was not as sophisticated as that in ImagePro and it would often over detect or under-detect the grain boundaries. ImageJ was also much slower and much more user intensive.

3.9.1 IMAGE CALIBRATION

The microscope needed to be calibrated to ensure that the optical measurements were accurate. To confirm, a precision stage Nikon micrometre slide was used to capture calibration images at all the magnifications used in this research, namely 50, 100, 200, and 500×, as shown in Figure 3-17. The images were used to set the calibrations in ImagePro.

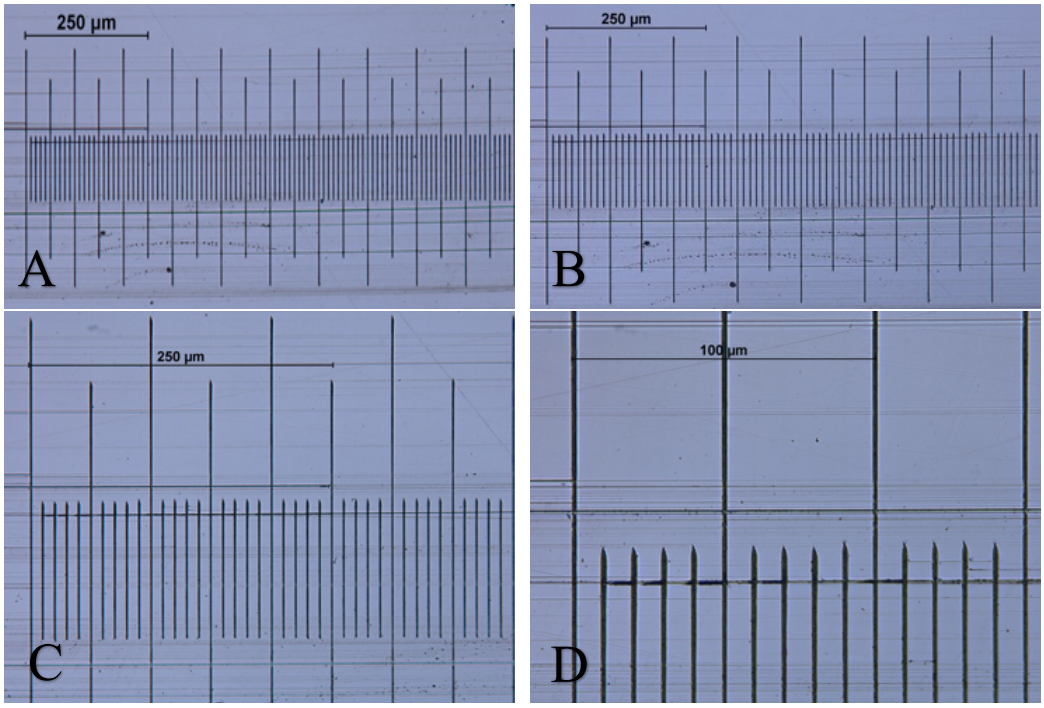

Figure 3-17 Precision microscope slide used to calibrate the scale bar on the microscope and ImagePro. The microscopes scale bar was added to all the images. A) Taken at 50 ×. B) Taken at 100 ×. C) Taken at 200 ×. D) Taken at 500 ×

3.10 Hardness testing.

Hardness testing was preformed using a LECO M400 with a Vickers indenter and a load of 1 kg. The largest dimension of an indent was ~ 180 µm measured on a diagonal. Indents were spaced at least 1 mm away from any other indents and at least 2 mm from an edge, the sample thicknesses were all well over 20x the depth of the indent as per ASTM E92 [86]. A minimum of six indents were taken at each site on the samples and averaged.

Hardness indents were taken on Sample 3a, after being strained to 40 % and after a 12-minute recrystallisation heat treatment. The homogeneous samples were tested after every heat treatment.

3.11 Validation of Methods

To validate the techniques used in this research, experiments were conducted to correlate the results and compare the accuracy from known and previously validated techniques and devices to those used.

3.11.1 DIC vs Axial Measurements

The strain measurements from DIC were compared against the strain measurements taken using a MTS axial extensometer during the deformation of the homogenous samples. The stress vs strain plot from the extensometer is shown in Figure 3-18. The peak strains for the three samples are shown in Table 3-5 along with the maximum displacement of the cross head, which was measured internally in the MTS tester using a digital linear displacement sensor.

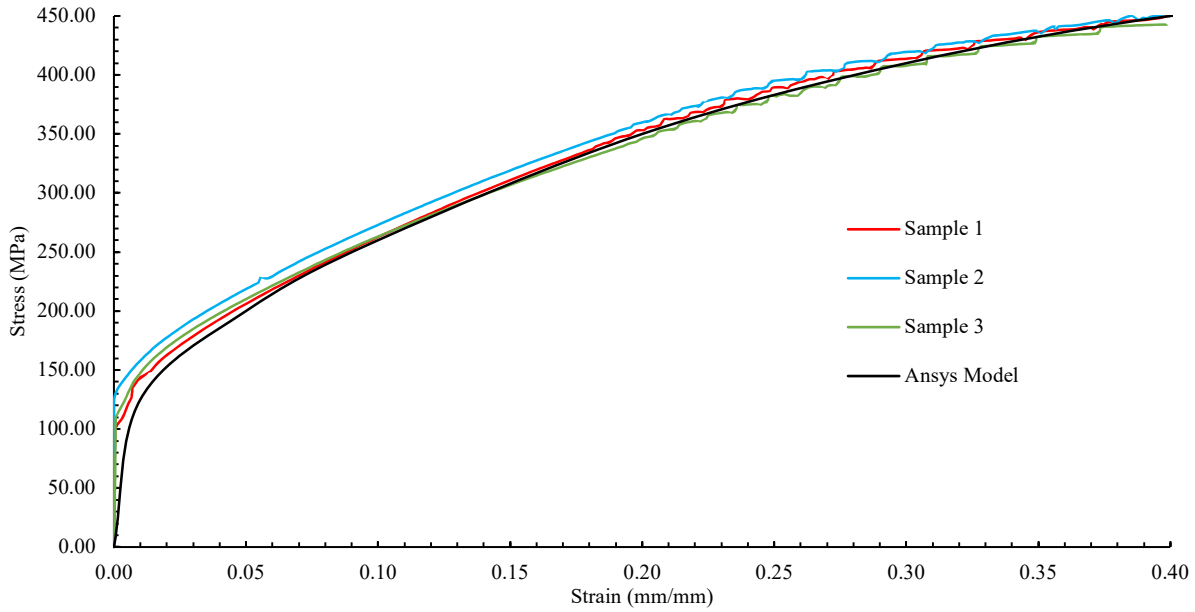

Figure 3-18 Engineering Stress vs Strain of the three homogenous samples measured using a MTS axial extensometer and linear displacement sensors. The Ansys model used to design the samples is shown for completeness.

The strain measurements from centrelines profiles drawn in GOM for the same three homogeneous samples is shown in Figure 3-19. The average readings from these profiles is recorded in Table 3-5. The maximum crosshead displacement was also measured in GOM for these samples and is also shown in Table 3-5.

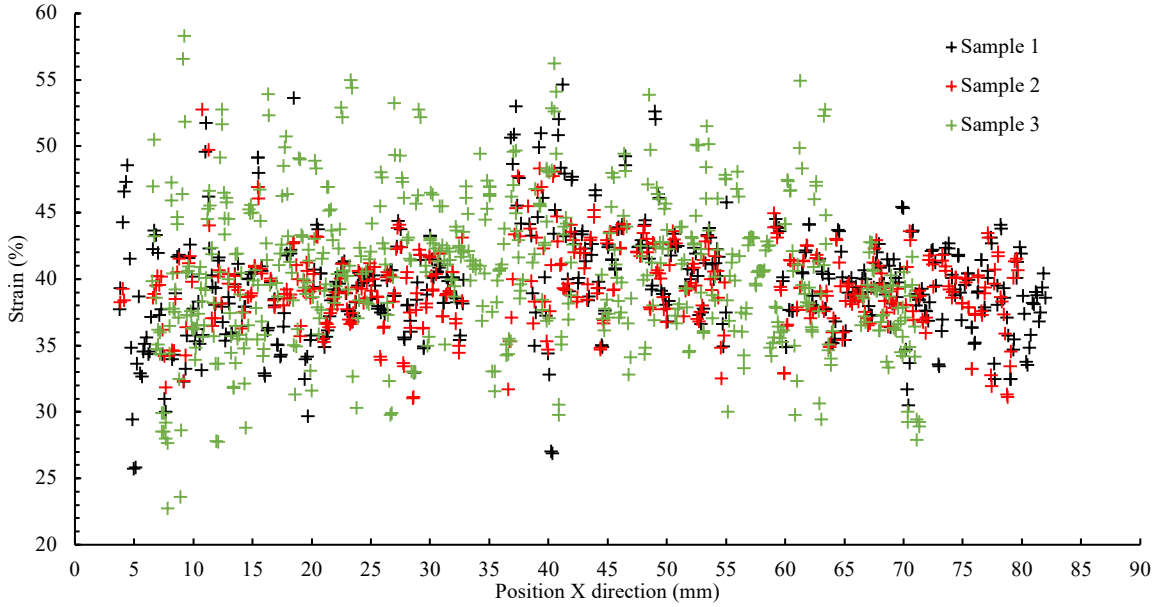

Figure 3-19 DIC Strain vs Position, for centre line profiles from three homogenious samples. Note the increased spread in Sample 3 is due to the poor speckle used in DIC. The gaps at ~ 35 mm and ~ 57 mm, on sample 1 and 2, were caused by the metal tabs used by the axial extensometers to affix to the sample covered the speckle on the front face stopping DIC from working effectivly in these locations, but supprisingly the overall length of the extension was still accurate.

Table 3-5 Comparison between Strain Gauges vs DIC when measuring strain, and linear displacement sensors vs DIC measuring maximum displacement during deformation of the homogenous samples.

Sample Number		*Strain (%)*	*Extension (mm)*
1	*Direct measurement*	*40.00*	*39.64*
	DIC	*39.71*	*39.56*
2	*Direct measurement*	*40.00*	*34.80*
	DIC	*39.45*	*35.13*
3	*Direct measurement*	*39.99*	*36.52*
	DIC	*40.06*	*36.48*

This show that DIC was able to accurately measure the strain as well as the absolute extension of the cross head with reliability for these three homogeneous samples.

3.11.2 DIC vs FEA

The predicted strain maps generated in ANSYS for the gradient samples shown in Figure 3-6 were compared to the strain maps generated from DIC, for the X direction. Horizontal centreline profile was constructed in both programs to measure the strain along the line. The result shows a close correlation between the two methods as shown in Figure 3-20. DIC does have a noisy scatter due to the numerous data points however the overall trend is similar.

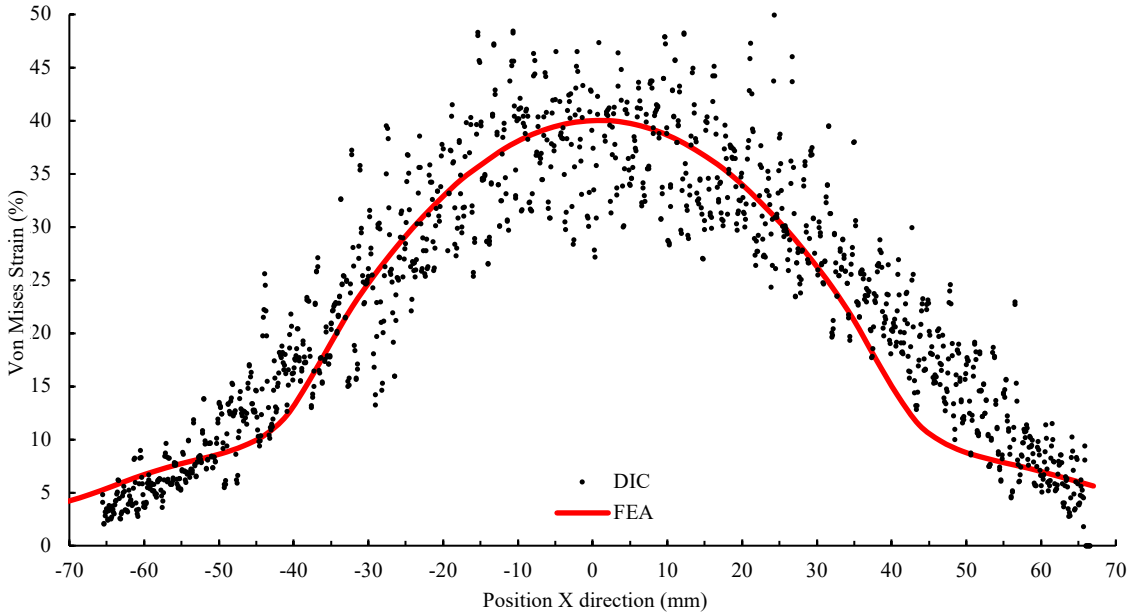

Figure 3-20 Comparison between centreline strain profiles for the gradient samples from FEA shown in red, and DIC shown in black. Note the averaged peak strain measures 40 % in DIC using a vertical profile.

3.11.3 Optical Methods for Grain Boundary Identification vs EBSD

EBSD is the obvious standard for accurately mapping grain boundaries. However, EBSD is slow and costly in microscope time. There are also limitations when using EBSD as the step size that the microscope takes determines the resolution. If the sample has very small grains, then the step size needs to be set very small to get the minimum 100 pixels (Data points) to call a grain a grain. The 100

pixels was based off Oxford instruments (manufacture of the detector) recommendations. This was the drive behind using optical methods in this project.

To verify that optical methods were accurate a large scale EBSD map was taken of a gradient sample. The SEM used was a JEOL IT300LV variable pressure scanning electron microscope with an Oxford EBSD detector. The step size was 4 μm and the total size of the image was 57 mm by 5 mm. This image took over 36 hours of beam time, as well as requiring a much higher level of polish than optical methods. The image was then processed in the Oxford software to identity the grains by eliminating any grains with less than 100 pixels according to ASTM E2627, and defining a grain boundary as an orientation change in the lattice of over 10 ° as shown in Figure 3-21.

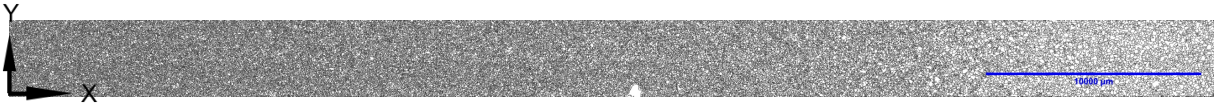

Figure 3-21 EBSD grain boundary map taken of a gradient grain sample, note the small grains on the left.

The oxford software also identified the locations of the centroids, area, and perimeter lengths of each grain. Further analysis of the information shows the distribution in grain size and perimeter length as a function of frequency as shown in Figure 3-22.

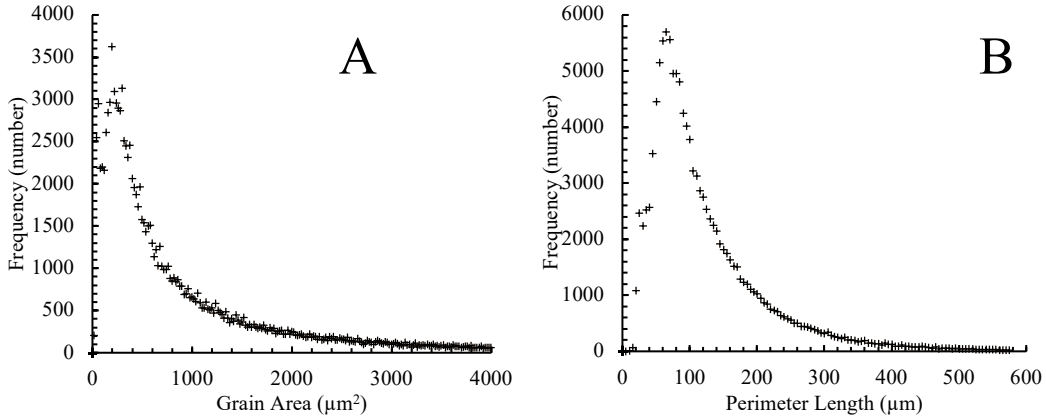

Figure 3-22 EBSD data recorded from a deformed gradient sample after a 12-minute heat treatment at 500 °C A) Grain area distribution. B) Grain perimeter distribution.

The discontinuity or kink in the above plots at a grain area of ~ 400 μm² and perimeter length of ~ 40 μm originates from the coarse step size used to generate the EBSD maps. The 4 μm step size reduced the time to image the sample, but also reduced the resolution. This affects the smaller grains disproportionally more than the larger grains.

Using the location of the centroids the individual grains were able to be put into the same bin locations as the optical images that were taken of the same sample, so that a direct comparison could be made between the two methods. The results are displayed in Figure 3-23.

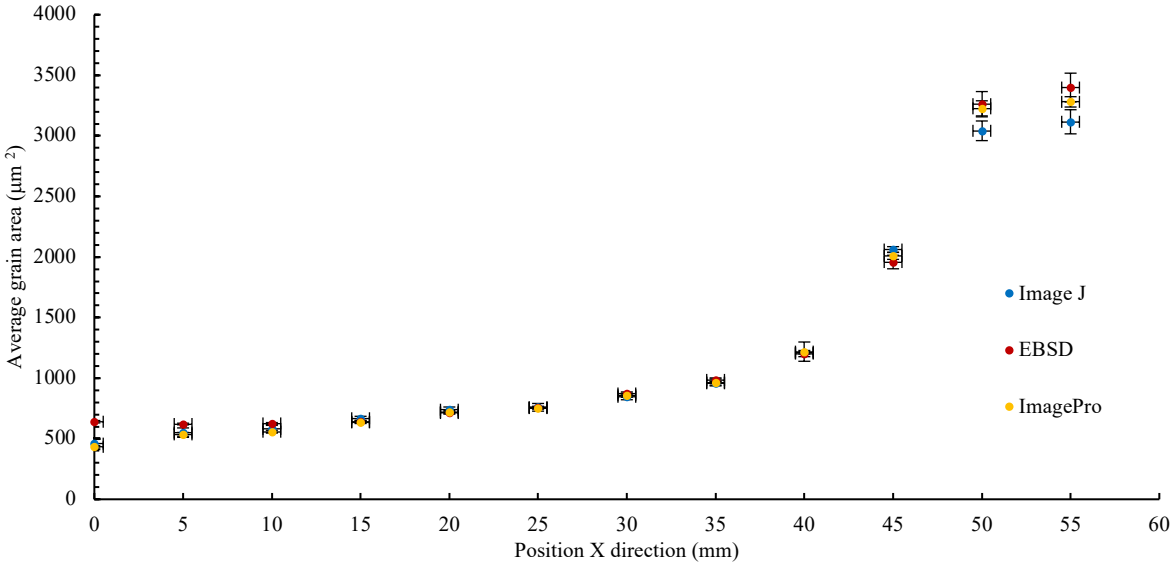

Figure 3-23 Grain area comparison between EBSD, ImagePro 10 and ImageJ. The error is the standard error of the mean.

Figure 3-23 shows that the automatic grain boundary detection in ImagePro is able to accurately record the same grain area as EBSD.

However, there is a small deviation between EBSD and the optical methods at the first three bin locations (0, 5, 10 mm). This was suspected to have originated from the step size used in the SEM being too large, and therefore missing grains under a certain size. This was confirmed by the kink or discontinuity in the plots shown in Figure 3-22.

There is also a deviation at the larger grain sizes, this is because when the grains are still deformed (i.e. before recrystallisation has happened) there are visible slip line in the micrographs which optical methods incorrectly identifies large slip lines as a grain boundary. Hence it is hard for ImagePro to distinguish between a grain boundary and a slip line. Optical methods will generally underestimate the average grain size if the sample is deformed.

4 RESULTS

INTRODUCTION

All the raw data is presented in this chapter. The chapter is broken into five sub sections,

- Strain measurements
- Average grain size vs time and temperature
- Temperature vs time of a gradient sample during heating and cooling
- Hardness of gradient and homogenous samples.
- Composition changes with time and temperature.

4.1 STRAIN

During deformation of all the gradient and homogenous samples, images were taken so that strain measurements could be extracted using DIC.

Vertical line profiles were added to a gradient sample in DIC to extract the von Mises strain in the 13 bin locations as indicated by the black vertical lines in Figure 4-1.

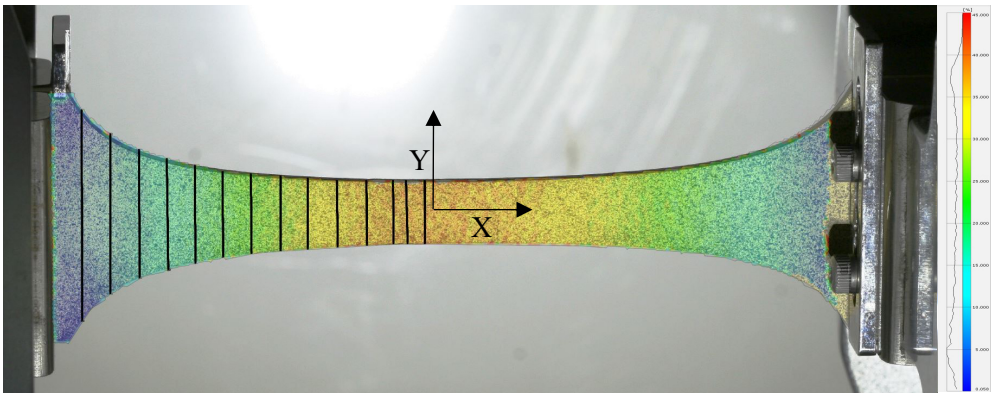

Figure 4-1 DIC image showing the lines used in GOM correlate to obtain the strain profiles plotted in Figure 4-2. The scale shown on the right is the von Mises strain, and also shows a historgram of strain in the sample.

The slightly mottled red and dark yellow colors in the centre of the sample are due to localised yielding. The von Mises strain from the line profiles are shown in Figure 4-2.

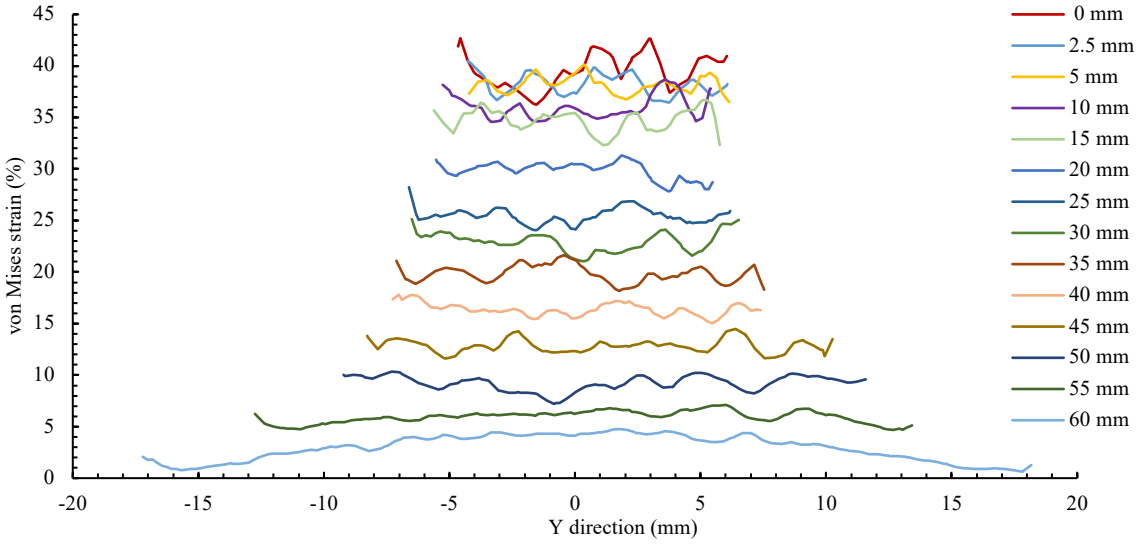

Figure 4-2 Strain measurements recorded from DIC at the bin locations.

The higher the strain the nosier the data, this is because the sample is going through local yielding and slip bands are visible in the sample this is discussed in 0 and shown in Figure 7-3.

The von Mises strain along each line profile in Figure 4-1 excluding the sporadic effects at the edges was averaged and is shown in Table 4-1 along with the standard deviation.

Table 4-1 von Mises strain and standard deviation for the 13 bins as measured by DIC

X (mm)	*Mean von Mises Strain*	*Standard deviation*
0	*39.53*	*1.75*
2.5	*38.21*	*1.08*
5	*37.54*	*0.82*
10	*36.55*	*1.13*
15	*34.92*	*1.09*
20	*30.45*	*0.88*
25	*25.70*	*0.67*
30	*22.83*	*0.95*
35	*20.00*	*0.82*
40	*16.70*	*0.49*
45	*13.31*	*0.67*
50	*8.81*	*0.74*
55	*6.96*	*0.60*
60	*2.92*	*0.60*

4.2 Grain Size vs Time

The average grain area was measured using ImagePro, from the large-scale optical images, taken for all the samples, at all bin locations, after each heat treatment according to the times recorded in Table 3-2, Table 3-3 and Table 3-4

The homogenous samples grain measurements are shown in Figure 4-3. The gradient sample grain measurements are shown in Figure 4-4 through to Figure 4-9.

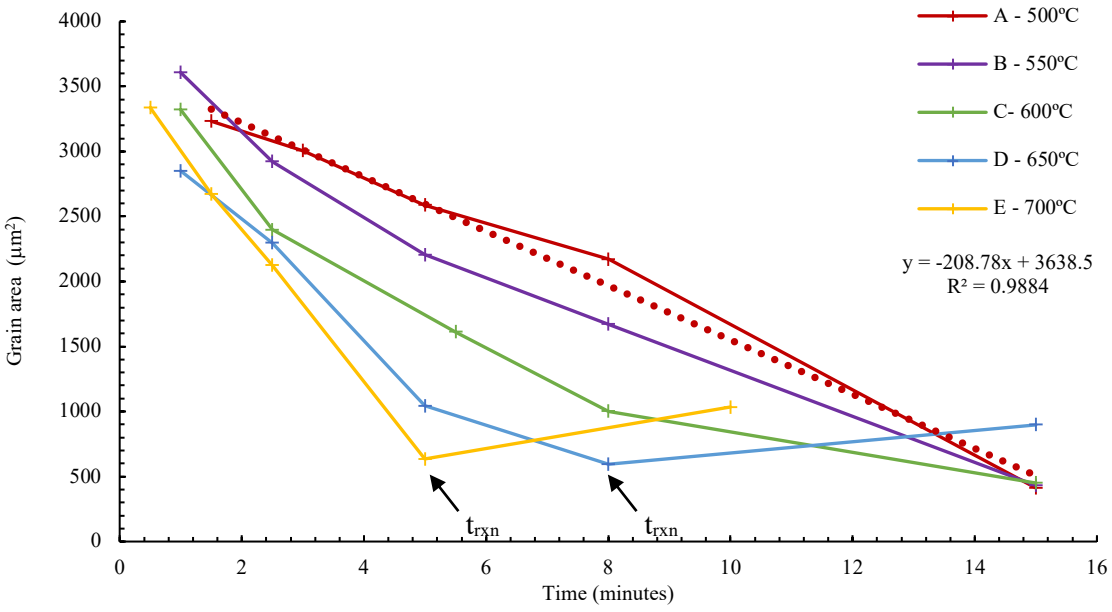

Figure 4-3 Average grain area vs time for the homogeneous samples. Samples D and E have gone through recrystallisation as indicated by t_{rxn}. Note sample A has a linear trendline shown with red dots for discussion.

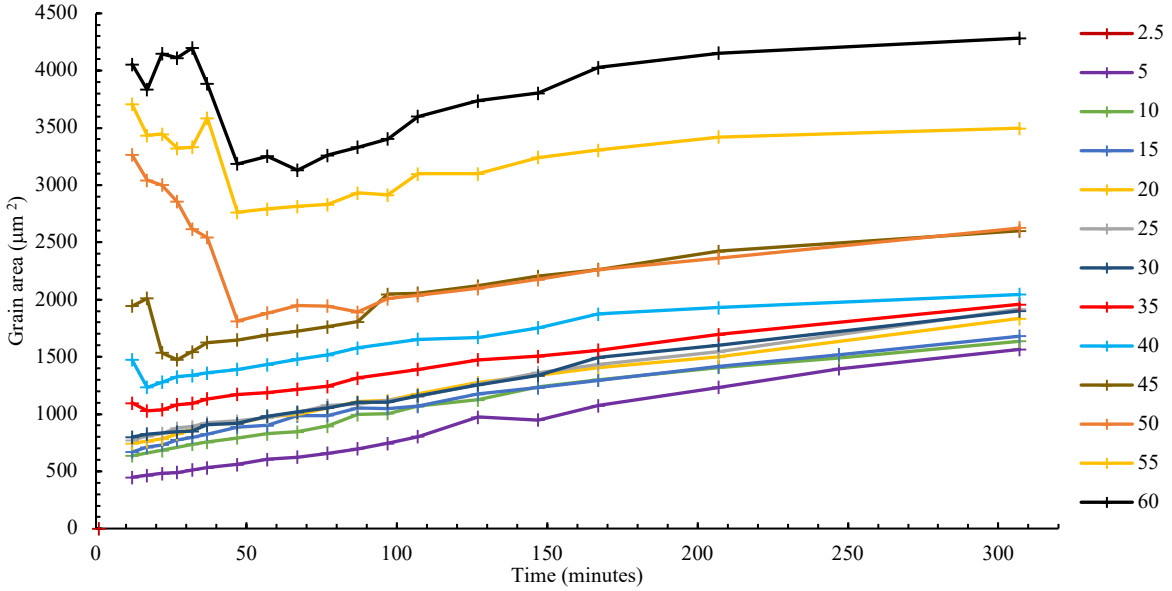

Figure 4-4 Average grain area per bin vs time for sample 1a which was heat treated at 500 °C.

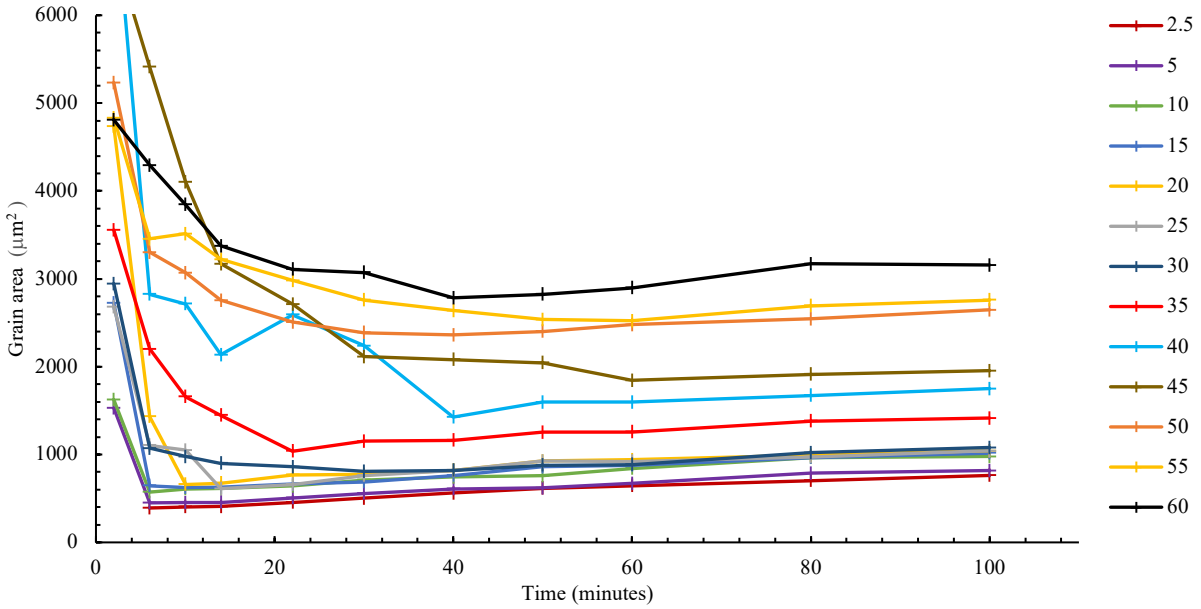

Figure 4-5 Average grain area per bin vs time for sample 5a which was heat treated at 500 °C.

The 40 mm bin location at 22 and 30 minutes was imaged poorly due to localised electro pitting and therefore the results from ImagePro are dubious. The grains size before and after are reliable.

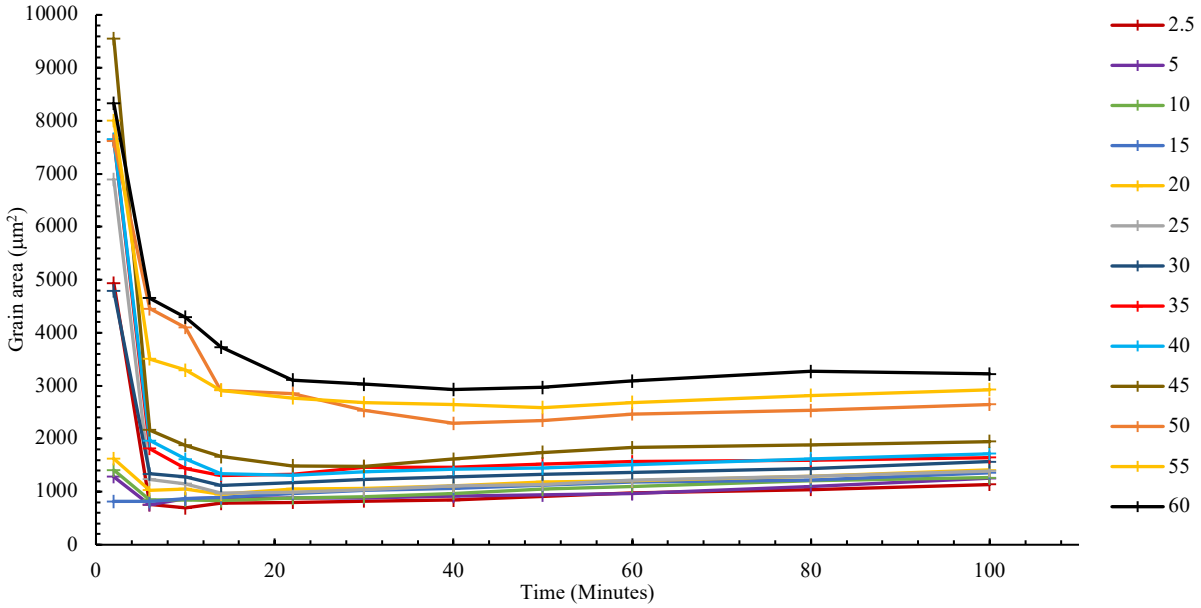

Figure 4-6 Average grain area per bin vs time for sample 6a which was heat treated at 550 °C.

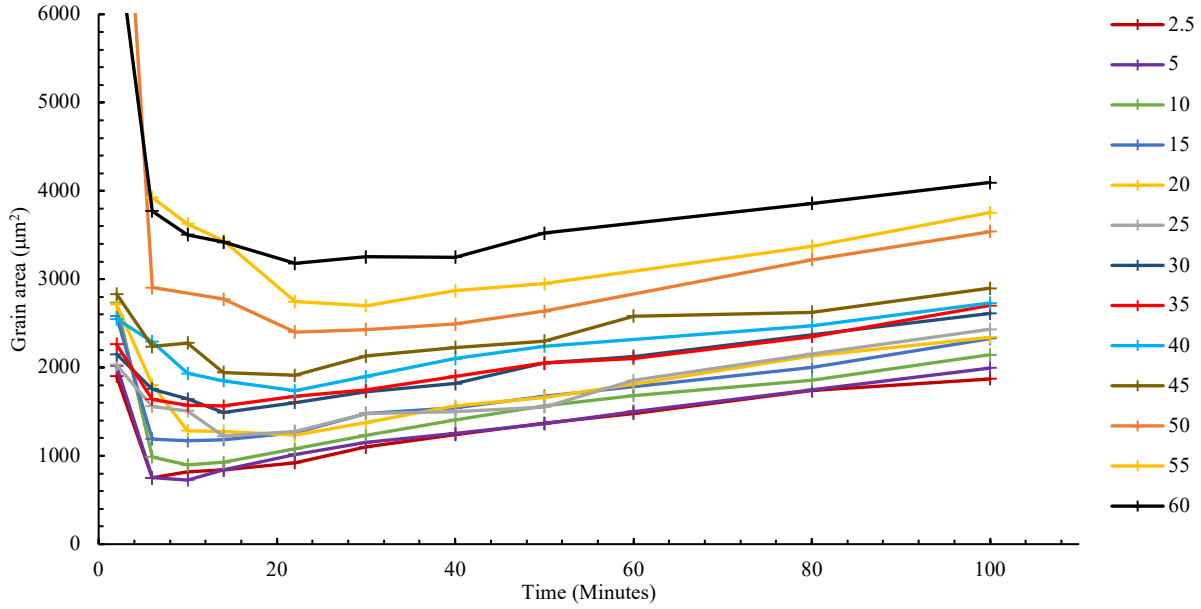

Figure 4-7 Average grain area per bin vs time for sample 7a which was heat treated at 600 °C.

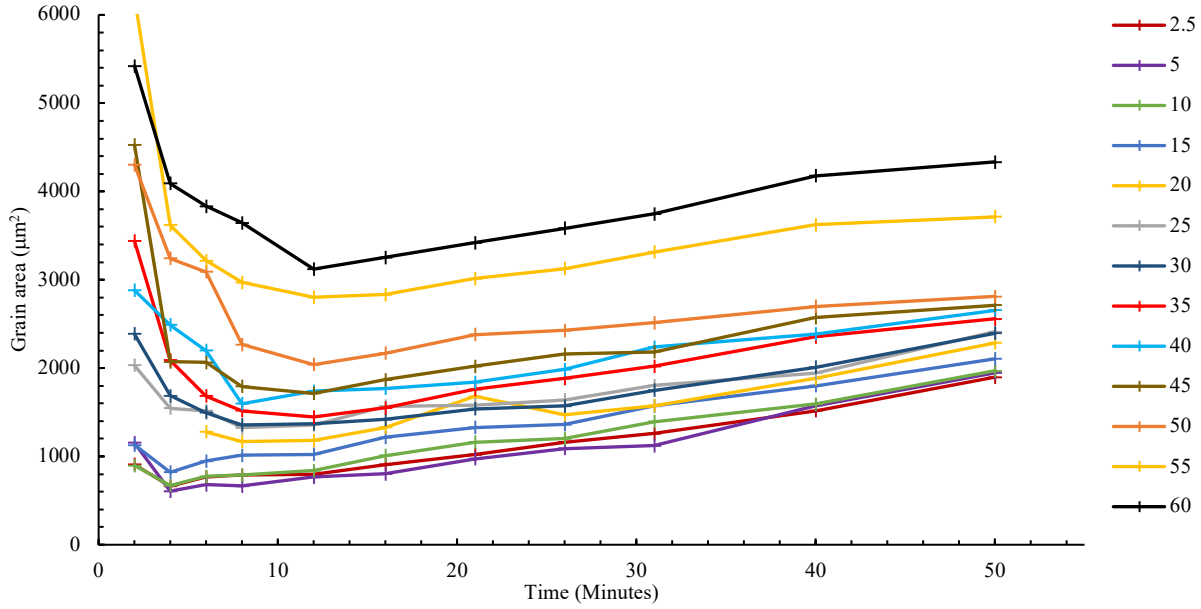

Figure 4-8 Average grain area per bin vs time for sample 8a which was heat treated at 650 °C.

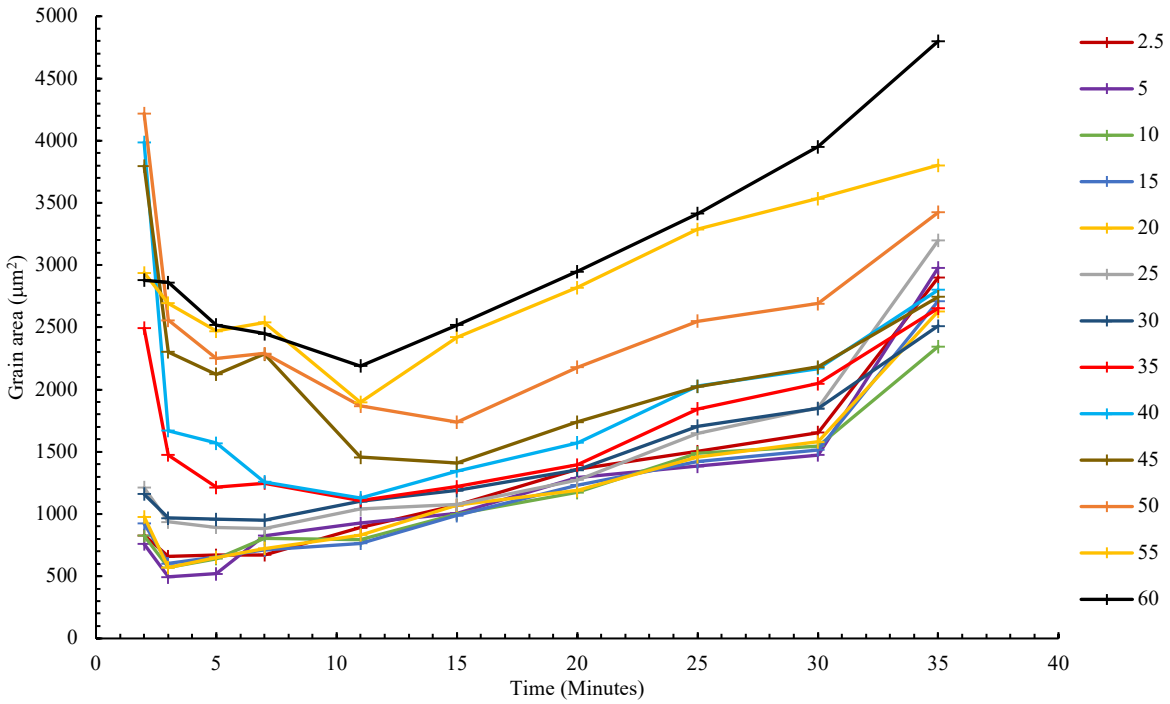

Figure 4-9 Average grain area per bin vs time for sample 9a which was heat treated at 700 °C.

4.3 TEMPERATURE

The internal temperature of a dummy gradient sample was recorded while being placed into the furnace at the five different heat treatment temperatures and is shown in Figure 4-10

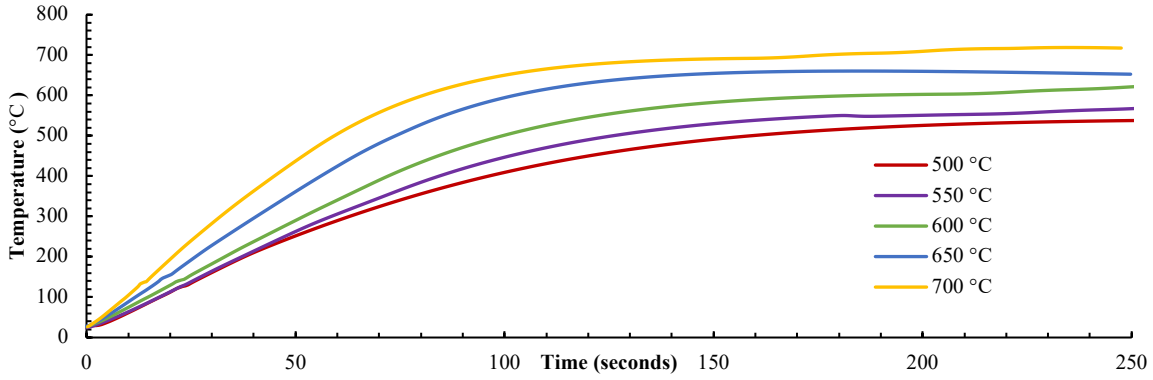

Figure 4-10 The internal temperature of gradient sample as a function of time while heating in the furnace for the five different furnace temperatures.

The same sample was also recorded being quenched in water that was at room temperature to record the cooling cycle, and is shown in Figure 4-11.

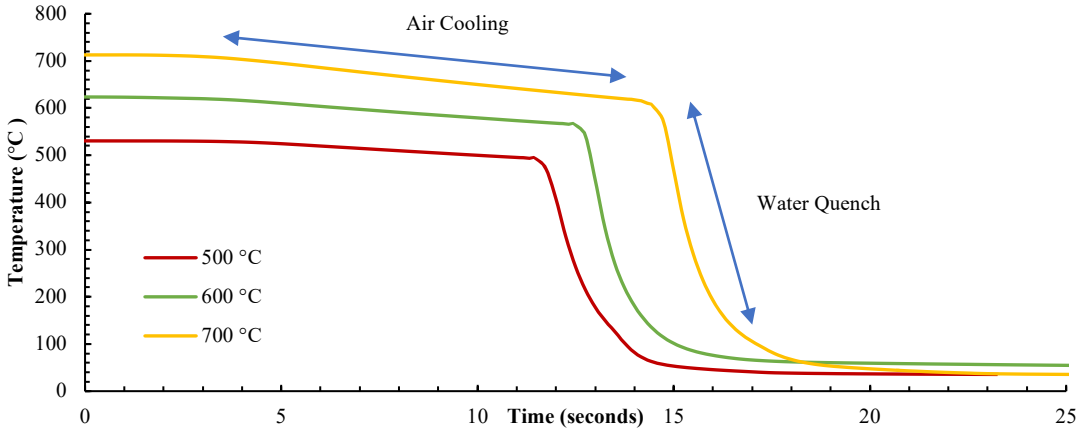

Figure 4-11 The internal temperature of gradient sample as a function of time while being quenched in water, note the initial 10 second air cooling before the sample was quenched was due to the thermocouple wire preventing instant quenching and should be ignored, but is shown for completeness.

4.4 HARDNESS

The hardness of a gradient sample 4a was measured after a 12-minute heat treatment at 500 °C and is shown in Table 4-2.

Table 4-2 Hardness vs position on a gradient sample after 12 min heat treatment at 500 °C.

Position Bin	*Average Hardness (Micro Vickers)*	*Standard Deviation (Sample)*
2	*78*	*3*
2.5	*76*	*4*
5	*77*	*5*
10	*77*	*7*
15	*76*	*4*
20	*75*	*3*
25	*72*	*3*
30	*69*	*3*
35	*67*	*2*
40	*67*	*3*
45	*65*	*2*
50	*69*	*3*
55	*75*	*2*
60	*71*	*3*

The hardness of the homogeneous samples was measured after each heat treatment. The hardness values are recorded in Table 4-3.

Table 4-3 Hardness values for the homogeneous samples along with the Standard deviation.

Name of Sample and Temperature	*Time (Minutes)*	*Average Hardness (Micro Vickers)*	*Standard Deviation (Sample)*
As deformed	*0.0*	*131*	*4*
A - 500℃	*3.0*	*127*	*5*
	5.0	*131*	*8*
	8.0	*119*	*4*
	15.0	*72*	*1*
B - 550℃	*2.5*	*129*	*3*
	5.0	*122*	*5*
	8.0	*122*	*4*
	15.0	*69*	*1*
C - 600℃	*2.5*	*135*	*4*
	5.5	*109*	*4*
	8.0	*97*	*4*
	15.0	*61*	*3*
D - 650℃	*2.5*	*131*	*3*
	5.0	*71*	*2*
	8.0	*67*	*1*
	15.0	*59*	*2*
E - 700℃	*1.5*	*129*	*5*
	2.5	*131*	*5*
	5.0	*67*	*3*
	10.0	*58*	*2*

4.5 COMPOSITION

The composition of the samples was measured with OES to identify if there were any changes in composition due to heat treatments. Two samples of the as received brass were taken from opposite ends of the brass sheet along with two gradient samples 5B and 9B after heat treatments and one sample heat treated at 700 °C for 240 min were measured.

Table 4-4 The average composition in weight percent as measured from the centre of the samples by OES. A minimum of 4 measurements were taken from each sample and was averaged.

	As Received #1	*As Received #2*	*350 min at 500 ℃*	*45 min at 700 ℃*	*240 min at 700 ℃*
Cu	*68.1*	*69.3*	*66.1*	*67.6*	*66.4*
Zn	*31.8*	*30.6*	*33.9*	*32.3*	*33.5*
Pb	*0.0211*	*0.0176*	*0.0172*	*0.0172*	*0.0220*
Sn	*< 0.0005*	*<0.0005*	*< 0.0005*	*< 0.0005*	*< 0.0005*
P	*0.0015*	*0.0017*	*0.0012*	*0.0011*	*0.0013*
Mn	*0.0019*	*0.0046*	*0.0029*	*0.003*	*0.0026*
Fe	*0.0204*	*0.0569*	*0.0149*	*0.0118*	*0.0149*
Ni	*0.0076*	*0.0081*	*0.0062*	*0.0059*	*0.0065*
Si	*0.0012*	*<0.0002*	*0.0037*	*0.0034*	*0.0128*
Mg	*0.0006*	*0.0005*	*0.0008*	*0.0007*	*0.0009*
Cr	*0.0007*	*0.0115*	*0.0006*	*0.0006*	*0.0006*
Al	*< 0.0005*	*<0.0005*	*<0.0005*	*< 0.0005*	*< 0.0005*
S	*< 0.0001*	*<0.0001*	*<0.0001*	*< 0.0001*	*< 0.0001*
As	*<0.0004*	*<0.0004*	*<0.0004*	*<0.0004*	*<0.0004*
Ag	*0.0045*	*0.0039*	*0.0046*	*0.0045*	*0.0048*
Co	*< 0.0010*	*0.0061*	*0.0016*	*0.0014*	*0.0021*
Bi	*0.0033*	*0.0035*	*0.0038*	*0.0032*	*0.0033*
Cd	*0.0014*	*0.0013*	*0.0014*	*0.0014*	*0.0014*
Sb	*<0.100*	*<0.100*	*<0.100*	*<0.100*	*<0.100*
Zr	*0.0003*	*0.0004*	*0.0004*	*0.0003*	*0.0004*

5 RECRYSTALLISATION

OVERVIEW

The process of recovery and recrystallisation is thermally driven. This section shows the time for recrystallisation of five gradient samples which have had interrupted heat treatments at five different temperatures.

Traditionally to find the recrystallisation time vs strain for a material, a whole series of samples would be coldworked/strained to the same amount, then heat treated to predetermined times in the hope that recrystallisation would be captured. This process would then be repeated for a higher or lower amount of strain. The process is time consuming and requires many different samples. Using a gradient sample, the same information can be captured from one sample.

5.1 INTRODUCTION

The origin of this set of experiments was inspired by the change in hardness down a gradient sample which was believed to have fully recrystallised after a 12-minute heat treatment at 500 °C. The sample was still going through recrystallisation in the 6 least strained bins, X > 40 mm. This was supported by the Grain Orientation Spread (GOS) data and the sharp change in grain size at the same location.

GOS is the amount of misorientation that is present in a grain. The GOS of grain i is calculated by

$$GOS_i = \frac{1}{J_i}\sum_j w_{i\,j}$$

Where J_i is the number of pixels in grain i, and $w_{i\,j}$ is the mis-orientation angle between the mean grain orientation and the orientation of the pixel [87].

The recrystallisation samples (5a-9b) were initially heat treated at very short time intervals which gradually increased in length as the experiments progressed as per The recrystallisation samples did not have an initial 12-minute heat treatment, and the first heat treatments were at very short times so that recrystallisation could be measured in the high strain portions of the sample. The heat treatment times are shown in Table 3-3.

Table 3-3. The exact time of recrystallisation was difficult to measure. This was because it was a progressive process with new small grains forming from the larger strained grains while there were still large regions of strained grains. An image of incomplete recrystallisation is shown in Figure 5-1. In this research complete recrystallisation was identified as the time corresponding to a minimum in measured mean grain area for that bin location.

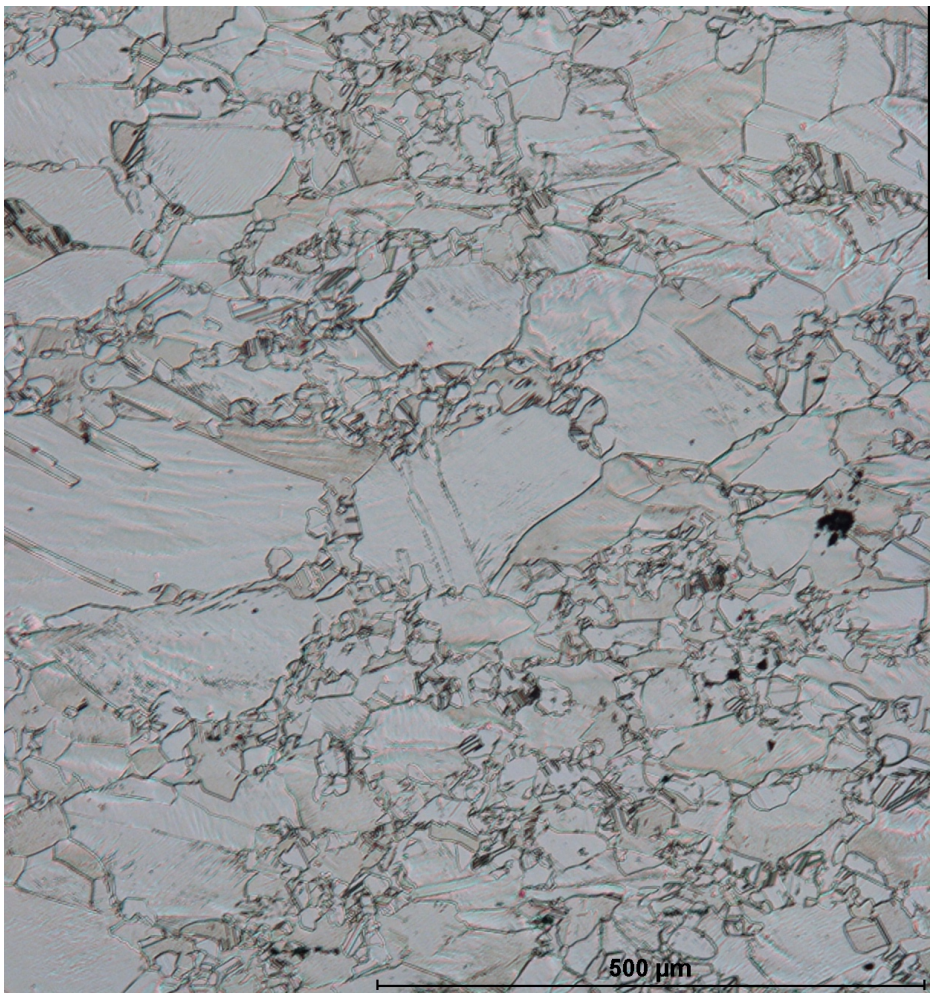

Figure 5-1 A small proportion of a large-scale image from homogeneous sample (C after 8 minutes at 600 °C). Note the nucleation of new small strain free grains and the larger parent grains which are still in a strained state and are yet to recrystallise. This creates a large grain size spread.

5.2 EBSD Recrystallised Fraction

The large scale EBSD map taken from the first gradient sample was further analysed in Oxford to show the GOS, as shown in Figure 5-2. What this map shows is that the sample is mostly recrystallised up until the 35 mm bin location by the predominant blue colour. However, all the locations greater than the 35 mm bin are shown with a decreased recrystallised fraction and an increase in deformed grains, shown by the red colour.

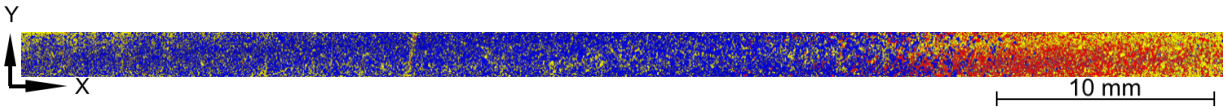

Figure 5-2 Grain Orientation Spread (GOS) map of a gradient sample 4a taken after a 12-minute heat treatment at 500 °C, Red is a deformed grain, Yellow is substructured and Blue is recrystallised.

The mean GOS was also plotted as a function of the X position as shown in Figure 5-3. This confirms that the transition is around the 35 mm bin location. Incomplete recrystallisation was also supported by the change in grain area in both the optical and EBSD data, and by the increase in measured hardness shown in Figure 5-4.

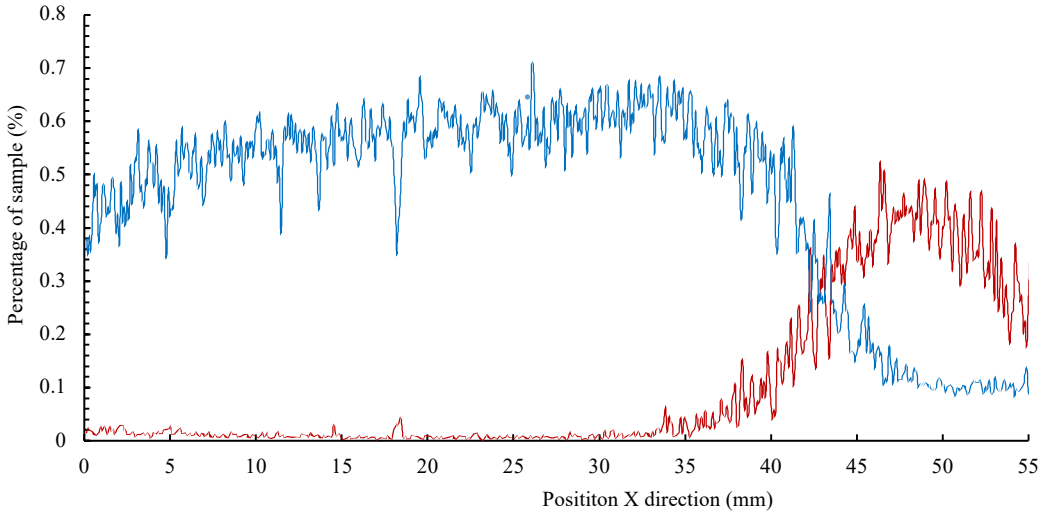

Figure 5-3 Deformed and recrystallised grains vs position for a gradient sample 4a after a 12-minute heat treatment at 500 °C

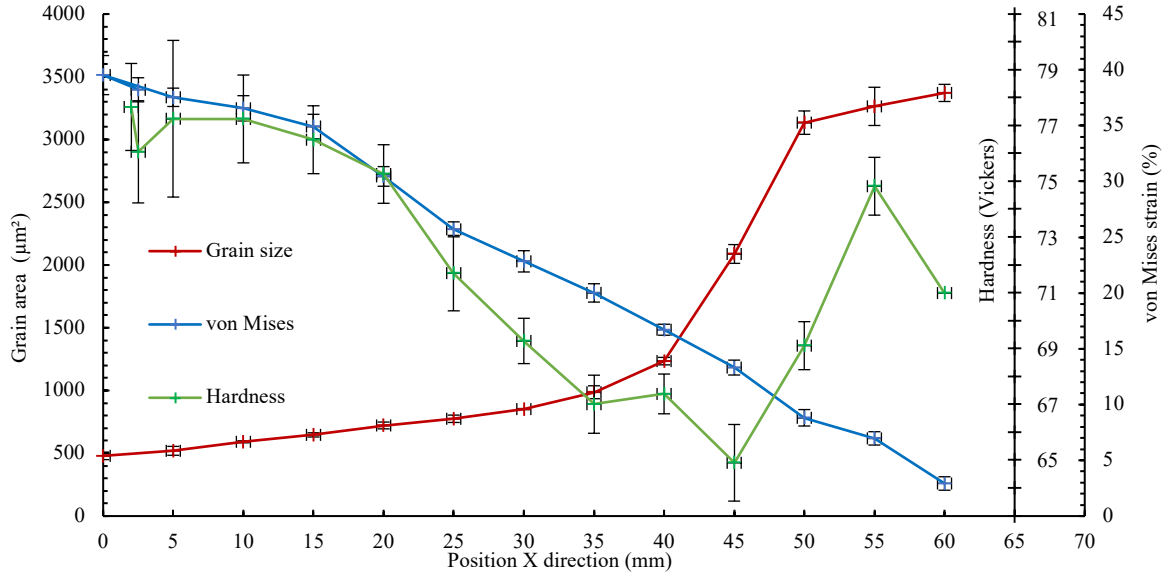

Figure 5-4 Grain size, von Mises strain, and hardness vs position for sample 4a after a 12-minute heat treatment at 500 °C. The error bars are the standard deviation of the mean.

5.3 Grain Area vs Time

What is presented in this section is the grain area for each bin as a function of time. It is broken into two sections, first the homogeneous samples followed by the gradient samples.

5.3.1 Homogeneous Samples

The recrystallisation time vs grain area of the homogeneous samples is shown in Figure 4-3. There was an expected trend where the time until recrystallisation reduced with increased temperature. The heat treatment time increments started out short but increased slightly in the later heat treatments as per Table 3-4.

Sample D and E heat treated at 650 °C and 700 °C both entered grain growth at 8 and 5 minutes. The decrease in grain area vs time looks to have a linear trend shown with a red dotted line for sample A.

The linear trend is unexpected and is not seen in the gradient samples as the recrystallisation process it a continuum, even after the average grain size is starting to increase there will still be new recrystallised grains forming at a reduced rate. However, they will be limited and will be dominated by the bulk grain growth. An expected trend line would be exponential/parabolic, as the strained grains are consumed by the new grains there would be a decrease in the nucleation rate. This may be caused by the interrupted heat treatments, as a material recrystallises it releases small amounts of strain energy which can help initiate recrystallisation in neighbouring grains and because the heat treatment was interrupted this energy was wasted. This will cause the sample to recrystallise over a much longer time than predicted.

5.3.2 Gradient Samples

The grain area vs time for the gradient samples is shown in Figure 4-4 through to Figure 4-9. The samples showed a gradual trend of the recrystallisation time decreasing as the temperature increased. The samples also showed an increasing time until recrystallisation as the amount of cold work decreased down the sample. This is expected and well documented in literature.

5.4 Critical Strain Anneal

The critical strain anneal is the minimum amount of cold work that a material must have to initiate recrystallisation. The critical strain for this brass was below the 2.9 % strain, which was in the 60 mm bin.

Chotinuchit found the critical strain in 70/30 brass at set time intervals using tensile cold work and at temperatures of 650 °C, 700 °C, 750 °C, and 800 °C as shown in Figure 5-5.

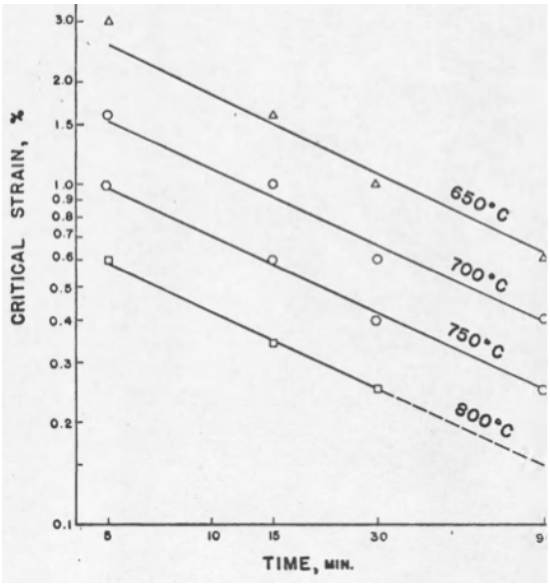

Figure 5-5 Chotinuchit critical strain from tensile cold work vs annealing time for 70/30 brass at indicated temperatures [15].

Figure 5-5 shows the time for recrystallisation at 3 % strain at 650 °C was 5 minutes. This time is much shorter than in this work, which was measured at 11 minutes. The samples in Chotinuchit's work were 1/16" (1.59 mm) thick and were heat treated in a molten salt bath without interruption [15]. The thin sample and the salt bath would decrease the thermal lag and therefore, it is expected that the time in this work would be slightly longer. However, there was little mentioned about how the strain

was measured. Therefore, it is unknown if the strain was measured as a reduction in cross sectional area or as a tensile strain.

Walker showed that the critical strain in 70/30 brass was 10 % using cold rolled samples at a temperature of 500 °C and 5.3 % for 550 °C as shown in Figure 2-5 [34]. Therefore, in bins greater than 50 mm at temperatures lower than 550 °C the grains should not have recrystallised and should have only grown in size. This was not the case as all the samples in this research have gone through recovery, recrystallisation and grain growth for all temperatures. There may be a change in the critical strain anneal depending on different methods of cold work, in Walkers research the cold work was due to rolling, whereas this research used tensile cold work. This difference may be because of the surface effects caused by rolling. A sample which has been cold rolled will have much higher deformation of the lattice at the surface than the centreline. With very low amounts of stored cold work (less than 10 %) the surface deformation may be easily polished off. This would result in a sample with much less cold work where the sample is imaged. Whereas tensile cold work which may have more consistent cold work through the thickness of the material and thus lowering the critical strain.

5.4.1 Strain, Temperature and Time

The minimum time required to recrystallise the different bins on the all the gradient samples was measured as the time which the grain size started to increase. The time is plotted against the strain for the different bin locations as measured by DIC and is shown in Figure 5-6.

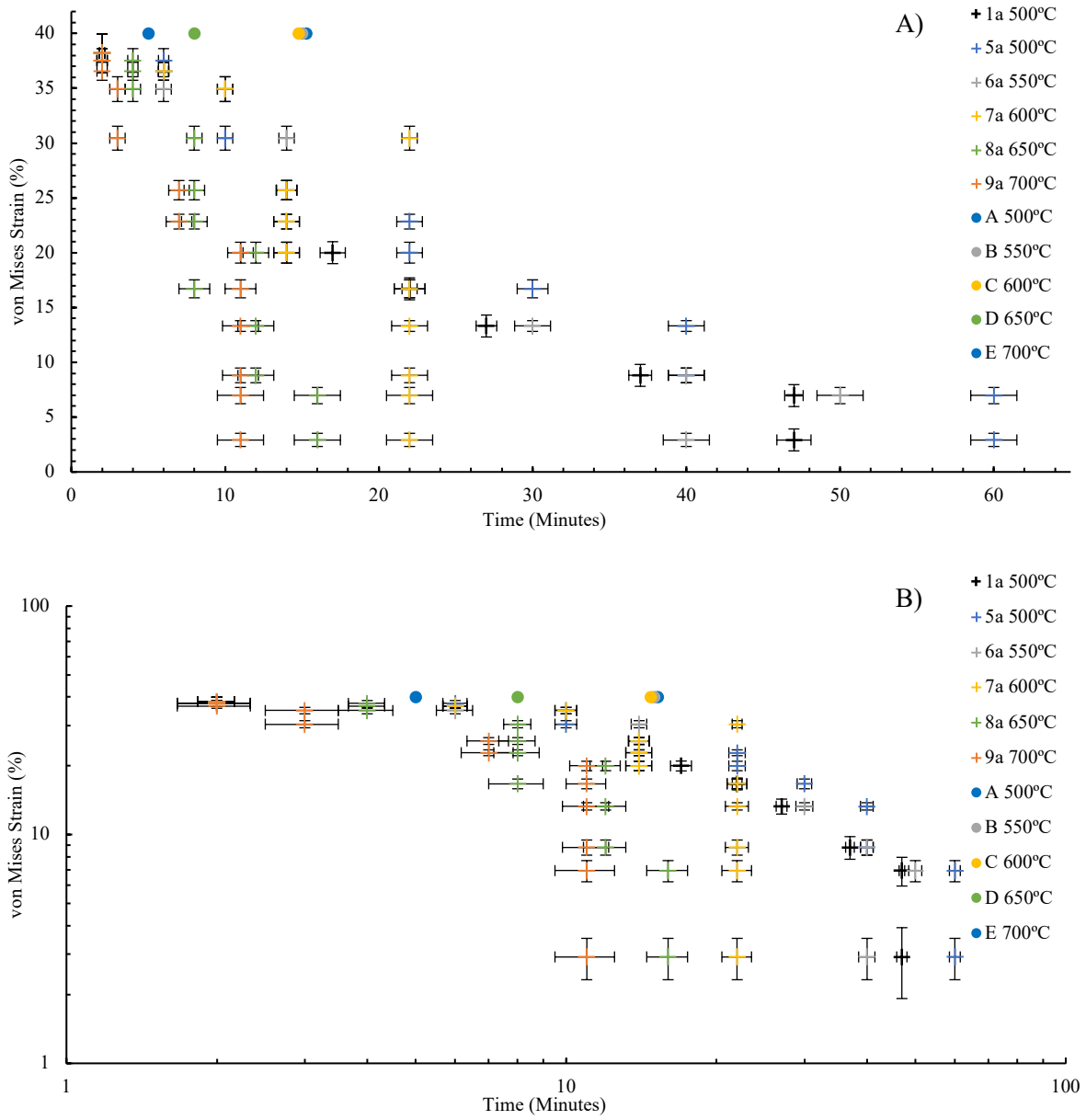

Figure 5-6 Strain as a function of time until recrystallised in 70/30 Brass when heat treated at 500, 550, 600, 650 and 700 °C. Plotted in two formats linear (A) and on log scales (B). The error bars correspond to the standard deviation.

Figure 5-6A and B show that the higher the temperature, the shorter the time to recrystallise. They also show that the higher the strain the shorter the recrystallisation time. This is as expected and is well documented in literature [25], [34], [26], [36].

Figure 5-6B show that there may be two different relationships, time invariant at low strain and power law at higher strain. The time invariants at low strains may be caused by the increase in the duration of the heat treatment at longer times, and thus the exact recrystallisation time is not being captured as accurately as for the shorter heat treatment times.

A suspected cause of the discrepancy between the homogeneous samples and the gradient samples is thermal lag. The homogeneous sample A was heat treated five times (1.5, 3, 5, 8, and 15 minutes) before recrystallisation was captured, whereas the gradient sample 5a was only heat treated twice, (2, and 6 minutes). The shorter times limited the peak temperatures to approximately 378 °C, 445 °C then 500 °C, in the first three heat treatments for the homogeneous sample whereas the gradient sample

reached 445 °C and 500 °C before recrystallisation was measured. Another cause of error was the last heat treatment for the homogenous sample A was 7 minutes, which is longer than the total time the gradient took to recrystallise. The time increase was much too large for the final heat treatment. Which has also caused disagreement with samples B and C.

The thermal lag was also suspected to be the source of discrepancy between the gradient sample 1a and 5a which were both heat treated at 500 °C. 1a has recrystallised much sooner than 5a. Sample 1a had an initial heat treatment of 12 minutes, and only required 7 heat treatments and 47 minutes to recrystallise the 60 mm bin, while sample 5a required 9 heat treatments and 60 minutes.

5.5 Activation Energy for Recrystallisation

The activation energy for recrystallisation for the bin locations at the five different heat treatments was calculated from the empirical relationship

$$\frac{1}{t} = A\, e^{\frac{-Q}{RT}}$$

Where t is the time for full recrystallisation, A is a temperature independent constant, Q is the activation energy for recrystallisation, R is the ideal gas constant and T is the absolute temperature. By plotting the natural log of one over the recrystallisation time against one over the temperature shown in Figure 5-7 gives the slope value of Q/R and the intercept gives A. The 2.5 mm bin location was found to have recrystallised at approximately the same times at all temperatures. This was caused by the thermal lag and the very short heating times.

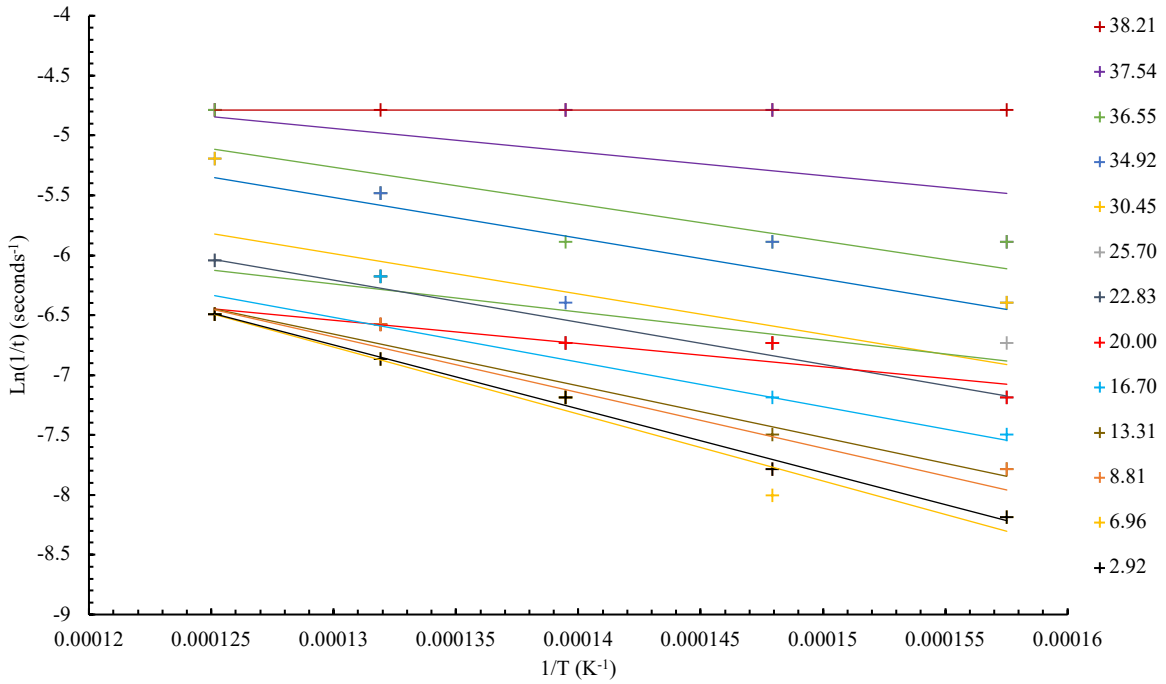

Figure 5-7 Arrhenius plot for recrystallisation for different amounts of von Mises strain.

The activation energy of recrystallisation (Q) and intercept (A) values are recorded of each bin in Table 5-1.

Table 5-1 Calculated values for the activation energy of recrystallisation (Q) and the preexponent factor (A).

Cold Work, ε_{vm} (%)	*Ln(A)*	*A*	*Activation Energy, Q (J/mole)*	*R^2 (-)*
38.21	*-4.79*	*0.01*	*0*	*1.00*
37.54	*-2.38*	*0.09*	*19700*	*0.24*
36.55	*-1.26*	*0.28*	*30800*	*0.68*
34.92	*-1.10*	*0.33*	*34000*	*0.65*
30.45	*-1.61*	*0.20*	*33700*	*0.34*
25.70	*-3.20*	*0.04*	*23400*	*0.75*
22.83	*-1.64*	*0.19*	*35200*	*0.93*
20.00	*-4.02*	*0.02*	*19400*	*0.86*
16.70	*-1.67*	*0.19*	*37300*	*0.75*
13.31	*-1.05*	*0.35*	*43200*	*0.96*
8.81	*-0.64*	*0.53*	*46500*	*0.91*
6.96	*0.50*	*1.65*	*55900*	*0.96*
2.92	*0.18*	*1.20*	*53300*	*0.99*
average	*-1.74*	*0.4*	*36000*	*0.77*

The activation energy for recrystallisation is plotted against the prior cold work and is shown in Figure 5-8

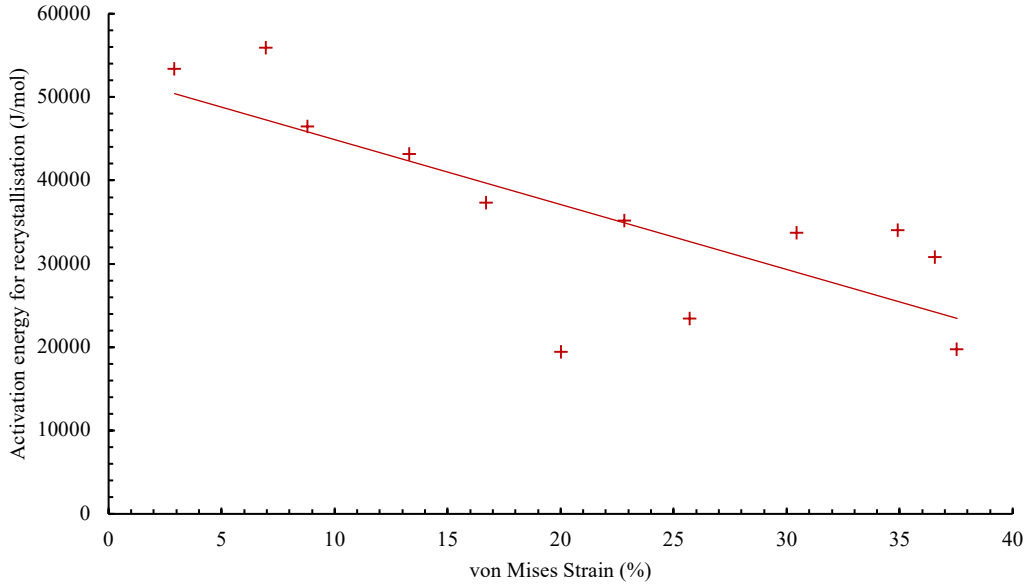

Figure 5-8 Activation energy for recrystallisation vs strain

The activation energy for complete recrystallisation for this work was found to lie between 19700 J/mol and 55900 J/mol with an average of 36000 J/mol. This value agrees with other work with 70/30 brass.

The activation energies reported in literature vary widely such as reported by Jägle et.al. [88]. Experimental methods such as, deformation mode, temperature, initial grain size and if recrystallisation was measured at the start of nucleation or the end, all alter the results.

Shafiei et.al. found the activation energy for 50% recrystallisation to be twice this using simulations on an Artificial Neural Network at 11324.3 J/mol [89]. This may be due to experiments having non-ideal conditions and materials which may decrease the activation energy due to increased nucleation caused by defects.

Klein found the activation energy for the start of recrystallisation to be 1445 J/mol [25] in 75 % cold rolled 70/30 brass. This value is the lowest found recording which was because it is the start of recrystallisation. Also, Klein's work used a molten salt bath compared to the interrupted atmospheric furnace heat treatments used in this work which would reduce thermal lag. It would be hard to compare Klein's work to this set of work as the start of recrystallisation would be almost impossible to detect using ImagePro.

5.6 Discussion

Trends can be obtained using this data but due to the interrupted nature of the heat treatments, comparison to continuous heat treatments will be challenging due the thermal lag from so many heating and cooling cycles. The last two grain area measurements for sample 9a heat treated at 700 °C for all bin sizes were growing much faster than the rest of the measurements as a result of the increased time spent at temperature. This was due to the thermal lag of using an atmosphere furnace. Both of these problems could be reduced if a different method was used for heating the samples, such as a molten salt baths or induction heating.

The highest strained location on the sample, the 2.5 mm bin was very hard to electro polish and etch, therefore the quality of the micrographs was lower than the rest of the bins on all samples. This may have affected the recrystallisation time at this bin location noted by the activation energy for recrystallisation, and ultimately the grain growth data. A solution would be to change the shape of the gradient sample to include a parallel portion to reduce the edge effects during polishing.

A different metric for determining when recrystallisation is complete could be to measure the standard deviation of the grain size when compared to the mean grain size. When there is a minimum in the standard deviation then maybe this time could be used as the recrystallisation time instead of just using a minimum in grain size.

6 GRAIN GROWTH

OVERVIEW

The relationship between the grain size, time and temperature is well understood and documented for homogeneous samples of brass. This chapter focuses on the grain growth in gradient samples measured using interrupted isothermal heat treatments. Six gradient samples were heat treated at five different temperatures. The average grain size was recorded from large scale optical images and was analysed using ImagePro software. The data presented here is a continuation from chapter 5, the grain size has reached a local minimum signalling that recrystallisation is complete and now has entered grain growth.

6.1 Grain Area vs Time

This section is dedicated to the grain area vs time during interrupted isothermal heat treatments of six different gradient samples. The six gradient samples were deformed to a peak strain of 40 %. This stored various amounts of cold work into the samples which were then heat treated at times according to The heat treatments for the first grain growth samples started with an initial heat treatment of 500 °C for 12 min. This was based on preliminary work. The times for each heat treatment are recorded in Table 3-2.

Table 3-2, Table 3-3, and Table 3-4. Large scale optical micrographs were taken of the samples at the 13 bin locations after each heat treatment. The average grain area was measured with ImagePro and grain growth was measured once the grain size had reached a local minimum.

The grain growth plots are based off a simplified form of Equation 2

$$\boldsymbol{a^{n} - a_{o}^{n} = kt}$$

Equation 5 Simple grain growth

where a is grain areas at time t, a_0 is the starting grain area, n is a exponent and t is time and $k = k_o e^{\frac{-Q}{RT}}$. This was done to compare the results to published literature.

The same data was plotted with n=1 and then replotted where the best value of n was calculated for the sample. The method to determine n for the sample was to find the least squares fit for a linear trendline of grain size vs time for each bin, then average the R^2 value of all the bins in that sample. Then solver was used to modify n to maximise the average of the least squares.

Sample 1a was heat treated at 500 °C with an initial heat treatment of 12 minutes and is shown in Figure 6-1.

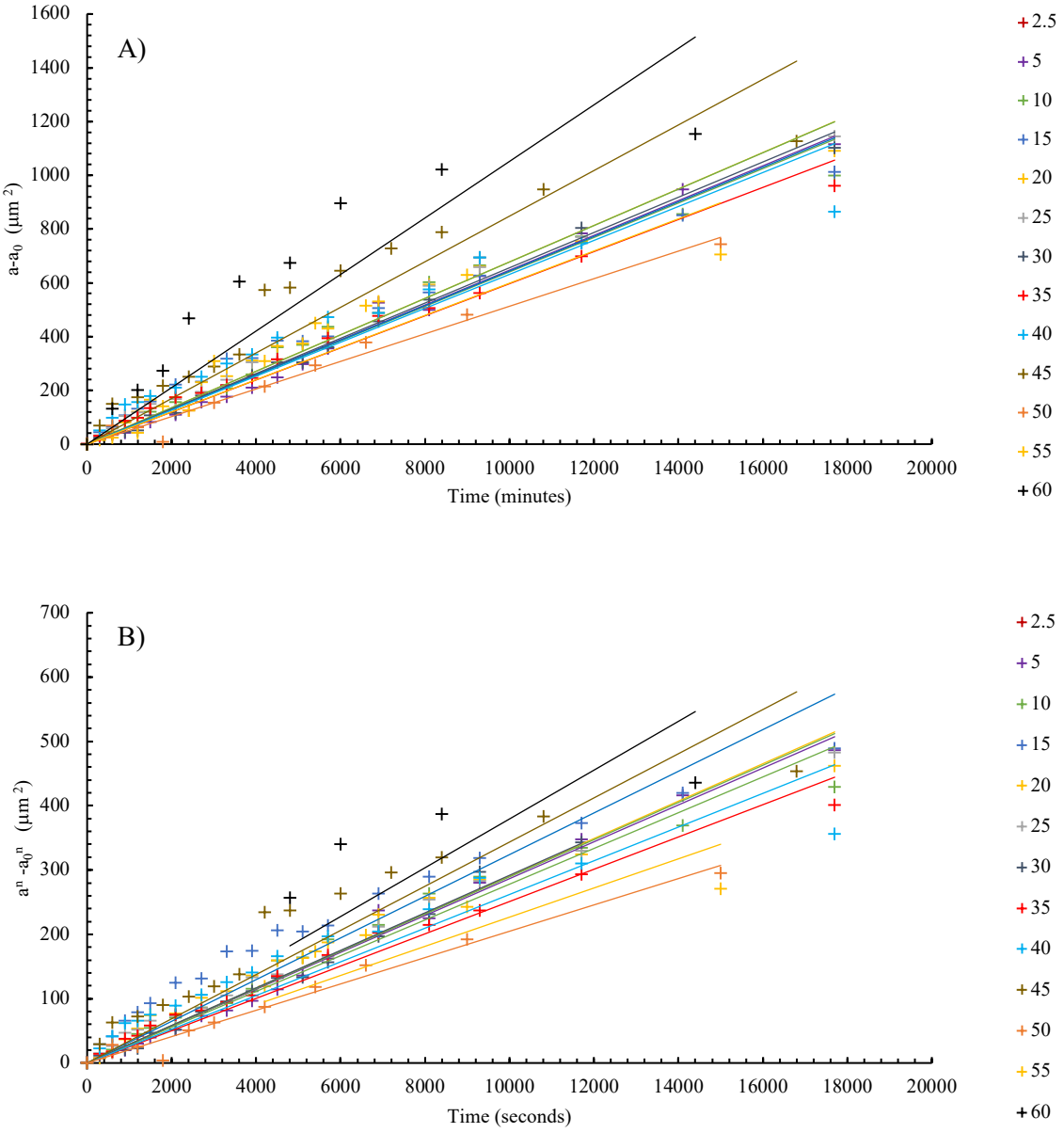

Figure 6-1 Mean grain size with annealing time for fully recrystallised regions corresponding to the bins in the legend for sample 1a annealed at 500 °C. A) Grain growth in form of equation 5 where n = 1. B) Grain growth in from of equation 5 where n was calculated to be 0.89.

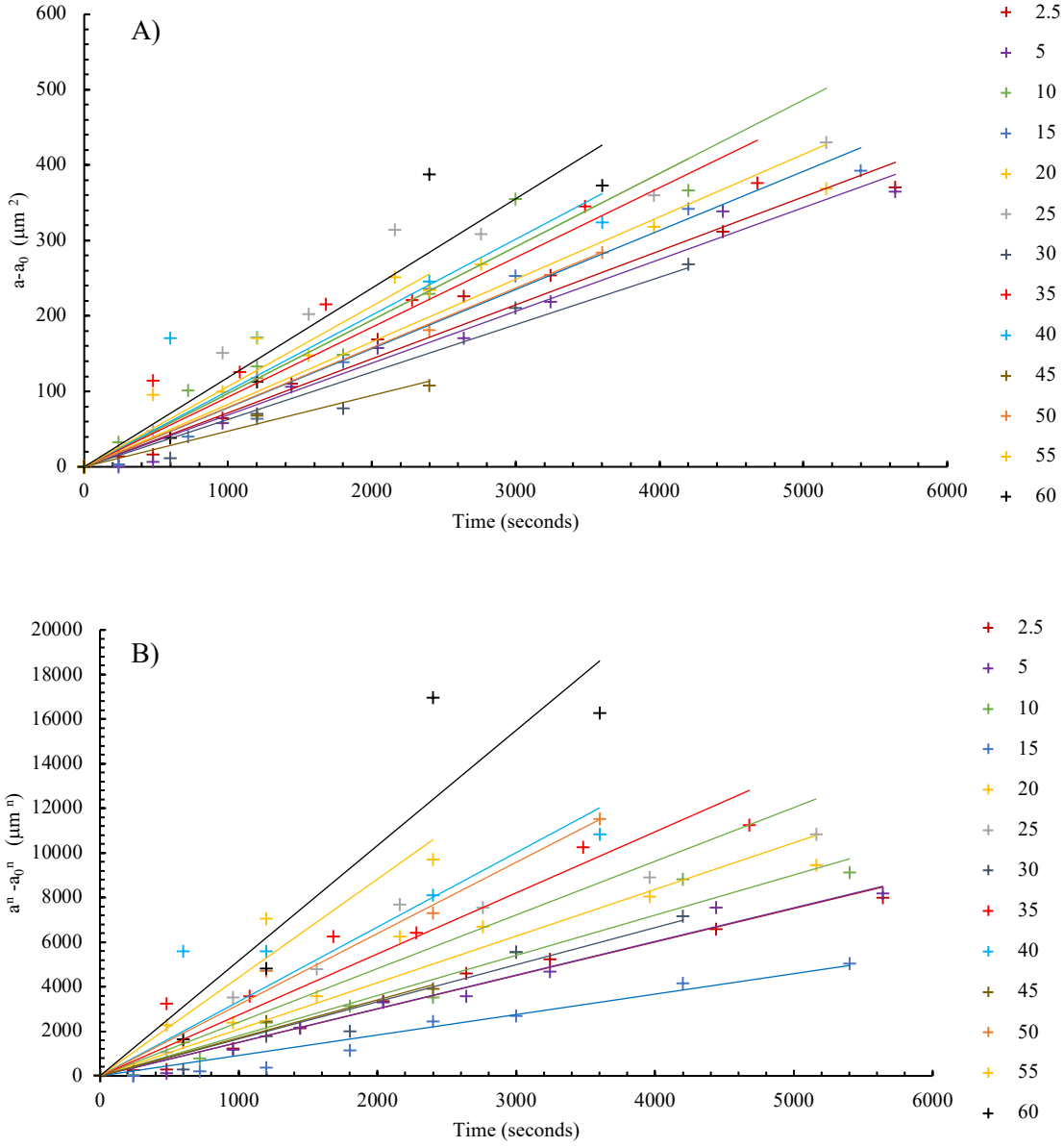

Figure 6-2 Mean grain size with annealing time for fully recrystallised regions corresponding to the bins in the legend for sample 1a annealed at 500 °C. A) Grain growth in form of equation 5 where n = 1. B) Grain growth in from of equation 5 where n was calculated to be 1.42.

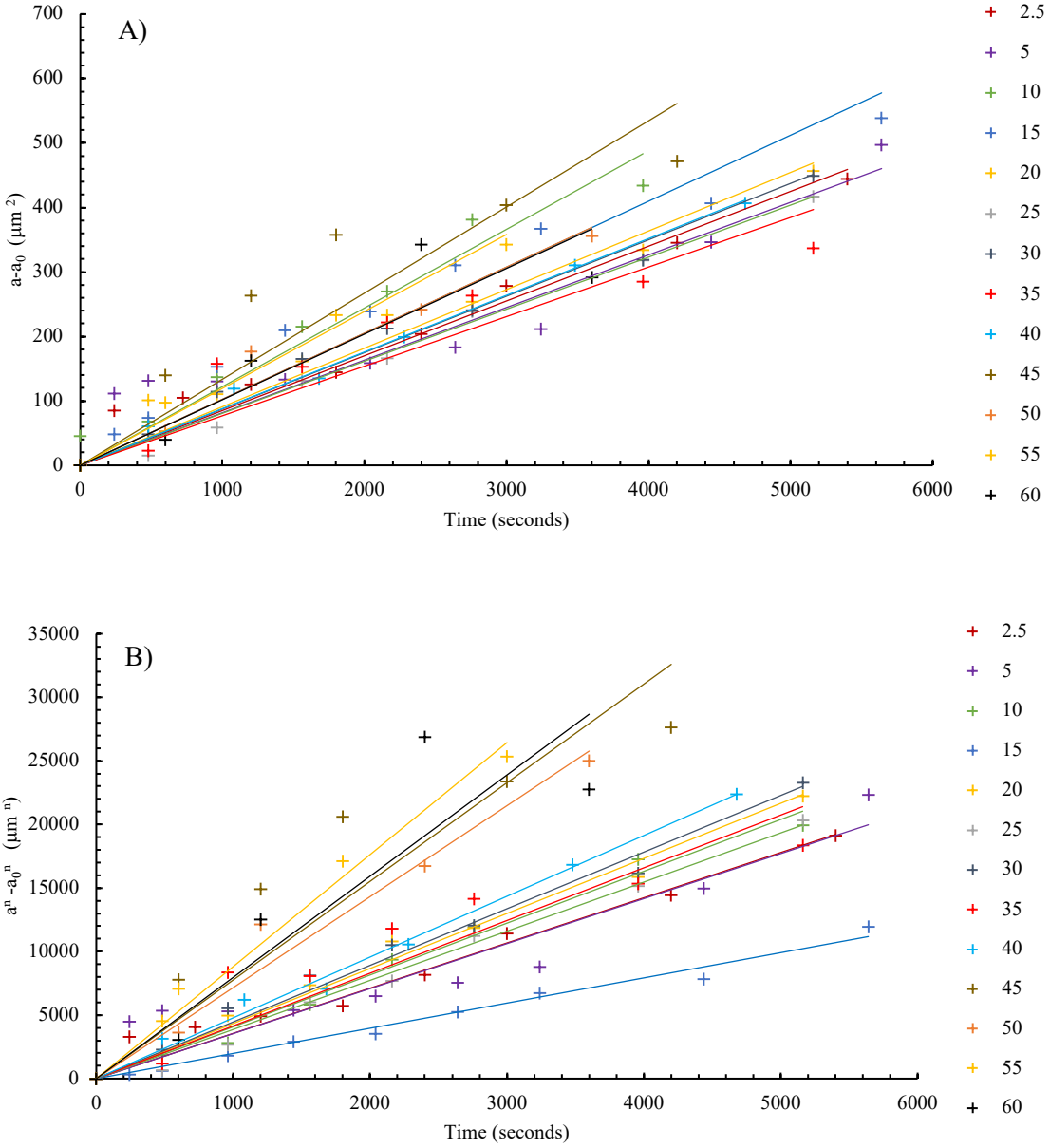

Figure 6-3 Mean grain size with annealing time for fully recrystallised regions corresponding to the bins in the legend for sample 1a annealed at 550 °C. A) Grain growth in form of equation 5 where n = 1. B) Grain growth in from of equation 5 where n was calculated to be 1.49.

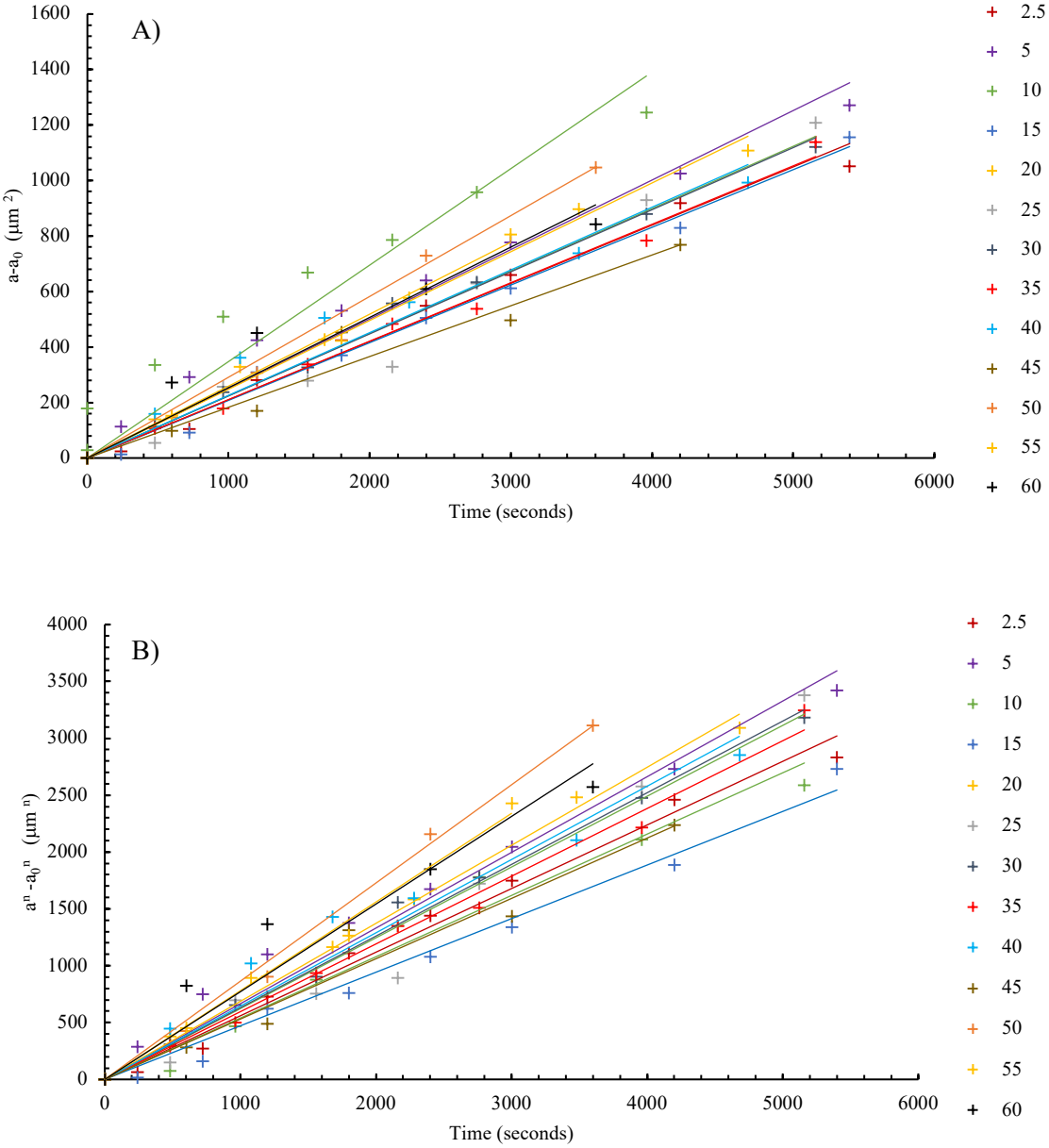

Figure 6-4 Mean grain size with annealing time for fully recrystallised regions corresponding to the bins in the legend for sample 1a annealed at 600 °C. A) Grain growth in form of equation 5 where n = 1. B) Grain growth in from of equation 5 where n was calculated to be 1.17.

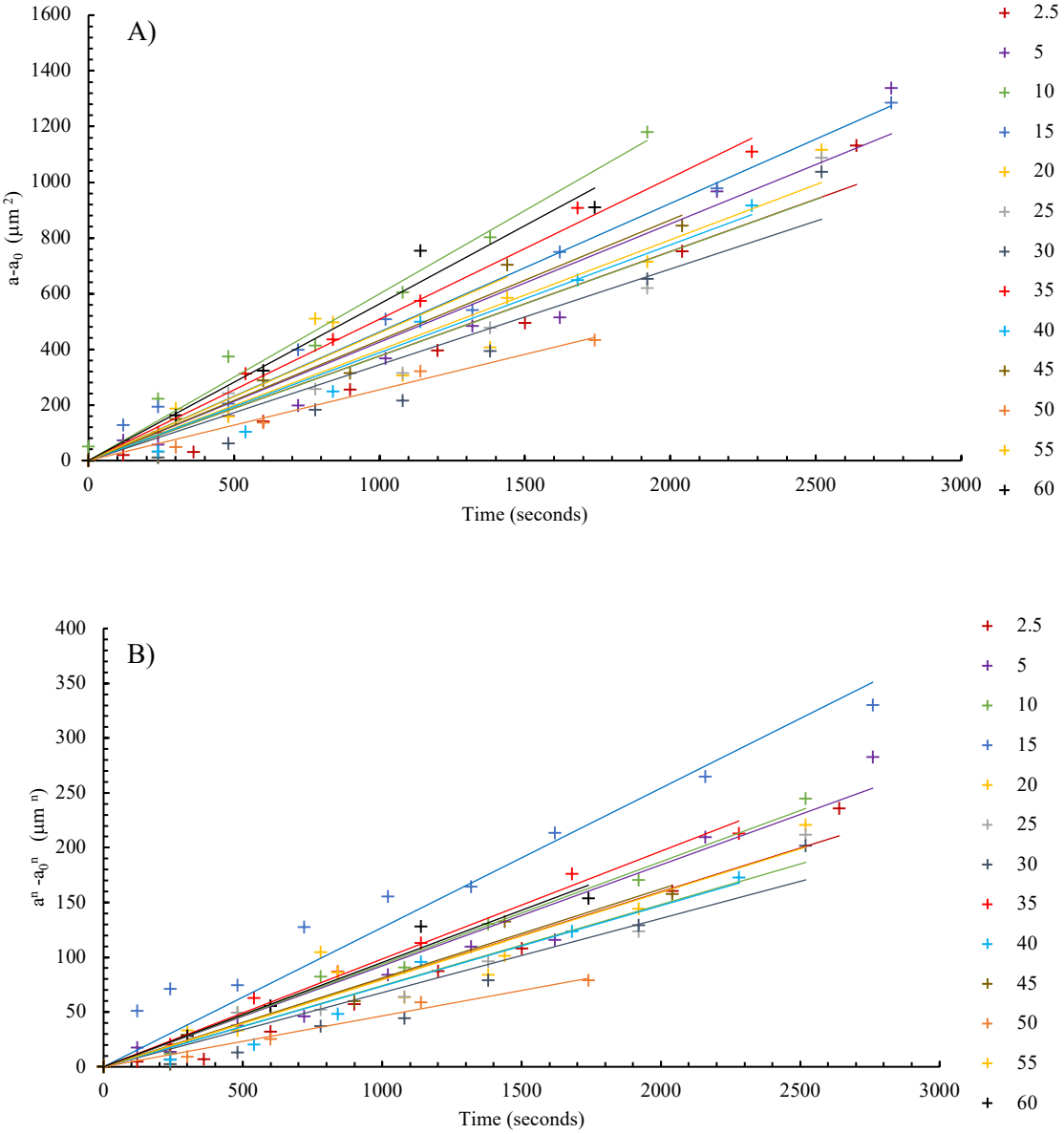

Figure 6-5 Mean grain size with annealing time for fully recrystallised regions corresponding to the bins in the legend for sample 1a annealed at 650 °C. A) Grain growth in form of equation 5 where n = 1. B) Grain growth in from of equation 5 where n was calculated to be 0.97.

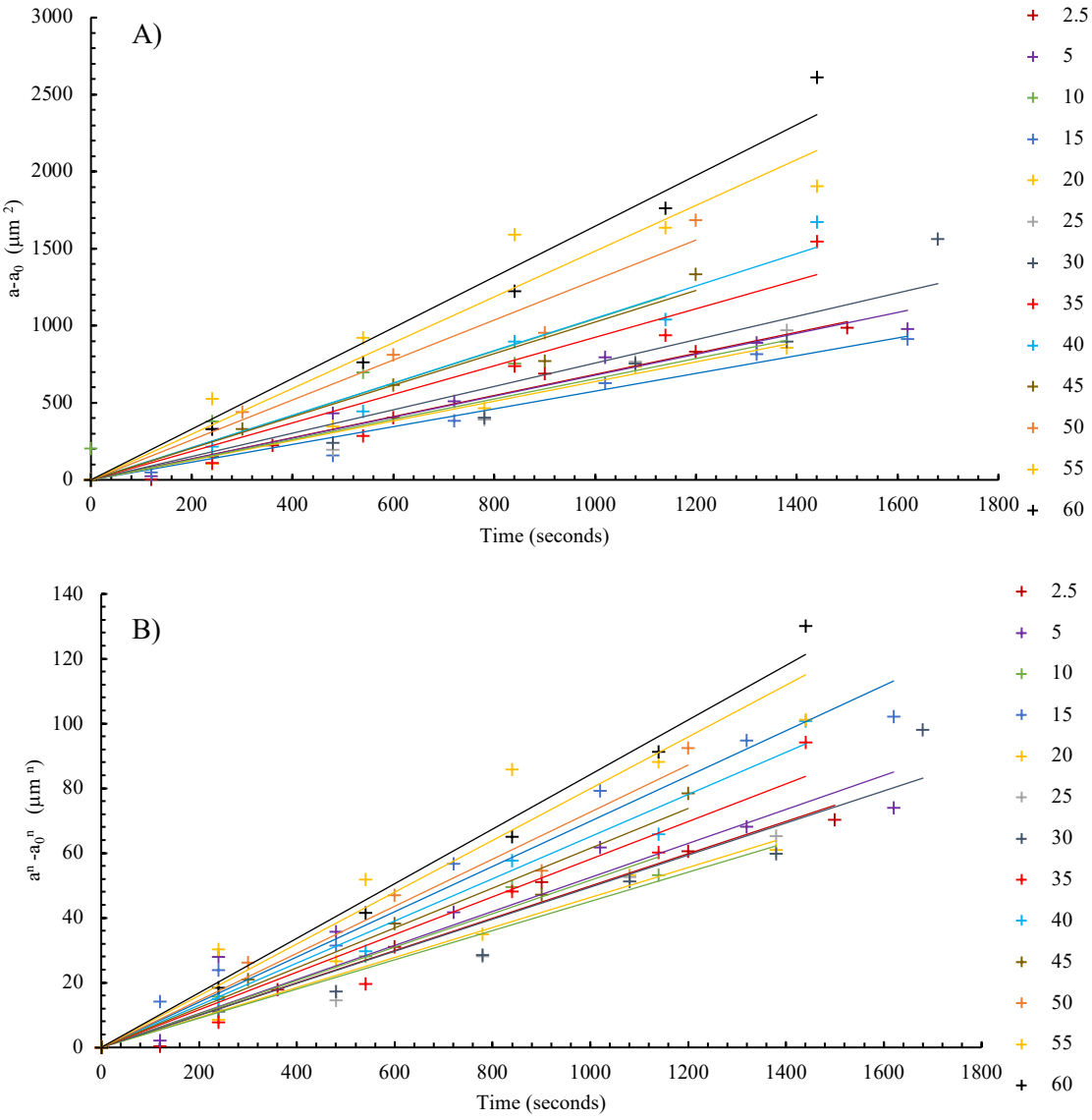

Figure 6-6 Mean grain size with annealing time for fully recrystallised regions corresponding to the bins in the legend for sample 1a annealed at 700 °C. A) Grain growth in form of equation 5 where n = 1. B) Grain growth in from of equation 5 where n was calculated to be 0.98.

The calculated grain growth exponent n varied between 0.89 and 1.49 with an average of 1.15 and had no detectable dependence on the temperature.

6.2 Grain Area vs Temperature

The grain growth constants, k, from the best fit lines measured off the grain growth plots Figure 6-1 to Figure 6-6 have been recorded in the Table 6-1 for the different bin locations.

Table 6-1 Parabolic grain growth constant (k) for all bin locations

		Sample number					
		1a	*5a*	*6a*	*7a*	*8a*	*9a*
Bin location	*2.5*	*Blank*	*0.072*	*0.085*	*0.210*	*0.376*	*0.684*
	5	*0.065*	*0.069*	*0.082*	*0.227*	*0.425*	*0.679*
	10	*0.064*	*0.073*	*0.090*	*0.201*	*0.443*	*0.722*
	15	*0.064*	*0.078*	*0.102*	*0.188*	*0.462*	*0.676*
	20	*0.068*	*0.083*	*0.091*	*0.201*	*0.397*	*0.638*
	25	*0.068*	*0.097*	*0.081*	*0.225*	*0.375*	*0.656*
	30	*0.068*	*0.063*	*0.087*	*0.224*	*0.344*	*0.758*
	35	*0.060*	*0.093*	*0.077*	*0.211*	*0.394*	*0.615*
	40	*0.063*	*0.101*	*0.088*	*0.226*	*0.387*	*1.049*
	45	*0.085*	*0.047*	*0.134*	*0.183*	*0.432*	*1.024*
	50	*0.051*	*0.079*	*0.103*	*0.291*	*0.254*	*1.297*
	55	*0.060*	*0.106*	*0.119*	*0.259*	*0.459*	*1.475*
	60	*0.105*	*0.118*	*0.102*	*0.253*	*0.563*	*1.646*
average		*0.068*	*0.083*	*0.095*	*0.223*	*0.409*	*0.917*
standard deviation		*0.013*	*0.019*	*0.016*	*0.029*	*0.069*	*0.338*

The parabolic grain growth constants were plotted against position, starting grain area and final grain area which all showed a slight trend of increasing grain gradients with larger bin location as shown in Figure 6-7 to Figure 6-9.

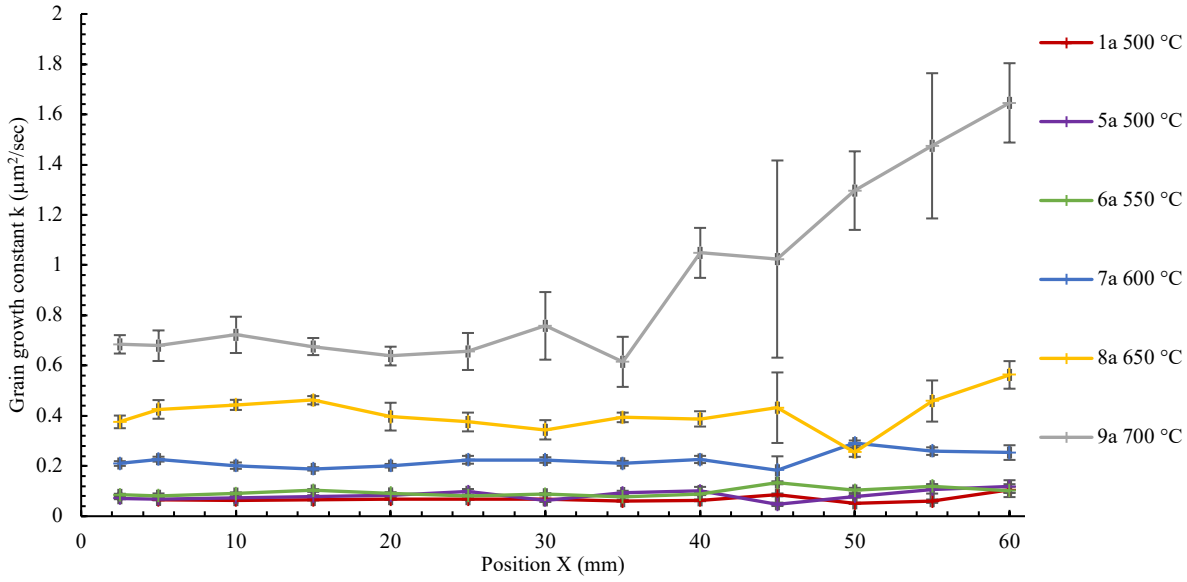

Figure 6-7 Parabolic grain growth constants k from the a-t_0 plots as a function of bin location and temperature. The error bars correspond to the standard deviation.

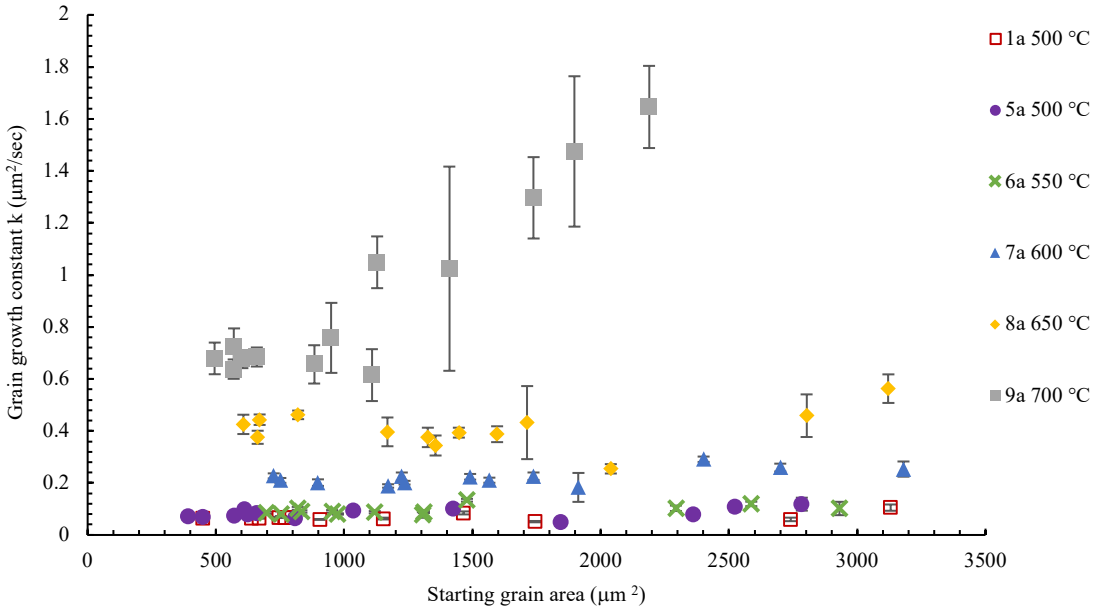

Figure 6-8 Parabolic grain growth constants k from the a-t_o plots as a function of temperature and the starting grain area. The error bars correspond to the standard deviation.

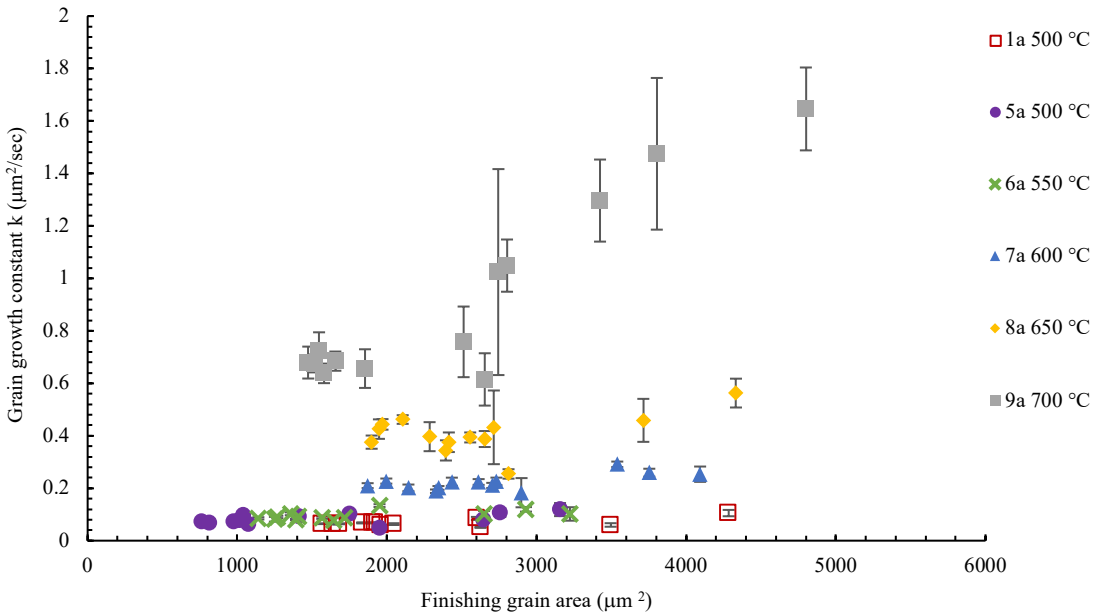

Figure 6-9 Parabolic grain growth constants k from the a-t_o plots as a function of temperature and finishing grain area. The error bars correspond to the standard deviation.

The increasing trend in the growth rate as the average grain size increases may be caused by the larger grains being removed from analysis of the large scale images due to touching an edge of the micrograph. The chance of excluding a large grain would be disproportional to excluding a small grain. This would skew the data to have a higher growth rate.

One would expect to see a reduction in the growth rate of the larger bins due to the grain boundary area decreasing with increased grain size. Given a set volume, if the grains that occupy that area grow in size consuming half the other grains, the grain boundary area has reduced by 21 %. The grain boundaries have energy associated with them and therefore the reduction in grain boundary area will cause a reduction in the growth rate.

Another reason to expect to see a reduction in the growth rate in the larger bins is the grains are bigger than in the smaller bins and therefore will reach the limiting grain size sooner. However, the maximum grain size in all the samples was still under 1/3 the maximum grain size seen in a sample that was heat treated continuously at 700 °C for 4 hours. This sample was used to check for pinning of the grain boundary due to the interaction with the surfaces of the sample. The largest grain diameter was also less than 1/3 the thickness of the sample at ~ 400 µm.

6.2.1 Arrhenius Equation

The activation energy for grain growth from Equation 2, was calculated by plotting $\ln(k)$ against $\frac{1}{RT}$, so that Q is the slope and the intercept is $ln(k_0)$ as shown in Equation 6 and Equation 7.

$$a - a_o = k_0 t\, e^{\frac{-Q}{RT}}$$

Equation 6 Arrhenius equation.

$$Ln\left(\frac{a - a_o}{t}\right) = Ln(k_0) - \frac{1}{RT}Q$$

Equation 7 Rearranged by dividing by t then taking the natural log.

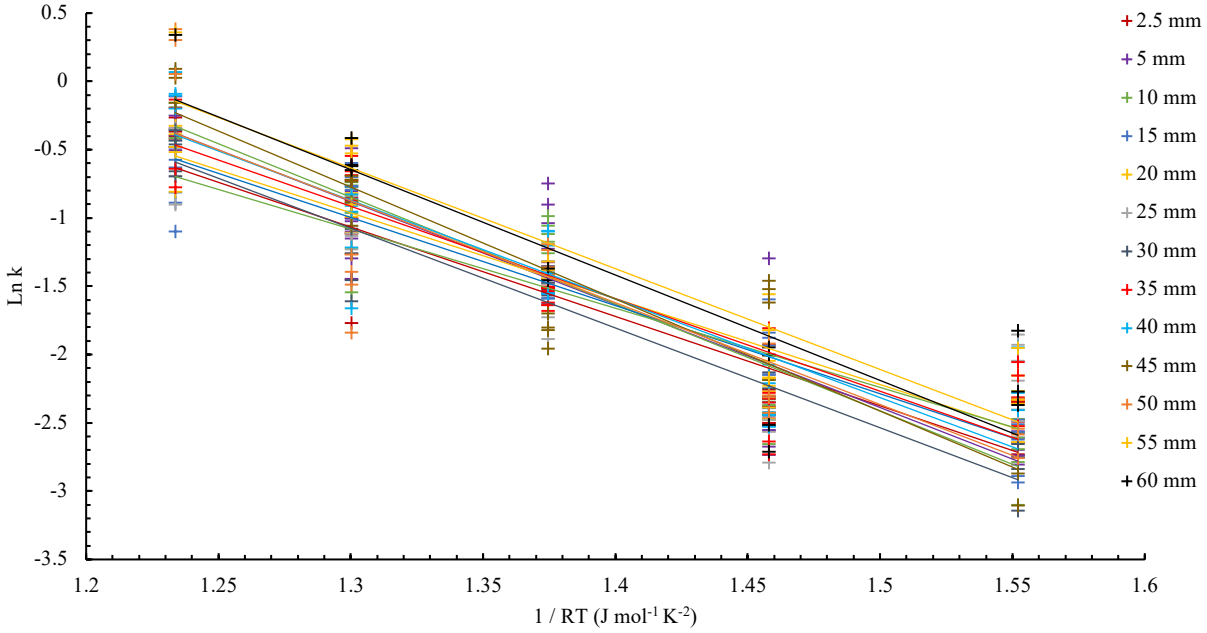

Figure 6-10 Arrhenius plot of parabolic grain growth constants for bin locations given in legend.

The constants for the trend lines from Figure 6-10 are shown in Table 6-2.

Table 6-2 Calculated Q and k_o values from the Arrhenius equation.

Cold Work, ε_{vm} (%)	*Ln (ko)*	*ko*	*Activation Energy, Q (J/mole)*	*R^2 (-)*
38.21	*7.44*	*1710*	*6.54*	*0.87*
37.54	*8.93*	*7540*	*7.54*	*0.84*
36.55	*9.32*	*11200*	*7.82*	*0.90*
34.92	*7.39*	*1620*	*6.45*	*0.91*
30.45	*7.21*	*1350*	*6.29*	*0.87*
25.70	*6.45*	*635*	*5.80*	*0.75*
22.83	*8.42*	*4550*	*7.31*	*0.93*
20.00	*7.89*	*2660*	*6.77*	*0.83*
16.70	*8.52*	*5010*	*7.22*	*0.80*
13.31	*9.89*	*19700*	*8.20*	*0.86*
8.81	*8.82*	*6740*	*7.45*	*0.78*
6.96	*8.96*	*7770*	*7.38*	*0.86*
2.92	*9.38*	*11900*	*7.72*	*0.80*
average	*8.36*	*6340*	*7.11*	*0.85*

The activation energy for grain growth for this work was between 5.8 and 8.2 J/mol with an average of 7.11 J/mol. These values agree within the large range of values found in literature.

Klein found the activation energy for grain growth to be 25 J/mol, using 0.044 inch (1.1 mm) thick 70/30 brass that was heated in a salt bath [25]. The thin samples and using a salt bath without interrupted heat treatments would greatly reduce the thermal lag that was measured in this work and would thus increase the growth rate.

Ghauri et.al. found the activation energy for grain growth to be 0.54 J/mol using 2, 3 and 4 mm diameter wires of 70/30 brass heated in an tube furnace under a vacuum of 1.3 mPa (10^{-5} Torr) [36]. The vacuum furnace would decrease the conduction and would result in a higher thermal lag than this work and would cause a lower growth rate than this work.

Burke measured the activation energy for grain growth to be 16 J/mol in commercially pure 70/30 brass and 25 J/mol in high purity 70/30 brass [90].

Beck et.al. measured the activation energy for grain growth to be 27 kJ/mol with little explanation of methods used [91].

Most of the classical grain growth data has made an assumption that the initial grain size (a_o) is very small compared to the final grain size and hence the starting grain size can be ignored. This was not the approach in this work and therefore comparison to this work is not straightforward.

6.3 THERMAL LAG

The internal temperature of a dummy gradient sample was recorded while being placed into the furnace at the five different heat treatment temperatures and is shown in Figure 4-10.

The same sample was also recorded being quenched in water that was at room temperature to record the cooling cycle, which is shown in Figure 4-11.

The time that the sample took to heat up was unexpected as rough hand calculations showed that the sample should reach the furnace temperature much sooner at around 3 seconds shown in the Appendix 10.1. This was suspected to have partially been caused by a poor thermal connection between the sample and thermocouple. This could not be rectified and retested due to the relatively large thermocouple size to the sample thickness. Also, the time the furnace spent with the door open when installing the sample was significant and thus the internal temperature of the furnace would have drop significantly before the door was re-closed.

One of the biggest issues of doing interrupted heat treatments is the time spent heating and cooling the samples, so that the time analysed is only the time spent at the desired temperature. This set of work has only looked at the unadjusted time that the samples have spent in the furnace, and not the equivalent time of a non-interrupted heat treatment. This is a larger issue with the recrystallisation experiments as the heat treatment times were much shorter than the grain growth experiments and would therefore cause a larger effect.

6.4 COMPOSITIONAL CHANGES

Two samples of the as received brass were taken from opposite ends of the brass sheet and were analysed with OES along with two gradient samples 5B and 9B after heat treatment and a sample heat treated at 700 °C for 240 min to measure any changes in the composition of the brass. The copper, zinc and lead content were plotted and are shown in Figure 6-11.

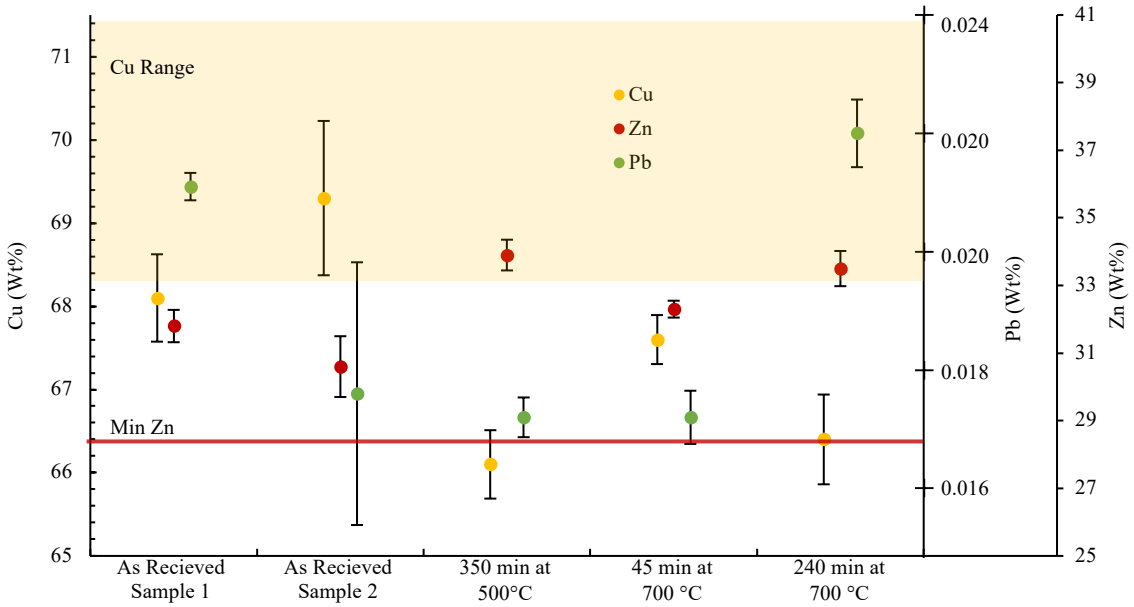

Figure 6-11 Average composition of copper, zinc and lead as measured by OES. The as received samples were taken at opposite ends of the sheet. The red line is the minimum zinc content and the yellow shaded region is the copper content required to confirm to C26000. The As received samples were tested at 0.1-0.3 mm from the surface while the heat-treated samples were tested at the mid plane. The error bars are the standard deviation from the four measurements taken at each sample.

Figure 6-11 shows there is no discernible change in the composition from the as received condition to any of the heat-treated samples. However, the copper content in the As Received Sample 1 is slightly lower than the standard C26000 but is within the error bars, and all the heat-treated samples were lower than the standard.

The dezincification that was measured by Giacobbe was much higher than measured here [11]. This is because dezincification is a thermally driven phenomenon and the temperatures used in this research were much lower than the 900 °C heat treatments used by Giacobbe.

The lead concentration in this batch of brass is an order of magnitude below 0.5 wt. % where lead was seen to precipitate during heat treatment which reduced the grain growth rates through particle drag. Therefore, the growth rates should not be affected by any of the compositional changes in the samples nor by grain boundary drag [13].

7 COLD WORK, GRAIN SIZE AND HARDNESS

OVERVIEW

This chapter discusses the relationship between rolled and tensile cold work.

Two calculations were done to compare tensile cold work to rolled cold work. The first was a comparison using the change in thickness, then another using the reduction in cross sectional area.

Following is a comparison between the original grain area and the recrystallised grain area showing that the same reduction was obtained from both rolled cold work and tensile cold work for the same amount of deformation.

The strain of a gradient sample was measured in the 13 bin locations using DIC, which includes an explanation into the sources of errors with using optical strain measurements.

Comparisons are made between the recrystallised grain area and the position on the gradient sample. The relationship between cold work and the recrystallised grain size is discussed.

The hardness is validated as a proxy for recrystallisation. Lastly the grain size relationship to hardness from this work is compared to literature.

7.1 Cold Work

7.1.1 Comparison Between Rolled and Tensile Cold Work.

The relationship between tensile cold work and rolled cold work is not well documented; therefore, a calculation was done in an attempt to compare rolled or compressive cold work to tensile cold work. All the existing literature is based on rolled cold work. The calculations were based of the FEA model in Ansys and were checked with experimental data.

During rolling the thickness of the sample is reduced however the other two dimensions will increase, whereas in tensile cold work, the length is increased, and the other two dimensions decrease.

The change in dimensions of a gradient sample was measured in Ansys by putting nodes at the thinnest section (X = 0).

7.1.1.1 Thickness Reduction

The change in thickness (Z direction) of a gradient sample was measured after deformation to be 2.7968 mm. The tensile equivalent to cold rolled work was calculated by measuring the change in thickness divided by the original thickness.

$$\frac{3\text{ mm} - 2.7968\text{ mm}}{3\text{ mm}} = 0.06773$$

= 6.7 % equivalent rolled cold work

Using the reduction in thickness gives an extremely low equivalent to cold rolled work.

7.1.1.2 Area Reduction

The displacement of the four nodes after deformation was measured in Ansys and is recorded in Table 7-1. The tensile equivalent to rolled cold work was measured by the change in the area divided by the original area.

Table 7-1: Displacement in the cross section of the FEA model as measured by four tracking nodes on the sample at the vertices at X = 0 of a gradient sample.

Node	δ_y (mm)	δ_z (mm)
1	+0.418	-0.1016
2	+0.418	+0.1016
3	-0.418	+0.1016
4	-0.418	-0.1016

The cross section remained rectangular after deformation. The deformed cross section area was calculated as the original size – the reduction.

$$\text{Y direction} \qquad 12.5\text{ mm} - 2 \times 0.418\text{ mm} = 11.664\text{mm}$$

$$\text{Z direction} \qquad 3\text{ mm} - 2 \times 0.1016\text{ mm} = 2.7968\text{mm}$$

Therefore, the deformed area is

$$11.664\text{ mm} \times 2.7968\text{ mm} = 32.622\text{ mm}^2$$

The original area was

$$12.5\ \text{mm} \times 3\ \text{mm} = 37.5\ \text{mm}^2$$

The reduction in area is

$$\frac{37.5\ \text{mm}^2 - 32.622\ \text{mm}^2}{37.5\ \text{mm}^2} = 0.13$$

= 13 % equivalent rolled cold work.

This calculated value was comparable to measurements taken on the homogeneous samples using a digital ball micrometer. The reductions in area were 12.8 % for samples A and B, 12.9 % for sample C and D and 13.3 % for sample E and F with a von Mises strain of 40 %. The values of area reduction are unreasonably low to give the same numeric value of cold rolled work and tensile cold work.

7.1.2 Grain Size Comparison Between Rolled and Tensile Cold Work.

The three homogeneous samples were deformed to a von Mises strain of 40 %. The average grain area was reduced from 5014 μm^2 to 431 μm^2. This is a 11.7-fold reduction in the original grain area. Walker measured an 11.3-fold reduction in grain area using a 42.5 % reduction in thickness from cold rolled work in 70/30 brass [34]. Figure 7-1 shows a comparison in the grain size reduction obtained after cold work followed by annealing at 650 °C between Walker's cold rolled samples with cold work expressed as percent reduction in thickness and this research with tensile cold work in a gradient sample with cold work expressed as von Mises strain.

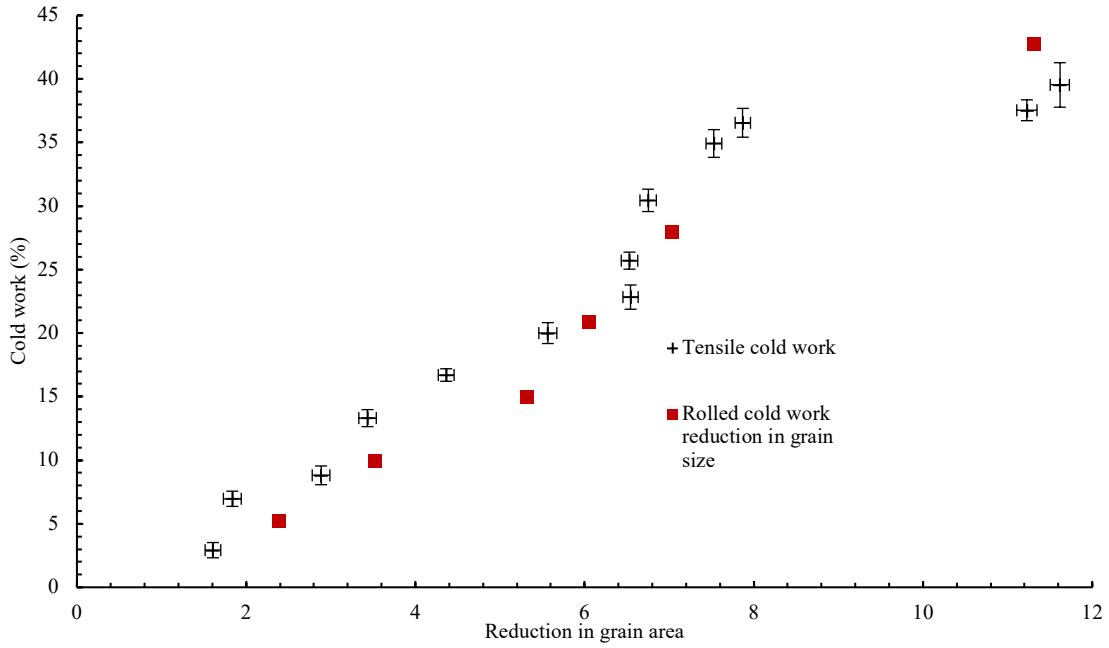

Figure 7-1 Comparison between the reduction in grain area between rolled cold work as recorded by Walker expressed as a reduction in thickness [34] and tensile cold work from this research expressed as von Mises strain.

Figure 7-1 shows that von Mises strain from tensile cold work gives a similar grain refinement to rolled cold work in 70/30 brass. This is interesting because the deformation mechanism with rolled cold work is localised to the surface and decreases toward the centreline.

7.1.3 DIC STRAIN IN THE Y DIRECTION

The von Mises strain was extracted from line profiles across the gage at fixed X corresponding to analysis bins and indicated on Figure 4-1 with the raw data shown in Figure 4-2. The mean values are plotted with position along the gage X in Figure 7-2.

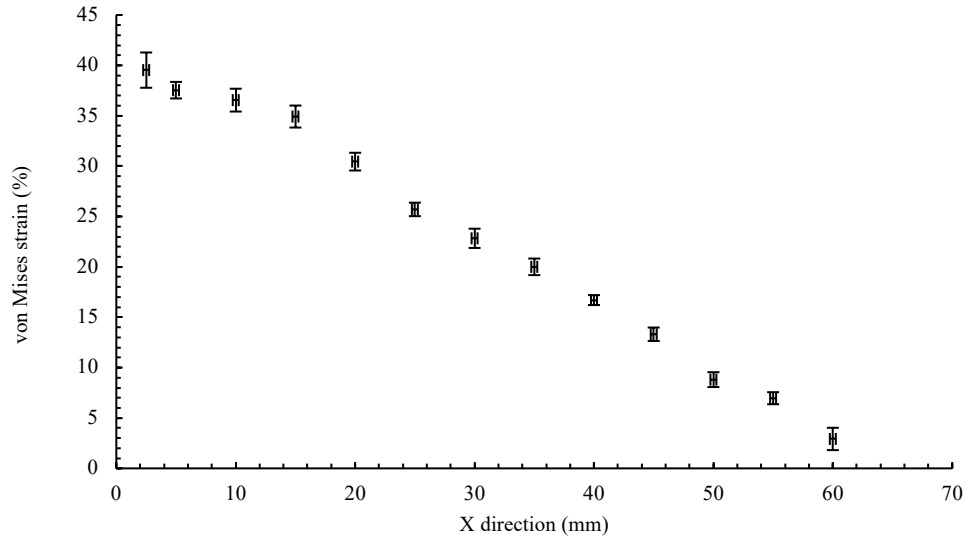

Figure 7-2 Mean von Mises strain with position along the gage at analysis bins at fixed X. The errors bars are the standard deviations.

Generally, the higher the strain, the nosier the data as shown by the high standard deviation in the 2.5 mm bin. This noise was suspected to have come from both material properties and DIC tracking anomalies.

The micro variations in strain were suspected to have come from tracking anomalies in DIC. These are a result of having a very small speckle which has crossed from one pixel to the next in the camera. This causes a large change in deformation over a short period of time (one frame) when, in fact, it was changing over a larger time frame, but the camera was unable to capture it. This can be reduced by using a slightly larger speckle or a higher resolution camera. Another cause is tracking errors. This is when the images are taken while the camera is slightly moving or vibrating. This causes the whole sample to change position in the camera's frame. GOM correlate can compensate for these changes, but this can cause these high local micro strains [79]. This can be reduced by a stable camera tripod.

The larger macro strain variations are cause by the material yielding locally in slip bands. These bands form at roughly 45 ° to the applied axial stress and travel the length of the gage leaving a wake of strain hardened material. Figure 7-3 shows slip bands forming in a series of images taken of a dog bone sample made of brass being deformed. The red indicates areas of higher von Mises strain and the blue are areas of lower strain.

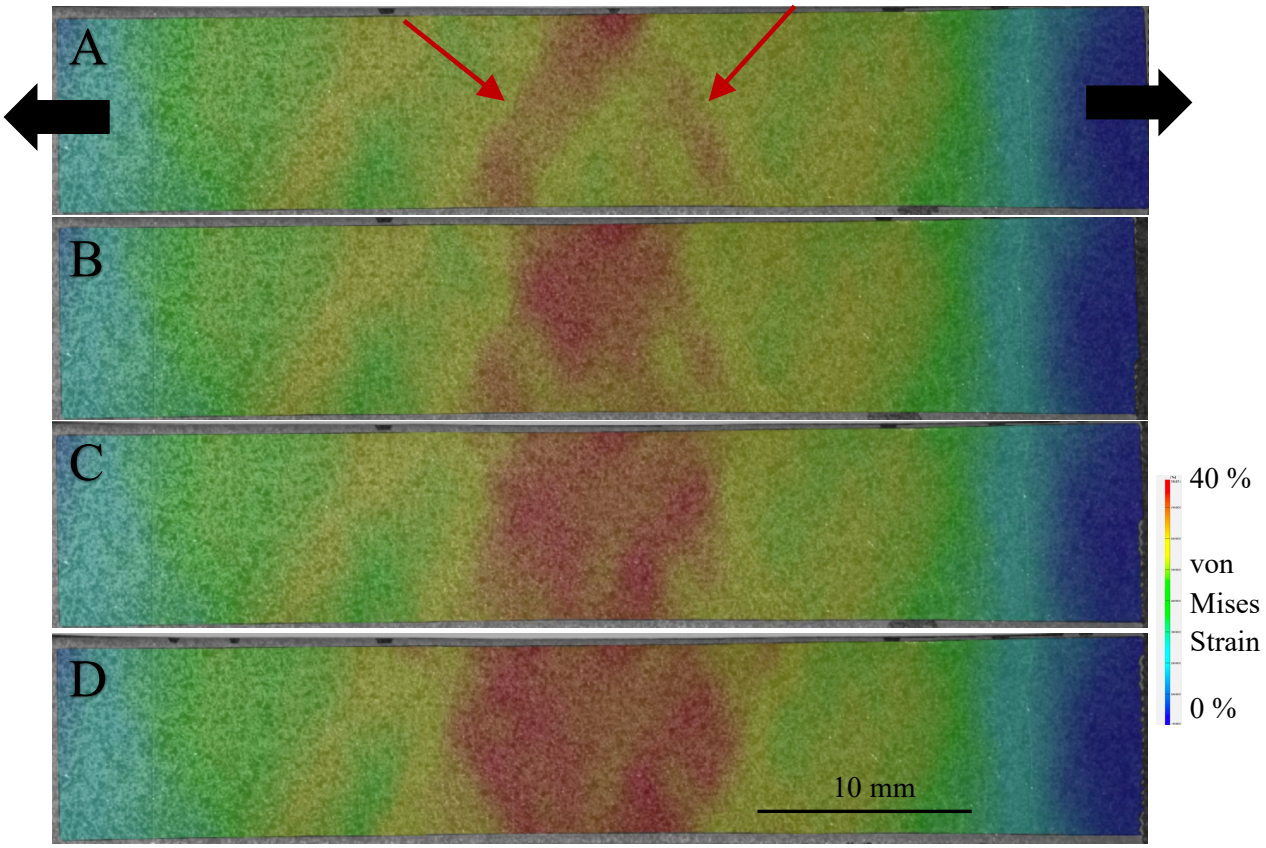

Figure 7-3 Slip bands observed forming in a 70/30 brass dog bone shaped sample during deformation. The colour corresponds to total von Mises strain from DIC. The slip bands are shown by the red colouring in the images and are indicated by red arrows. The direction of applied load is shown with black arrows. A) The first slip band has formed at approximately 45 ° to the applied stress on the left, and the second is just starting to form, also at 45 ° to the stress but perpendicular to the first. B) The first band is starting to grow to the right, while the second band is stagnant. C) The first band has grown both further to right and starting to grow to the left, while the second band is growing to the right. D) The first band is continuing to grow in both directions while the second has caught up to the first on the left side.

7.2 Grain Size

7.2.1 Grain Size vs Position

The minimum mean grain size identified at each bin location for the six gradient samples is plotted as a function of X position on the sample. The five homogenous samples were also plotted for completeness assuming their strains are equivalent to the X = 0 mm position on the gradient samples.

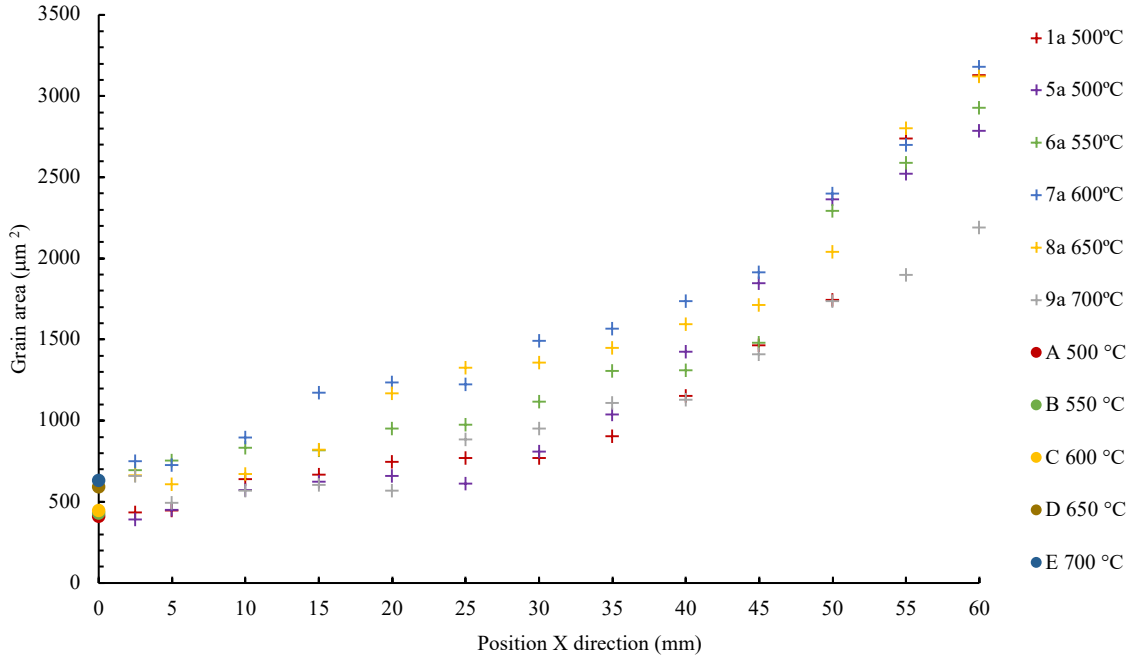

Figure 7-4 Minimum recrystallised grain area as a function of bin position along the gage X for all samples. Note that sample 1a was in grain growth for all bin locations under 35 mm but was left in for completeness.

Figure 7-4 shows that the higher the recrystallisation heat treatment temperature the larger the minimum grain size. This is typically observed, although there are reports of materials with temperature invariant recrystallised grain sizes [92]. The conventional explanation is that increased temperatures allow fewer sub grains to coarsen above the critical size before the entire microstructure has recrystallised, which yields a larger recrystallised grain size.

7.2.2 Grain Size vs Cold Work

The amount of cold work per bin location X was plotted against the minimum recrystallised grain area for each bin location X and is shown in Figure 7-5. The black crosses are from Walker's work where heat treatment was at 450 °C and 500 °C after cold rolling.

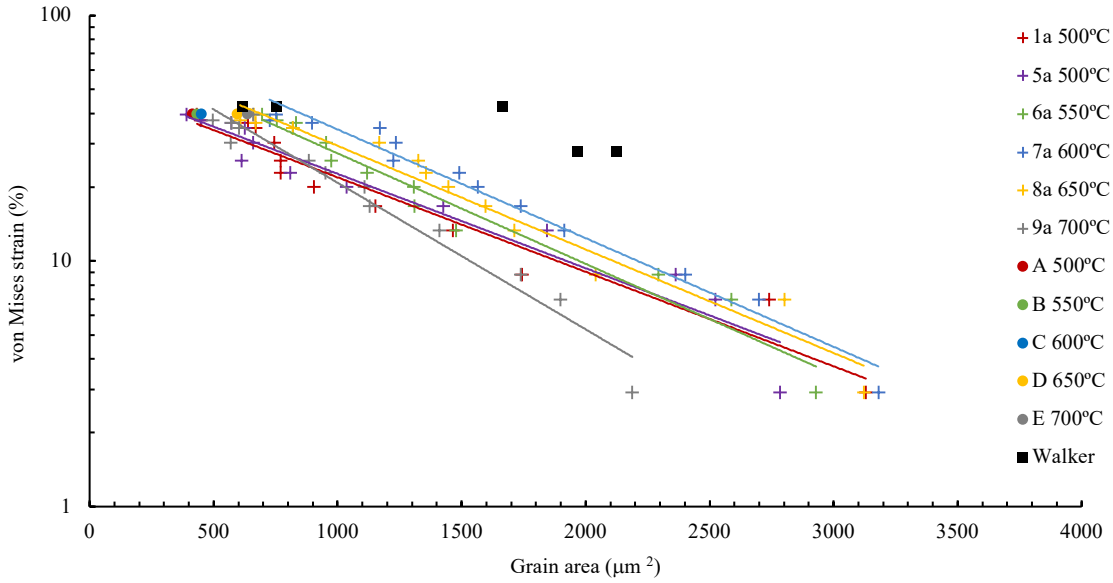

Figure 7-5 Minimum grain area vs strain for all gradient and homogeneous samples. Note that sample 1a, was already into the grain growth plase for all bin locations less than 35 mm but was left in for completeness.

The constants of the trend lines from Figure 7-5 are shown in Table 7-2 along with the R^2 value. As the von Mises strain is shown in a log scale the trend lines are exponential and are expresses in the form of Equation 8.

$$y = Ae^{Bx}$$

Equation 8 Exponental format for the constants in Table 7-2

Where y is the von Mises strain, A and B are constants and x is the grain area.

Table 7-2 Constants for the trendlines in Figure 7-5.

	Sample number					
	1a	*5a*	*6a*	*7a*	*8a*	*9a*
A	*53*	*55*	*77*	*95*	*78*	*82*
B	*-0.00089*	*-0.00089*	*-0.00104*	*-0.00102*	*-0.00097*	*-0.00137*
R^2	*0.94*	*0.94*	*0.96*	*0.97*	*0.96*	*0.96*

Figure 7-5 shows that there is an exponential relationship with the prior cold work and the recrystallised grain area. The higher the temperature the larger the base constant and more negative the exponent. The larger base constant would be expected with higher temperatures because the higher the recrystallisation temperature the larger the grain area.

7.3 Hardness

The hardness of the homogeneous samples was measured after each heat treatment. The hardness values are recorded in Table 4-3. The hardness values are plotted against time and are shown in Figure 7-6, which shows as the sample recrystallises the hardness decreases. This is expected because as the sample recrystallises there is a reduction in stored cold work within the lattice. While grain

refinement is also occurring, the hardening effect from strain hardening dominates over the hardening effect from grain refinement.

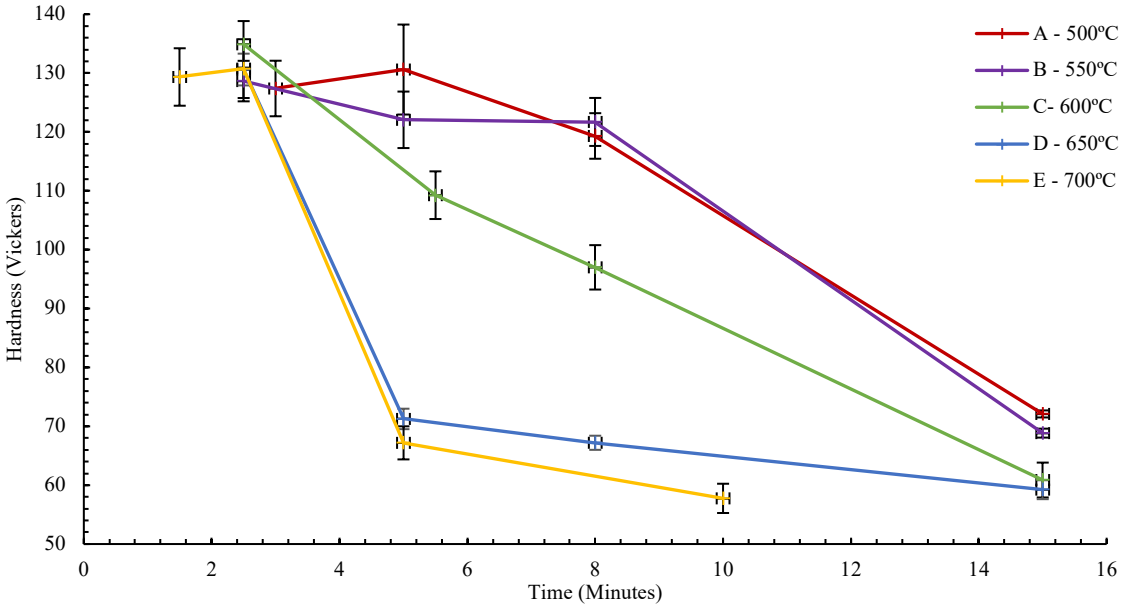

Figure 7-6 Hardness vs Time for the homogenious samples the vertical error bars are the standard deviation.

The hardness for the homogeneous samples was plotted against grain area$^{-0.25}$ so that a comparison could be made to the Hall Petch equation, with hardness being a proxy for strength and is shown in Figure 7-7.

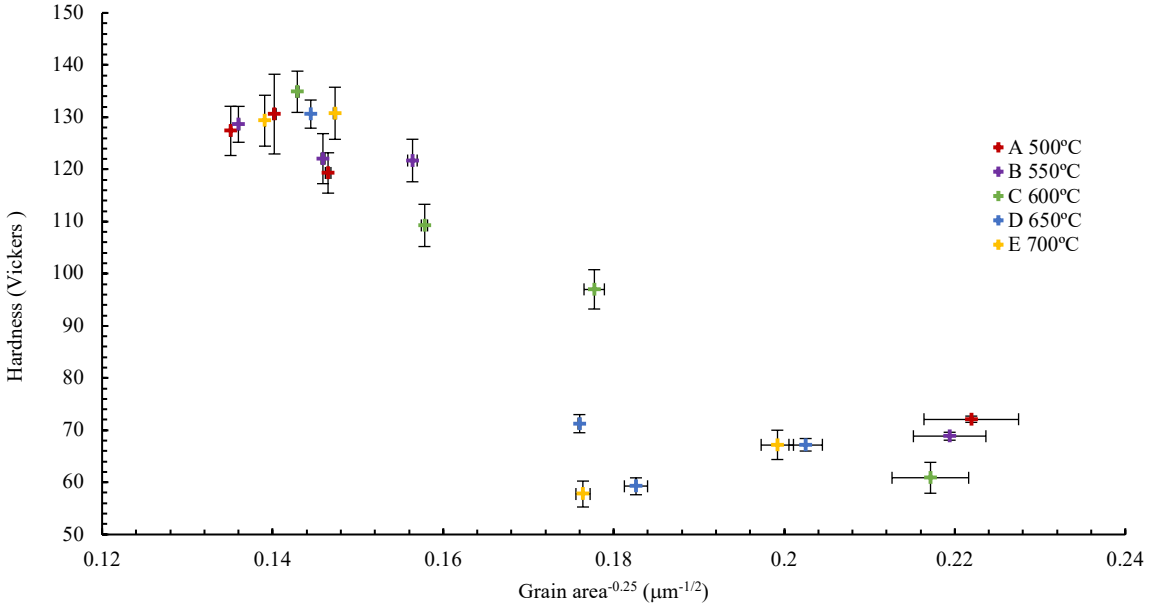

Figure 7-7 Hardness vs grain area$^{-0.25}$, as the homogenous samples go through recovery, recrystallisation and enter grain growth. The error bars are the standard deviation.

This shows an inverse Hall-Petch relationship which is consistent with recrystallisation. Figure 7-7 also shows that there is potentially some grain growth happening in sample D and E due to the hardness decreasing as the grains started getting larger. This is supported by the hardness almost plateauing in Figure 7-6. The same plot was made of gradient sample after a 12-minute heat treatment at 500 °C as shown in Figure 7-8. This sample has partially recrystallised and is shown with a trend

line. However, the largest 4 grain sizes shown with red were much harder and deviated from the expected trend. This is because these grains still had stored cold work and were still recrystalising.

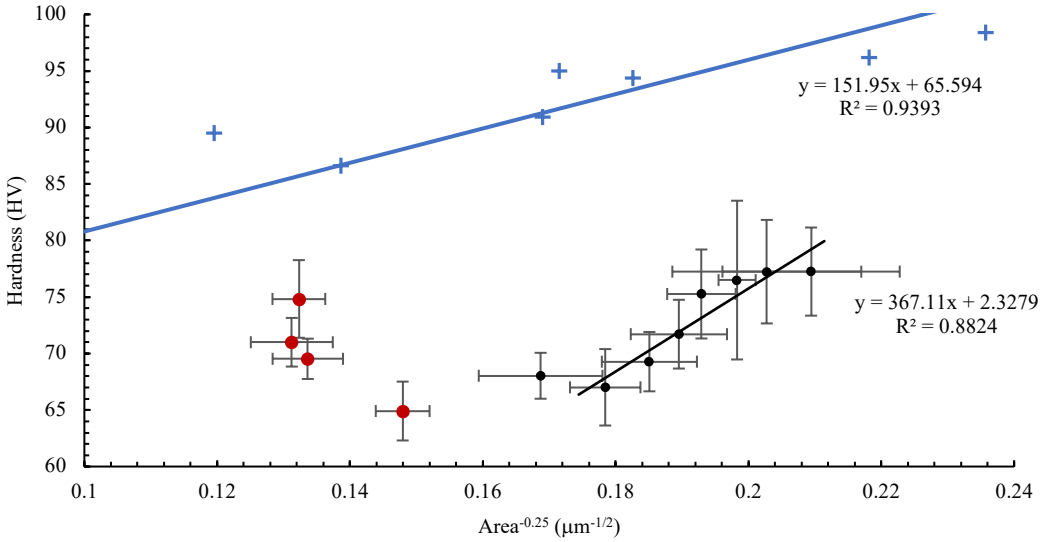

Figure 7-8 Hardness vs grain area$^{-0.25}$, measured from the gradient sample 1b, heat treated at 500 °C for 12 minutes. Data correspond to analysis bins where data points on the right have fully recrystalised and have a linear trendline, while the data indicated with red are not fully recrystallised. The blue line are measurements converted from Rockwell H taken by Walker during recrystallisation and grain growth of cold rolled 70/30 brass. The error bars are the standard deviation [34]

Figure 7-8 shows that there is a decrease in hardness as grain size increases with both Walker's study and this work. There is a discrepancy between Walker's research and this work. Cold rolling is deformation which is concentrated at the surface, while tensile work is not. Walker took the grain size measurements after he observed recrystallisation on the surface; however, there was no indication that the grains under the surface had recrystallised. The hardness scale that Walker reported was Rockwell H, which was converted to Vickers according to ASTM 140-12B [93], he used a 60 kg load and a 1/8" ball indenter according to ASTM E18 [94]. In comparison this research used the Vickers scale which uses a diamond indenter with a load of 1 kg according to ASTM E92-17 [86]. The larger load used by Walker will be testing a much larger hemisphere of material and thus if there are still some un-recrystallised grains under the surface then it will have an elevated hardness [95]. Another source of error in Walkers research is the single hardness test at each grain.

8 CONCLUSION AND FUTURE WORK

INTRODUCTION

The main conclusions from this work are summarised in this Chapter. Future work and process improvements are also discussed. The future work is broken into two sections: material properties, with items such as grain growth and recrystallisation kinetics; and process development, like improvements to DIC, better processing of the images and better heat treatment processes.

8.1 Summary and Conclusions

This masters project set out to exploit gradient tensile specimens to create gradient grain sizes to study the effect of the gradient on grain growth kinetics.

The gradient in grain sizes was created in this work by using tensile cold work. A sample with constantly changing cross sections was designed using ANSYS and deformed to a fixed crosshead displacement. Inhomogeneous strains were obtained from DIC on videos of the tensiometer process using GOM Correlate. Analysis was conducted on a series of subdomains (bins) spaced along the gage. This was followed by a series of interrupted heat treatments at temperatures of 500 °C to 700 °C to recrystallise, then grow, the grains. The grain size was measured after each heat treatment from large scale optical images analysed in ImagePro.

Because the stored cold work was dependant on the location along the gage, recrystallisation was able to be tracked as it progressed down the sample. Then recrystallisation and grain growth was quantified in samples with grain size gradients.

The main conclusions are

- This work showed that FEA was able to accurately predict the strain in a sample by comparison to DIC, even well past the elastic limit.
- The use of DIC for measuring strain and deformation was validated by direct comparison to strain gauges and linear extensometers.
- A method was developed to electropolish large samples with simple equipment to a quality suitable for EBSD.
- The equivalence of tensile and rolled cold work to achieve the same reduction in original grain size was validated.
- A gradient in grain sizes was able to be created in one sample using tensile cold work.
- Digital grain boundary detection using large scale optical images was shown to be more effective and efficient than EBSD in this study.

- There was a detectable increase in the grain growth rate depending on the starting grain size, however this was hypotheses to have been from the largest grains being excluded from analysis due to touching the edges of the micrographs.
- The activation energy for recrystallisation and grain growth behaviour measured here in the gradient samples loosely agreed with values from literature.

- A new method to determine the critical strain anneal conditions using a single sample was developed. This will enable high-throughput materials engineering when developing new engineering metals.

8.2 Future Work

8.2.1 Grain Growth and Recrystallisation

The amount of micrographs taken during this work was extensive (well over 25,000) and 2/3rds of the images were analysed, therefore a logical next step would be to process the rest of the images and look these and see how it add to the statistical significance of the data.

The metal used in this work was a classical material for preforming a grain growth study. A different composition could be chosen to see if the same trends are found in other metals. A candidate is an interstitial free steel.

The strain used in this work was between 2.9 - 40 % von Mises which could be both reduced to look at the critical strain anneal and then increased to look at reducing the minimum grain size. During the initial testing of methods in creating a gradient of grain sizes, two stages of cold work were used. A gradient sample was taken to 40 % von Mises strain then heat treated for 20 minutes at 500 °C, then cold worked to a further ~ 30 % von Mises strain then heat treated again for 15 minutes at 500 °C. This was done in an attempt to increase the gradient in grain size. However, the grain size stayed at approximately the same minimum size. The thought was that the reduction in grain size had increased the yield strength of the smallest cross section, and thus most of the second stage cold work had been in the mid to larger cross section proportions in the sample. This was because the grain size in the larger bin locations was lower than the single stage cold worked samples. This technique may still work if the gradient sample shape was altered to have factored this in. An alternative method to increase the gradient in grain size is to grow the starting grain size to close to the limit of the material then deform it to a much higher peak von Mises strain

The largest grain diameter in this work was approximately 0.4 mm which is much smaller than the 3 mm thickness of the sample. However, there may be surface effects which are altering the grain growth rates. If the sample thickness was increased there would be more material that could be removed during polishing so that the grain size could be measured away from the surface and thus hopefully any surface effects will be negated.

The hardness tests in this work were limited to one gradient sample at 12 minutes at 500 °C and all the homogeneous samples. Hardness reduces during recovery and recrystallisation. Therefore, a local minimum in hardness could also be used alongside a minimum in grain size to identify when a sample has begun grain growth.

8.2.2 Method Improvements

The methods improvements section is broken into a few areas, improvements to DIC, the polishing process and finally improving the large-scale micrograph quality.

8.2.2.1 DIC

This work has shown that DIC is accurately able to measure the strain on a brass sample up to 40 % von Mises strain when compared to an extensometer. The quality of the speckle greatly affects the results of DIC and so altering the process used in this work could increase the resolution and accuracy.

The samples in this work were dry sandblasted using a very fine granite, however this still produced a sample that was very clean but shiny metal, the sample surface was also rough which may have contributed to the speckle. There are alternative methods to flatten the surface such as an acid etch, tumbling in media, vapor blasting or even an undercoat of paint. There are a few limits to these techniques though, if the preparation causes surface deformation such as sand blasting, vapour blasting and tumbling then this will cause stored cold work and hence the reason that the samples in this work were only imaged on the non DIC side. Also, if an undercoat is used then the undercoat must adhere to the surface without cracking or flaking and deform with the sample.

The speckle in this work was applied via a spray can. A pressurised spray can, is unable to produce a consistent mist of paint particles and hence in this work the sample was coated using an overspray from wind. If the speckle was applied using a spray gun or even an air brush, then the size of the paint particles could be greatly reduced along with much finer control of the particle size and quantity.

In this work the speckle was black on an uncoated metallic brass surface. The contrast was not very high and could also be improved. If a black undercoat was applied or even if the metal was left in a heavily oxidised state (either from the furnace anneal, or from an intentional acid attack) then the speckle could be white. White would illuminate much better under intense white light such as the strong LED used in this work and thus the speckle would have a higher contrast.

The tripod and camera used in this work was somewhat stable however there were micro variations in the images. The causes of these variations were a combination of the shutter action from the DSLR shaking the camera, and the

8.2.2.2 Thermal Lag

A factor in the inaccuracy of any interrupted type heat treatment is the time required to heat the samples. This work used an atmospheric furnace which was shown to be slow at heating the samples. If this experiment was to be repeated, then an alternative and faster method of heating the samples would be to use a molten salt bath. The most common molten salt bath uses a combination of sodium chloride, potassium chloride and magnesium chloride salts and these can be liquid as low as 400 °C. Liquid salts have a similar heat capacity as water and thus are able to heat samples much more rapidly.

An alternative to a salt bath would be to use an induction heater. These are able to transfer large amounts of energy very quickly. Some of the issues with using induction heating are similar to those of electro polishing where the sample shape can cause localised heating. This may not work in such large samples which have constantly changing cross sections.

Another method to reduce thermal lag would be to use set duration heat treatments and not interrupted heat treatments. This would reduce the thermal lag to only one cycle. This would assume all the samples are identical replicates with all the same starting grain sizes.

8.2.2.3 Electro Polishing

The electro polishing in this piece of work was by for the hardest and required the most trial and error. The sample shape did not help as the constantly varying shape caused a variation in the current density down the sample. If the sample was sectioned after deformation into a rectangular shape this may reduce the effects as shown in Figure 8-1.

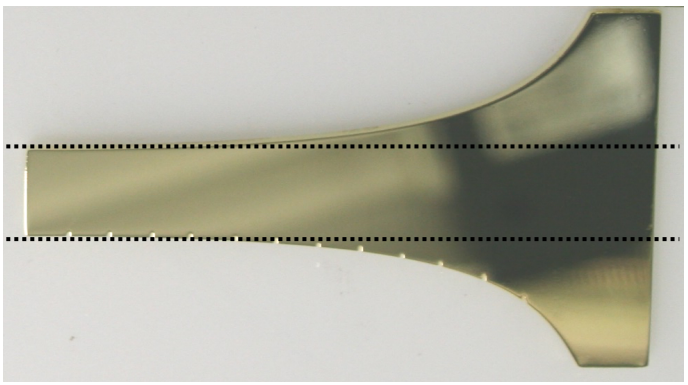

Figure 8-1 Gradient sample with cutting lines. Having a rectangular sample will help reduce the electro pitting during polishing by not having a constantly varying cross section which caused the current density down the sample to vary in the gradient samples.

Another change would be to increase the overall size of the gradient sample, then section after deformation as in Figure 8-1. The reason is for increasing the sample size is to enable enough material to get large scale micrographs while still having a rectangular sample for ease of polishing.

Alternatively if the sample design was changed to have a straight section at the x = 0 mm for 10 mm. This would enable the first 5 mm of each replicate to be disregarded as it would have uniform strain. This would help the problems that were experienced with polishing the 2.5 mm bin location.

8.2.2.4 Micrographs

The optical microscope used in this work was a Leica DMIRM inverted microscope fitted with a Nikon camera. The operation of the manual stage was time consuming and resulted in a few errors when combining the large scale images which had gaps. Also the small variation in the overlap altered the area of each large scale image. If an automated stage microscope was used then the overlap errors would be eliminated and each large scale image would be the same size. The time spent stitching the micrographs together would also be reduced or eliminated if the microscope was able to do it

8.2.3 New Material Design and Testing

Grain size influences material properties and therefore grain size manipulation and control is important when both designing and testing new alloys.

If material properties and kinetics are measured for a new alloy using current methods then a complex series of tests are needed. Measuring the critical strain anneal (the minimum amount of cold work before a metal will recrystallise), recrystallisation time for various amounts of cold work vs temperature and time, Grain growth data, creep resistance etc require many different samples to be individually tested [96]. If a gradient sample was used then the critical strain anneal, recrystallisation time vs strain and once fully recrystallised then grain growth kinetics could be measured all in the one sample.

9 REFERENCES

[1] A. Lasalmonie and J. L. Strudel, "Influence of grain size on the mechanical behaviour of some high strength materials," *J. Mater. Sci.*, vol. 21, no. 6, pp. 1837–1852, 1986, doi: 10.1007/BF00547918.

[2] Porter DA, Easterling KE, Sherif MY, *Phase transformations in metals and alloys*, 3rd ed. Boca Raton, FL: CRC Press, 2009.

[3] W. D. Callister and D. G. Rethwisch, *Materials science and engineering: an introduction*, 9th edition. Hoboken, NJ: John Wiley and Sons, Inc, 2014.

[4] F. Torster, G. Baumeister, J. Albrecht, G. Lütjering, D. Helm, and M. A. Daeubler, "Influence of grain size and heat treatment on the microstructure and mechanical properties of the nickel-base superalloy U 720 LI," *Mater. Sci. Eng. A*, vol. 234–236, pp. 189–192, 1997, doi: 10.1016/S0921-5093(97)00161-5.

[5] M. Hatherly, A. Rollett, F. J. Humphreys, and G. S. Rohrer, *Recrystallization and Related Annealing Phenomena*. London, UNITED KINGDOM: Elsevier Science & Technology, 2004.

[6] N. K. Bourne, "Viewpoint: Unexpected Twins," *Physics*, vol. 9, Feb. 2016, Accessed: Apr. 11, 2019. [Online].

[7] J. W. Christian and S. Mahajan, "Deformation twinning," *Prog. Mater. Sci.*, vol. 39, no. 1, pp. 1–157, Jan. 1995, doi: 10.1016/0079-6425(94)00007-7.

[8] N. Hansen and D. J. Jensen, "Development of Microstructure in FCC Metals during Cold Work," *Philos. Trans. Math. Phys. Eng. Sci.*, vol. 357, no. 1756, pp. 1447–1469, 1999.

[9] G. H. Xiao, N. R. Tao, and K. Lu, "Effects of strain, strain rate and temperature on deformation twinning in a Cu–Zn alloy," *Scr. Mater.*, vol. 59, no. 9, pp. 975–978, 2008, doi: 10.1016/j.scriptamat.2008.06.060.

[10] "ASTM B36/36B -13 Standard Specification for Brass Plate, Sheet, Strip, And Rolled Bar." .

[11] F. W. Giacobbe, "Thermodynamic dezincification behaviour of brass during annealing," *J. Alloys Compd.*, vol. 202, no. 1, pp. 1837–1852, 1993, doi: 10.1016/0925-8388(93)90546-Y.

[12] U. Tabrizi, R. Parvizi, A. Davoodi, and M. H. Moayed, "Influence of heat treatment on microstructure and passivity of Cu–30Zn–1Sn alloy in buffer solution containing chloride ions," *Bull. Mater. Sci.*, vol. 35, no. 1, pp. 89–97, 2012, doi: 10.1007/s12034-011-0252-8.

[13] T. Konkova, S. Mironov, A. Korznikov, G. Korznikova, M. M. Myshlyaev, and S. L. Semiatin, "Grain growth during annealing of cryogenically-rolled Cu–30Zn brass," *J. Alloys Compd.*, vol. 666, pp. 170–177, 2016, doi: 10.1016/j.jallcom.2016.01.097.

[14] S. Mahalingam, P. E. J. Flewitt, and J. F. Knott, "Effect of pre-strain on grain size distributions in 316H austenitic stainless steel," *J. Mater. Sci.*, vol. 47, no. 2, pp. 960–968, 2012, doi: 10.1007/s10853-011-5875-z.

[15] P. Chotinuchit, "GRAIN GROWTH IN CRITICALLY. STRAINED COPPER AND COPPER-ZINC ALLOYS." The University of Arizona, 1962.

[16] M. Avrami, "Kinetics of Phase Change. I General Theory," *J. Chem. Phys.*, vol. 7, no. 12, 1939, doi: 10.1063/1.1750380.

[17] M. Avrami, "Kinetics of Phase Change. II Transformation-Time Relations for Random Distribution of Nuclei," *J. Chem. Phys.*, vol. 8, no. 2, 1940, doi: 10.1063/1.1750631.

[18] R. E. Smallman and R. J. Bishop, *Modern Physical Metallurgy and Materials Engineering - 6th Edition*. 1999.

[19] A. D. Rollett, G. Gottstein, L. Shvindlerman, and M. Molodov, "Grain boundary mobility - A brief review," *Z. Für Met.*, 2004, doi: http://dx.doi.org/10.3139/146.017938.

[20] J. Hu, X. Wang, J. Zhang, Z. Shen, J. Luo, and J. Luo, "A unified theory of grain growth in polycrystalline materials," *ArXiv190100732 Cond-Mat*, 2018, Accessed: Jan. 08, 2019. [Online]. Available: http://arxiv.org/abs/1901.00732.

[21] J. W. Martin, J. W. Martin, R. D. Doherty, and B. Cantor, *Stability of Microstructure in Metallic Systems*. Cambridge University Press, 1997.

[22] A. Pourrahimi, D. Liu, V. Ström, M. S. Hedenqvist, R. T. Olsson, and U. W. Gedde, "Heat treatment of ZnO nanoparticles: new methods to achieve high-purity nanoparticles for high-voltage applications," *J. Mater. Chem. A*, vol. 3, no. 33, 2015, doi: 10.1039/C5TA03120F.

[23] M. Hillert, "On the theory of normal and abnormal grain growth," *Acta Metall.*, vol. 13, no. 3, pp. 227–238, 1965, doi: 10.1016/0001-6160(65)90200-2.

[24] M. I. Mendelev and D. J. Srolovitz, "A regular solution model for impurity drag on a migrating grain boundary," *Acta Mater.*, vol. 49, no. 4, pp. 589–597, 2001, doi: 10.1016/S1359-6454(00)00358-X.

[25] J. Klein, "Recrystallization Behavior of 70/30 Brass." UNIVERSITY OF ILLINOIS AT CHICAGO, 2016, Accessed: Jul. 14, 2018. [Online].

[26] R. F. Kirby, “GRAIN GROWTH IN ALPHA BRASSES.” The University of Arizona., 1965.

[27] H. K. D. H. Bhadeshia, “Considerations of solute-drag in relation to transformation of steels,” *J. Mater. Sci.*, vol. 18, pp. 1473–1481, 1983.

[28] George F. Vander Voort, *Metallography Principles and Practices*. .

[29] N. Tsuji *et al.*, “Microstructural change of ultrafine-grained aluminum during high-speed plastic deformation,” *Mater. Sci. Eng. A*, vol. 350, no. 1, pp. 108–116, Jun. 2003, doi: 10.1016/S0921-5093(02)00709-8.

[30] C. Kwan, Z. Wang, and S.-B. Kang, “Mechanical behavior and microstructural evolution upon annealing of the accumulative roll-bonding (ARB) processed Al alloy 1100,” *Mater. Sci. Eng. A*, vol. 480, no. 1, pp. 148–159, May 2008, doi: 10.1016/j.msea.2007.07.022.

[31] J. S. Vetrano, S. M. Bruemmer, L. M. Pawlowski, and I. M. Robertson, “Influence of the particle size on recrystallization and grain growth in Al-Mg-X alloys,” *Mater. Sci. Eng. A*, vol. 238, no. 1, pp. 101–107, Oct. 1997, doi: 10.1016/S0921-5093(97)00445-0.

[32] C. N. Tomé, R. A. Lebensohn, and U. F. Kocks, “A model for texture development dominated by deformation twinning: Application to zirconium alloys,” *Acta Metall. Mater.*, vol. 39, no. 11, pp. 2667–2680, Nov. 1991, doi: 10.1016/0956-7151(91)90083-D.

[33] L. Rice, C. P. Hinesley, and H. Conrad, “Techniques for optical and electron microscopy of titanium,” *Metallography*, vol. 4, no. 3, pp. 257–268, Jun. 1971, doi: 10.1016/0026-0800(71)90017-6.

[34] H. L. Walker, “Grain sizes produced by recrystallization and coalescence in cold-rolled cartridge brass,” University of Illinois at Urbana Champaign, College of Engineering. Engineering Experiment Station., 1945.

[35] “Binary Alloy Phase Diagrams, 2nd Edition,” p. 3.

[36] I. M. Ghauri, M. Z. Butt, and S. M. Raza, “Grain growth in copper and alpha-brasses,” *J. Mater. Sci.*, vol. 25, no. 11, pp. 4782–4784, Nov. 1990, doi: 10.1007/BF01129942.

[37] S. K. Rhee, “Grain growth in alpha brass and in alpha iron,” *Mater. Sci. Eng.*, vol. 9, pp. 246–248, Jan. 1972, doi: 10.1016/0025-5416(72)90041-9.

[38] W. L. Phillips and R. W. Armstrong, “The strain dependence of the flow stress-grain size relation for 70:30 brass,” *Metall. Trans.*, vol. 3, no. 10, pp. 2571–2577, 1972, doi: 10.1007/BF02644231.

[39] M. A. Meyers, A. Mishra, and D. J. Benson, “Mechanical properties of nanocrystalline materials,” *Prog. Mater. Sci.*, vol. 51, no. 4, pp. 427–556, 2006, doi: 10.1016/j.pmatsci.2005.08.003.

[40] H. Conrad and J. Narayan, “On the grain size softening in nanocrystalline materials,” *Scr. Mater.*, vol. 42, no. 11, pp. 1025–1030, 2000, doi: 10.1016/S1359-6462(00)00320-1.

[41] G. Palumbo, U. Erb, and K. T. Aust, “Triple line disclination effects on the mechanical behaviour of materials,” *Scr. Metall. Mater.*, vol. 24, no. 12, pp. 2347–2350, 1990, doi: 10.1016/0956-716X(90)90091-T.

[42] P. G. Sanders, J. R. Weertman, and J. G. Barker, “Structure of nanocrystalline palladium and copper studied by small angle neutron scattering,” *J. Mater. Res.*, vol. 11, no. 12, pp. 3110–3120, 1996, doi: 10.1557/JMR.1996.0395.

[43] G. E. Fougere, J. R. Weertman, R. W. Siegel, and S. Kim, “Grain-size dependent hardening and softening of nanocrystalline Cu and Pd,” *Scr. Metall. Mater.*, vol. 26, no. 12, pp. 1879–1883, 1992, doi: 10.1016/0956-716X(92)90052-G.

[44] C. A. Schuh, T. G. Nieh, and H. Iwasaki, “The effect of solid solution W additions on the mechanical properties of nanocrystalline Ni,” *Acta Mater.*, vol. 51, no. 2, pp. 431–443, 2003, doi: 10.1016/S1359-6454(02)00427-5.

[45] H. Chang, H. J. Hfler, C. J. Altstetter, and R. S. Averback, “SYNTHESIS, PROCESSING AND PROPERTIES OF NANOPHASE TiAI,” *Scr. Metall.*, vol. 25, no. 5, p. 6, 1991.

[46] H. Van Swygenhoven, M. Spaczer, and A. Caro, “Microscopic description of plasticity in computer generated metallic nanophase samples: a comparison between Cu and Ni,” *Acta Mater.*, vol. 47, no. 10, pp. 3117–3126, 1999, doi: 10.1016/S1359-6454(99)00109-3.

[47] B. Cai, Q. P. Kong, L. Lu, and K. Lu, “Interface controlled diffusional creep of nanocrystalline pure copper,” *Scr. Mater.*, vol. 41, no. 7, pp. 755–759, 1999, doi: 10.1016/S1359-6462(99)00213-4.

[48] V. S. Tong and B. T. Britton, “Formation of very large `blocky alpha’ grains in Zircaloy-4,” *Acta Mater*, vol. 129, 2017, doi: 10.1016/j.actamat.2017.03.002.

[49] Oxford Instruments, “Simultaneous ESD and EBSD Analysis Using AZtec Large Area Mapping,” 2014.

[50] Y. Kok *et al.*, “Anisotropy and heterogeneity of microstructure and mechanical properties in metal additive manufacturing: A critical review,” *Mater. Des.*, vol. 139, pp. 565–586, Feb. 2018, doi: 10.1016/j.matdes.2017.11.021.

[51] A. Saboori, D. Gallo, S. Biamino, P. Fino, and M. Lombardi, “An Overview of Additive Manufacturing of Titanium Components by Directed Energy Deposition: Microstructure and Mechanical Properties,” *Appl. Sci.*, vol. 7, no. 9, p. 883, Aug. 2017, doi: 10.3390/app7090883.

[52] Z. Cheng, H. Zhou, Q. Lu, H. Gao, and L. Lu, “Extra strengthening and work hardening in gradient nanotwinned metals,” *Science*, vol. 362, no. 6414, p. 1925, 2018, doi: 10.1126/science.aau1925.

[53] J. Li and A. K. Soh, “Modeling of the plastic deformation of nanostructured materials with grain size gradient,” *Int. J. Plast.*, vol. 39, pp. 88–102, Dec. 2012, doi: 10.1016/j.ijplas.2012.06.004.

[54] R. B. Martin, D. B. Burr, N. A. Sharkey, and D. P. Fyhrie, *Skeletal tissue mechanics*, Second edition. New York ; Heidelberg: Springer, 2015.

[55] K. Brakke, *Surface Evolver Manual*. Selinsgrove, PA: Susquehanna University, 2013.

[56] A. Baskaran, D. Crist, and D. Lewis, “Effect of initial variance of microstructures on grain growth under mean curvature,” *Model. Simul. Mater. Sci. Eng.*, vol. 25, no. 6, p. 065010, 2017, doi: 10.1088/1361-651X/aa763c.

[57] N. J. Breeuwer, “Creating a Gradient of Grain Sizes in 70/30 Brass.” University of Canterbury, 2018.

[58] C. M. Bishop, S. P. Mucalo, M. V. Kral, and D. J. Lewis, “Continuous Grain Size Gradients in Austenitic Incoloy 800H: Design, Processing, and Characterization,” *Metall. Mater. Trans. A*, Jan. 2020, doi: 10.1007/s11661-019-05622-1.

[59] “ASTM E112-13 Test Methods for Determining Average Grain Size,” ASTM International. doi: 10.1520/E0112-13.

[60] George F. Vander Voort, *Metallography Principles and Practices*. McGraw-Hill, 1999.

[61] K. Dicks, “Introduction to EBSD.” Oxford Instruments Analytical, 2003.

[62] R. Erni, M. D. Rossell, C. Kisielowski, and U. Dahmen, “Atomic-Resolution Imaging with a Sub-50-pm Electron Probe,” *Phys. Rev. Lett.*, vol. 102, no. 9, Mar. 2009, doi: 10.1103/PhysRevLett.102.096101.

[63] R. A. Schwarzer, D. P. Field, B. L. Adams, M. Kumar, and A. J. Schwartz, *Present State of Electron Backscatter Diffraction and Prospective Developments*. Boston, MA: Springer US, 2009.

[64] M. M. Nowell, R. A. Witt, and B. True, “EBSD Sample Preparation: Techniques, Tips, and Tricks,” *Microsc. Microanal. Camb.*, vol. 11, no. S02, pp. 504–5, Aug. 2005.

[65] J. H. Bunge and P. R. Morris, *Texture analysis in material science*, 2nd Edition. 1982.

[66] R. A. Schwarzer, “Automated crystal lattice orientation mapping using a computer-controlled SEM,” *Micron*, vol. 28, no. 3, pp. 249–265, Jun. 1997, doi: 10.1016/S0968-4328(97)00010-3.

[67] G. L. Donati, R. S. Amais, and C. B. Williams, “Recent advances in inductively coupled plasma optical emission spectrometry,” *J. Anal. At. Spectrom.*, vol. 32, no. 7, pp. 1283–1296, Jul. 2017, doi: 10.1039/C7JA00103G.

[68] “NIST ASD Output: Lines.” https://physics.nist.gov (accessed Feb. 13, 2020).

[69] G. L. Wynick and C. J. Boehlert, “Use of electropolishing for enhanced metallic specimen preparation for electron backscatter diffraction analysis,” *Mater. Charact.*, vol. 55, no. 3, pp. 190–202, Sep. 2005, doi: 10.1016/j.matchar.2005.04.008.

[70] E. Goins, “Digital image analysis in microscopy for objects and architectural conservation,” p. 16.

[71] T. J. Collins, “ImageJ for microscopy,” *BioTechniques*, vol. 43, no. 1S, pp. S25–S30, Jul. 2007, doi: 10.2144/000112517.

[72] A. Campbell, P. Murray, E. Yakushina, S. Marshall, and W. Ion, “New methods for automatic quantification of microstructural features using digital image processing,” *Mater. Des.*, vol. 141, pp. 395–406, Mar. 2018, doi: 10.1016/j.matdes.2017.12.049.

[73] "ASTM E562-19 Test Method for Determining Volume Fraction by Systematic Manual Point Count," ASTM International. doi: 10.1520/E0562-19.

[74] W. Montero, R. Farag, V. Díaz, M. Ramirez, and B. L. Boada, "Uncertainties Associated with Strain-Measuring Systems Using Resistance Strain Gauges," *J. Strain Anal. Eng. Des.*, vol. 46, no. 1, pp. 1–13, Jan. 2011, doi: 10.1243/03093247JSA661.

[75] N. McCormick and J. Lord, "Digital Image Correlation," *Mater. Today*, vol. 13, no. 12, pp. 52–54, Dec. 2010, doi: 10.1016/S1369-7021(10)70235-2.

[76] "Precision Strain Gages - 1-Axis General Purpose." Accessed: Feb. 13, 2020. [Online]. Available: https://www.omega.ca.

[77] "How to Select the Right Extensometer for Your Material Testing Application." Jan. 21, 2019, Accessed: Feb. 13, 2020. [Online]. Available: https://www.azom.com.

[78] Y. L. Dong and B. Pan, "A Review of Speckle Pattern Fabrication and Assessment for Digital Image Correlation," *Exp. Mech.*, vol. 57, no. 8, pp. 1161–1181, Oct. 2017, doi: 10.1007/s11340-017-0283-1.

[79] Corrolated Solutions, *Speckle Pattern Fundamentals*. .

[80] R. Vayeda and J. Wang, "Adhesion of coatings to sheet metal under plastic deformation," *Int. J. Adhes. Adhes.*, vol. 27, no. 6, pp. 480–492, Sep. 2007, doi: 10.1016/j.ijadhadh.2006.08.003.

[81] ASTM, "Specification for Brass Plate, Sheet, Strip, And Rolled Bar," ASTM International. doi: 10.1520/B0036_B0036M-18.

[82] *GOM Correlate By GOM Gmbh Schmitzstraße 2 38122 Braunschweig Germany*. .

[83] A. J. Schwartz, B. L. Adams, D. P. Field, and M. Kumar, *Electron Backscatter Diffraction in Materials Science*. New York, NY, UNITED STATES: Springer, 2010.

[84] H. S. Rawdon and M. G. Lorentz, "Metallographic etching reagents; I, for copper," *Sci. Pap. Bur. Stand.*, vol. 16, p. 641, Oct. 1920, doi: 10.6028/nbsscipaper.074.

[85] *ImagePro 10 By Media Cybernetics Inc. 1700 Rockville Pike, Suite 240 Rockville, MD 20852 USA*. .

[86] "ASTM E92 - Standard Test Methods for Vickers Hardness and Knoop Hardness of Metallic Materials - Engineering Workbench." .

[87] A. Hadadzadeh, F. Mokdad, M. A. Wells, and D. L. Chen, "A new grain orientation spread approach to analyze the dynamic recrystallization behavior of a cast-homogenized Mg-Zn-Zr alloy using electron backscattered diffraction," *Mater. Sci. Eng. A*, vol. 709, pp. 285–289, Jan. 2018, doi: 10.1016/j.msea.2017.10.062.

[88] E. A. Jägle and E. J. Mittemeijer, "The Kinetics of and the Microstructure Induced by the Recrystallization of Copper," *Metall. Mater. Trans. A*, vol. 43, no. 4, pp. 1117–1131, Apr. 2012, doi: 10.1007/s11661-011-0959-6.

[89] A. Shafiei M, A. Roshanghias, H. Abbaszadeh, and G. H. Akbari, “An Investigation into the Effect of Alloying Elements on the Recrystallization Behavior of 70/30 Brass,” *J. Mater. Eng. Perform. N. Y.*, vol. 19, no. 4, pp. 553–557, Jun. 2010.

[90] J. E. Burke and D. Turnbull, “Recrystallization and grain growth,” *Prog. Met. Phys.*, vol. 3, pp. 220–292, Jan. 1952, doi: 10.1016/0502-8205(52)90009-9.

[91] P. A. Beck, “Comments on ``Grain Growth in Alpha-Brass'',” *J. Appl. Phys.*, vol. 18, no. 11, pp. 1028–1029, Nov. 1947, doi: 10.1063/1.1697575.

[92] S. Wang, E. A. Holm, J. Suni, M. H. Alvi, P. N. Kalu, and A. D. Rollett, “Modeling the recrystallized grain size in single phase materials,” *Acta Mater.*, vol. 59, no. 10, pp. 3872–3882, Jun. 2011, doi: 10.1016/j.actamat.2011.03.011.

[93] “ASTM 140-12B Standard Hardness Conversion Tables for Metals Relationship Among Brinell Hardness, Vickers Hardness, Rockwell Hardness, Superficial Hardness, Knoop Hardness, Scleroscope Hardness, and Leeb Hardness.”

[94] “ASTM E18 - Standard Test Methods for Rockwell Hardness of Metallic Materials - Engineering Workbench.” .

[95] K. Herrmann, *Hardness Testing: Principles and Applications*. Materials Park, UNITED STATES: A S M International, 2010.

[96] “ASTM E139 Test Methods for Conducting Creep, Creep-Rupture, and Stress-Rupture Tests of Metallic Materials,” ASTM International. doi: 10.1520/E0139-11R18.

10 APPENDIX

10.1 ROUGH HAND CALCULATIONS FOR TEMPERATURE CHANGE

The time required to heat a sample of brass by conduction was calculated. This is only a rough calculation and was only used to justify the use of a conduction furnace and the short interrupted heat treatments.

$$\boldsymbol{Q = \frac{k \times A \times (T_{hot} - T_{cold})}{d}}$$ **Equation 9 Heat conduction**

Q = Conduction heat transfer (W)

k = Materials thermal conductivity (W/mK)

A = Cross sectional area (m²)

T_{hot} = Higher temperature (°C)

T_{cold} = Colder temperature (°C)

d = Material thickness (m)

$$\boldsymbol{q = m \times c \times \Delta T}$$ **Equation 10 Energy to heat a sample**

q = Energy required to heat the sample to temperature (j)

m = Mass of the sample (kg)

c = Specific heat capacity of the material

ΔT = Temperature change (°C)

$$\boldsymbol{t = \frac{q}{Q}}$$ **Equation 11 Time required to heat sample**

The thermal conductivity of 70/30 brass is 100.42 W/mK

The temperature of the furnace was 500 °C and the temperature of the sample was 25 °C.

The mass of the sample was 0.05 kg the surface area was 0.0056565 m^2 the thickness is 0.03 m.

$$Q = \frac{100.42 \times 0.0056565 \times (500 - 25)}{0.03}$$

$$Q = 8993.7\,W$$

$$q = 0.05 \times 920 \times 475$$

$$q = 21850\,j$$

$$t = \frac{21850}{8993.9}$$

$$t = 2.43\,seconds$$

The time required for a gradient sample to be heated from 25 °C to 500 °C should only be 2.5 seconds.